ABSTRACT

NUCLEAR SPECTROSCOPIC STUDIES OF SOME SHORT-LIVED AND NEUTRON DEFICIENT Ga AND Zn ISOTOPES

By

Gregg Carl Giesler

The decay schemes of ^{63}Zn, ^{62}Zn and ^{63}Ga were investigated by high-resolution γ-ray spectroscopy in an effort to further elucidate their nuclear properties. Also, a search for β-delayed α emission from the light Ga isotopes was conducted.

Such γ-ray spectroscopic techniques as Ge(Li) singles, Ge(Li)-Ge(Li) megachannel coincidence, Ge(Li)-NaI(Tl) coincidence, and Ge(Li)-time coincidence techniques have been utilized to study these isotopes. A He-jet thermalizer was utilized in the search for β-delayed α emission. Several programs written for data analysis are presented.

Forty-five γ rays have been assigned to the decay of 38.4-minute ^{63}Zn and have been incorporated into a decay scheme containing 24 levels with energies of 0, 669.71, 962.14, 1327.0, 1412.07, 1546.8, 1860.9, 1865.7, 2012.0, 2062.3, 2081.4, 2093.5, 2336.8, 2497.5, 2512.5, 2536.2, 2697.0, 2717.2, 2780.1, 2857.8, 2889.5, 3044.0, and 3100.3 keV. A search for γ rays with energies above 700 keV from the decay of 9.3-hour ^{62}Zn was conducted and six were found at energies of 881.4, 915.6, 1142.5, 1280.8, 1389.1, and 1429.9 keV. They were placed in a decay scheme containing seventeen γ-rays and ten levels with energies of 0, 40.94, 243.44, 287.98, 548.41, 637.53, 915.6, 1142.5, 1280.8, and 1429.9 keV. The decay of 32.4-second ^{63}Ga has sixteen γ rays which were placed

in a decay scheme containing nine levels with energies of 0, 193.0, 248.0, 627.1, 637.0, 650.1, 1065.2, 1395.4, and 1691.7 keV.

Spin and parity assignments for the nuclear states investigated are based on log ft values, relative γ-ray intensities to states of known spin and parity and charged particle scattering results.

A survey of and comparison with previously reported Ge(Li) detector results and with charged particle scattering results is presented for these isotopes. The structures of the low-lying states in these nuclei are discussed and compared with theoretical calculations and systematics of the region.

A search for β-delayed α emission from the short-lived (<5 sec) Ga isotopes through ^{60}Ga was conducted. The γ-ray and α-particle spectra from the nuclei produced are presented. An upper limit of ten parts per million was placed on β-delayed α branching from the decay of these nuclei.

NUCLEAR SPECTROSCOPIC STUDIES OF SOME SHORT-LIVED AND NEUTRON DEFICIENT Ga AND Zn ISOTOPES

By

Gregg Carl Giesler

A THESIS

Submitted to
Michigan State University
in partial fulfillment of the requirements
for the degree of

DOCTOR OF PHILOSOPHY

Department of Chemistry
Program in Chemical Physics

1971

ACKNOWLEDGEMENTS

I sincerely wish to thank Dr. Wm. C. McHarris for suggesting this region of study. His guidance, encouragement, and patience during the experimental work and preparation of this thesis are greatly appreciated.

I also wish to thank Dr. W. H. Kelly of the Physics Department for his help and advice. His suggestions and advice during this project were very useful.

Dr. H. G. Blosser, Mr. H. Hilbert, and Dr. W. P. Johnson assisted with the operation of the Michigan State University Sector-Focused Cyclotron, which was used to prepare the radioactive sources used for this investigation.

Dr. D. B. Beery, Mr. J. Black, Mr. W. B. Chaffee, Dr. J. B. Cross, Dr. R. E. Doebler, Dr. R. E. Eppley, Mr. R. B. Firestone, Dr. R. Goles, Mr. C. Morgan, and Mr. R. Todd all deserve special mention for their assistance and advice throughout the course of these experiments. I particularly wish to thank Mr. K. L. Kosanke for his assistance with and the development of the He-jet thermalizer and pneumatic rabbit systems.

Mr. R. Au, Mr. and Mrs. W. Merritt, and the cyclotron computer staff have aided greatly in the data aquisition and evaluation through the use of the XDS Sigma 7 computer. Their assistance in programming of the computer is greatly appreciated.

Help has also been received from Mr. R. N. Mercer and his staff

in the cyclotron machine shop, and from Mr. W. Harder and the cyclotron electronics shop.

The cyclotron drafting staff, especially Mr. A. Daudi, have been very helpful and quick in preparing the drawings for this thesis.

Our secretaries Mrs. P. Warstler and Mrs. M. Fedewa have helped in typing this thesis.

Mr. J. J. Chavda prepared the artwork for the cover.

I wish to thank the U. S. Army for allowing me to continue my education and obtain this degree.

I thank the National Science Foundation, U. S. Atomic Energy Comission, and Michigan State University for their financial support without which this study would not be possible.

Finally, I wish to thank my wife, Maryjane, for her encouragement, inspiration, perspiration, and patience during the course of this study.

TABLE OF CONTENTS

Chapter

Page

LIST OF TABLES

LIST OF FIGURES

Figure

Page

Chapter I

INTRODUCTION

Any study of the nucleus involves the use of many models, since no one model fits more than a small number of nuclei. Although these models vary widely in their description of the nucleus, they are all semi-empirical, that is, require a number of experimentally determined parameters in order to make any predictions. Therefore, any improvement in quality or quantity of the experimental results will not only aid in improving the results obtained from the model, but also aid in the further development of the model and the description of nuclei as a whole.

One of the most useful methods of obtaining information about nuclear properties is γ-ray spectroscopy. With the development of Ge(Li) detectors with their present efficiency and resolution, even the very weak γ rays in a complex spectrum can be seen and easily resolved from their neighbors. As a result, decay schemes previously considered relatively simple have become much more complex. γ-ray spectroscopy, therefore, has become an important part of the study of nuclear properties.

The nuclear shell model is one of the more popular models used to describe the nucleus. The nucleus, according to this model, is like an atom with the protons and neutrons individually going around in their own orbits. In addition, closed shells occur at neutron or proton "magic" numbers of 2, 8, 20, 28, 50, 82, and 126. It is found that this model only works well near these closed shells. Accordingly,

most of the study of this model has occurred in the following regions: nuclei with fewer than 23 protons, those with 28 protons, 50 neutrons or protons, 82 neutrons, and nuclei in the region of the ^{208}Pb doubly closed shell.

A primary interest is in the region with fewer than 23 protons, since in this region the β stability line lies on or near $N=Z$. Here also there is an abundance of doubly closed shells, and each closed shell consists of at most three low spin orbits which makes the calculations relatively easy. The stable isotopes of calcium which go from the doubly magic ^{40}Ca to the also doubly magic ^{48}Ca are found at the upper end of this region.

One more doubly magic nucleus occurs near this region, ^{56}Ni. It is different from the others because it is unstable to β decay and rather far from the line of β stability. The two closed shells are the $1f_{7/2}$ for both protons and neutrons. In the region immediately beyond this nucleus are the $2p_{1/2}$, $2p_{3/2}$, $1f_{5/2}$ and $1g_{9/2}$ orbits, which, even when considering only the lowest levels populated, require a complex set of calculations. Coupled with the complexity of the calculations is the small amount of information available about the isotopes just above this doubly closed shell. The present investigation is intended to help provide information about some of the nuclei outside this doubly closed shell.

In Figure 1, the portion of the Chart of the Nuclides covering this region is shown. When Nurmia and Fink (Nu65) reported the discovery

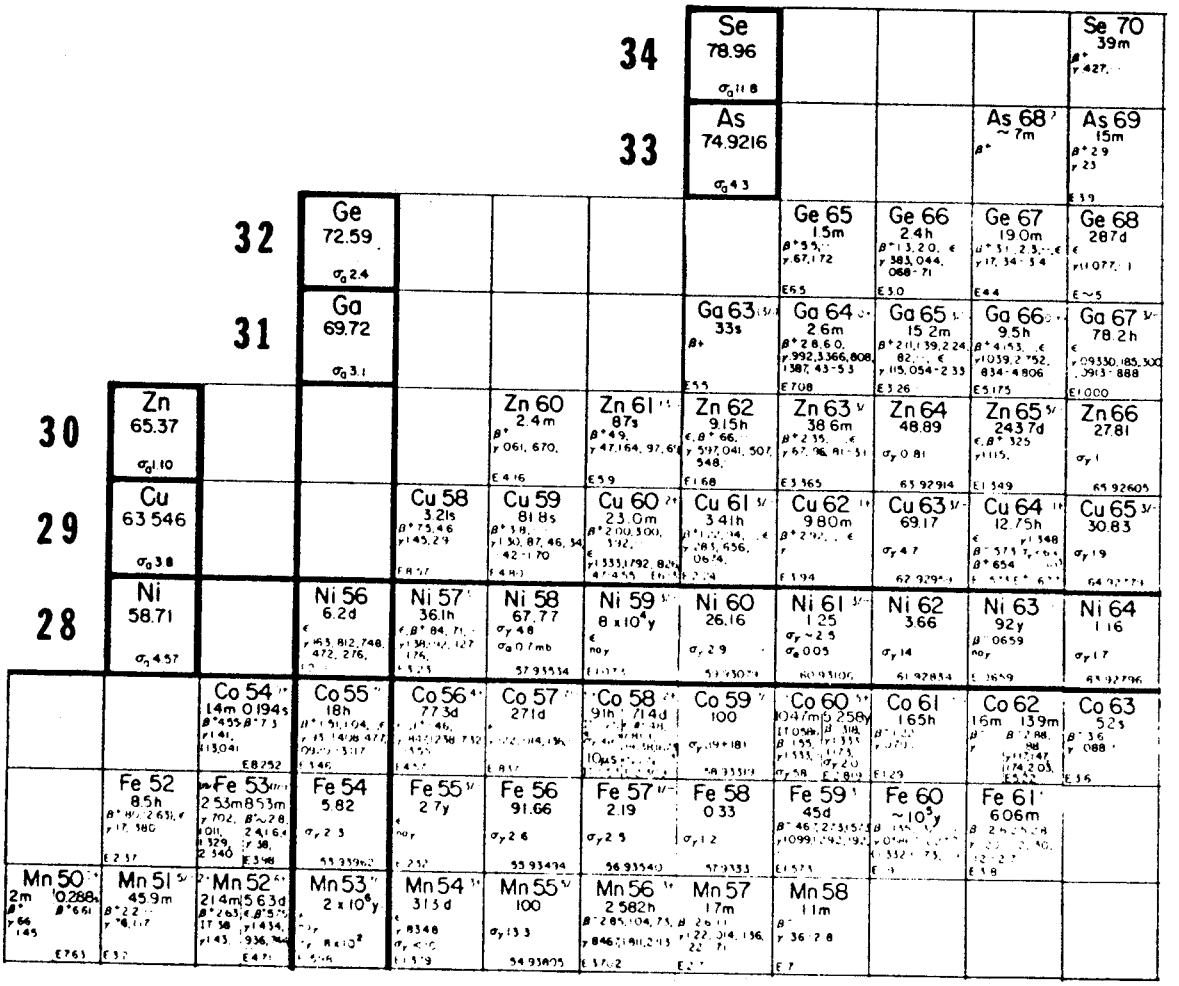

Fig. 1. Portion of the Chart of the Nuclides, including the copper-zinc-gallium region of interest in this thesis. Taken from the Chart of the Nuclides compiled by the Knolls Atomic Power Laboratory, Tenth Edition.

of ^{63}Ga, they mentioned the possibility of β-delayed α emission in this region. According to the calculations of Taagepera and Nurmia (Ta61), ^{63}Ga as well as the lighter Ga isotopes should all be β-delayed α emitters. Nurmia and Fink did not, however, report a decay scheme for the ^{63}Ga. This region of the neutron deficient Zn and Ga isotopes holds strong promise of providing valuable information that can be used for the application of the shell model to this region.

In Chapter II many of the techniques used in the course of this study of both the γ-ray decay and a search for β-delayed α emission in this region are discussed. Included in this chapter is the chemical separation used in the study of the decay of the Zn isotopes.

After the data are obtained, they must be analyzed to obtain the energies and relative intensities. The methods used for this analysis are described in Chapter III. Various computer programs written for or adapted for the XDS Sigma 7 computer at the Michigan State University Cyclotron Laboratory were used to sort the megachannel coincidence data, analyze the many singles spectra, and finally calculate the parameters needed for the final decay schemes.

The Ge(Li)-Ge(Li) megachannel coincidence system discussed in Chapter II has several interesting characteristics that have been studied further. These include the effects of the Compton scattering between detectors and the possibility of using the data obtained from a γ-γ coincidence experiment as γ-sum coincidence data. A study of these characteristics and the results are discussed in Chapter IV.

The results of this study of the neutron deficient Ga and Zn isotopes are described in the following chapters. Several interesting

results that were obtained in the study of ^{63}Zn comprise Chapter V. Chapter VI describes results obtained from a study of ^{62}Zn in a search for γ transitions above 700 keV. The decay of 33 second ^{63}Ga is described in Chapter VII. Chapter VIII presents the results obtained in the search for β delayed α emission in the light Ga isotopes.

Finally, in Chapter IX, these results and their application to this region of light Zn and Ga isotopes are discussed.

CHAPTER II

EXPERIMENTAL APPARATUS AND TECHNIQUES

Each of the isotopes of Zn and Ga studied in this investigation decayed by position emission and electron capture to states in its daughter. The excited states in the daughter in general then decayed by γ emission to the ground state. To study the γ emission and thereby learn about the excited states, many different techniques, both standard ones and newly-developed ones, were utilized. Some of the excited states also have the possibility of decaying by α emission. In order to examine this possibility, some new techniques were utilized to collect the radioactive parent so that this β-delayed α emission could be more precisely studied. This chapter describes the techniques and apparatus used for the data acquisition. Section 2.1. describes the γ-ray spectrometer systems used and the techniques involved in their utilization. In Section 2.2. the α spectrometer and the He jet thermalizer used to prepare the α sources and short-lived γ sources are described. Some of the experiments performed studying the decays of ^{62}Zn and ^{63}Zn required the chemical separation of the Zn from the Cu targets. This separation is described in Section 2.3.

2.1. γ-Ray Spectrometers

With the development of Ge(Li) detectors great interest developed in the examination of new decay schemes as well as many old ones. These decay schemes became more and more refined as Ge(Li) detectors with greater efficiencies and better resolution were developed. In the period of the four years involved in this study, the Ge(Li) γ-ray spectrometers used have gone from one with a resolution of ≈5.6 keV FWHM for the 1332-keV γ of ^{60}Co and an efficiency of <<1% as compared to a 7.6×7.6 cm NaI(Tl) detector with the source 25 cm from the detector to a Ge(Li) detector with a resolution of 2.1 keV FWHM and an efficiency of 10.4%.

The γ-ray spectrometers were not the only instruments to improve greatly over these few years. Many improvements have been added to the amplifiers used with these systems, including such developments as adjustable base-line restoration and pole-zero cancellation. Last but not least, the multichannel analyzers (MCA) have also shown vast improvements in going from a hardwired MCA with 1024 channels and a digitizing rate of 4 MHz to computer interfaced analog-to-digital converters (ADC) with 8192 channels and a digitizing rate of 50 MHz. The preamplifiers improved from room temperature FET's mounted in external units to ones with cooled FET's mounted along with the detector (with a corresponding decrease in noise).

2.1.1. Ge(Li) Singles Spectrometers

A typical γ-ray singles spectrometer system used in this study consisted of a Ge(Li) detector and its bias supply, a charge sensitive FET preamp, a spectroscopy amplifier, an ADC, and some type of memory

storage unit plus its associated readout. Almost all of the electronics equipment are in modular form and are mutually compatible so that equipment from various manufacturers may be used together for a particular experiment.

A variety of different Ge(Li) detectors were used for the experiments in this study. In Table 1 some of the detectors used are listed along with their characteristics. Since each detector is different, the choice of which detector to use for a particular experiment depended on several considerations. Some of them are the relative experimental importance of resolution to efficiency, the count rate involved, and, of course, whether the desired detector is in use for another experiment running concurrently. Another important consideration is whether we possessed the desired detector at the time of the experiment, since the detectors represent the improvements in the state-of-the-art over a period of several years.

The spectroscopy amplifiers which were used contain several features to improve the resolution, especially at higher count rates. Both unipolar and bipolar output pulses shaped with various time constants ranging from 0.25 μsec to 4 μsec can be obtained with various maximum amplitudes of either polarity for use as an input to an ADC or for timing purposes. These amplifiers have highly linear amplification responses and include such features as adjustable pole-zero cancellation, base-line restoration, and DC offset.

The use of pole-zero cancellation permits precise elimination of undershoot on the amplifier pulse after first differentation. This becomes important at higher count rates because succeeding pulses

Table 1. Ge(Li) Detector Characteristics

Manufacturer	Shape	Efficiency[a]	Resolution[b]	Peak to Compton Ratio	Preamp FET
MSU Cyclotron Lab.	Trapezoidal	0.42%	5.6 keV	4.5 to 1	room temperature
Nuclear Diodes	Trapezoidal	2.0%	3.4 keV	8 to 1	room temperature
Nuclear Diodes	Trapezoidal	2.5%	2.2 keV	16.5 to 1	cooled
ORTEC	True Coaxial	3.6%	2.0 keV	22 to 1	room temperature
ORTEC	True Coaxial	4.6%	1.9 keV	24 to 1	room temperature
Nuclear Diodes	True Coaxial	10.4%	2.1 keV	38 to 1	cooled

[a]With respect to the 1332 keV peak of ^{60}Co at 25 cm from a 7.6×7.6-cm NaI(Tl) detector.

[b]FWHM for the 1332 keV peak of ^{60}Co.

may fall into the undershoot and will have an apparent area smaller than the actual area, thus causing a loss in resolution. Base-line restoration also improves resolution at higher count rates by restoring the undershoot of the amplifier signals to a DC base-line after all other shaping has been performed. This improves the resolution by reducing the pileup distortion that is produced when one pulse occurs in the undershoot of another. The DC level adjustment matches the DC level of the amplifier unipolar output to the DC level of the direct input to the ADC. This input bypasses the ADC internal base-line restorer, amplifier, and pulse amplitude discriminator stages, thus lessening the distortion of the input pulse. Also eliminated is the fixed delay (1.25 μsec) added to each pulse to allow time for the discriminators to operate. Eliminating this delay allows a higher count rate for the same ADC dead time.

In this laboratory a variety of analyzers has been used for data acquisition and represents the change in the state-of-the-art over several years. Some of their characteristics are listed in Table 2. With the interfacing of ADC's to a computer, many different modes of data acquisition not available in hardwired analyzers became available. Some of these new modes were used in this study and are discussed in later sections.

2.1.2. Coincidence Spectrometers

Singles experiments are useful in determining the energies and intensities of γ rays from the decay of a nucleus but tell nothing of their placements in the decay scheme. To aid in the placement of these γ transitions, various coincidence experiments were performed.

Table 2. Characteristics of Some ADC's

ADC	Maximum Number of Channels	Digitizing Rate	Memory
Nuclear Data 160	1024	4 MHz	Hard wired
Nuclear Data 2200	4096	16 MHz	Hard wired
Northern Scientific 625	dual 4096	40 MHz	Interfaced to DEC PDP-9
Northern Scientific 629	quadruple 8192	50 MHz	Interfaced to XDS Sigma-7

These include anti-(revealing direct ground state transitions), prompt-(revealing cascade transitions), delayed- (revealing transitions in cascade with states having a measureable lifetime), and 511-511-γ (revealing double escape peaks and β^+-fed levels) coincidence experiments. Descriptions of these techniques are given in the following sections.

2.1.2.A. Ge(Li)-NaI(Tl) Split Annulus Spectrometer

One of the most useful spectrometers at MSU is the 20.3×20.3 cm NaI(Tl) split annulus. Several of its uses in conjunction with a Ge(Li) detector are described by Auble et al. (Au67). In the present study it was used as an anticoincidence spectrometer and a 511-511-γ coincidence spectrometer. Figure 2 gives a block diagram of the electronics used for these experiments.

For the anticoincidence experiment, a 7.6×7.6 cm NaI(Tl) detector was placed inside one end of the annulus tunnel to increase the solid angle subtended by the annulus. A Ge(Li) detector was placed inside the other end of the annulus with the sample between these two detectors, approximately in the center of the annulus. The timing signals from the three NaI(Tl) detectors were combined in an AND/OR gate to produce a timing signal whenever a signal was produced by any of the three NaI(Tl) detectors. An ORTEC universal coincidence unit with the coincidence requirement set to 1 was used for the AND/OR gate. The resolving time control on this unit therefore had no effect. The timing signal from this unit was then required to be in coincidence, within a 110-nsec resolving time, with the timing signal from the Ge(Li)

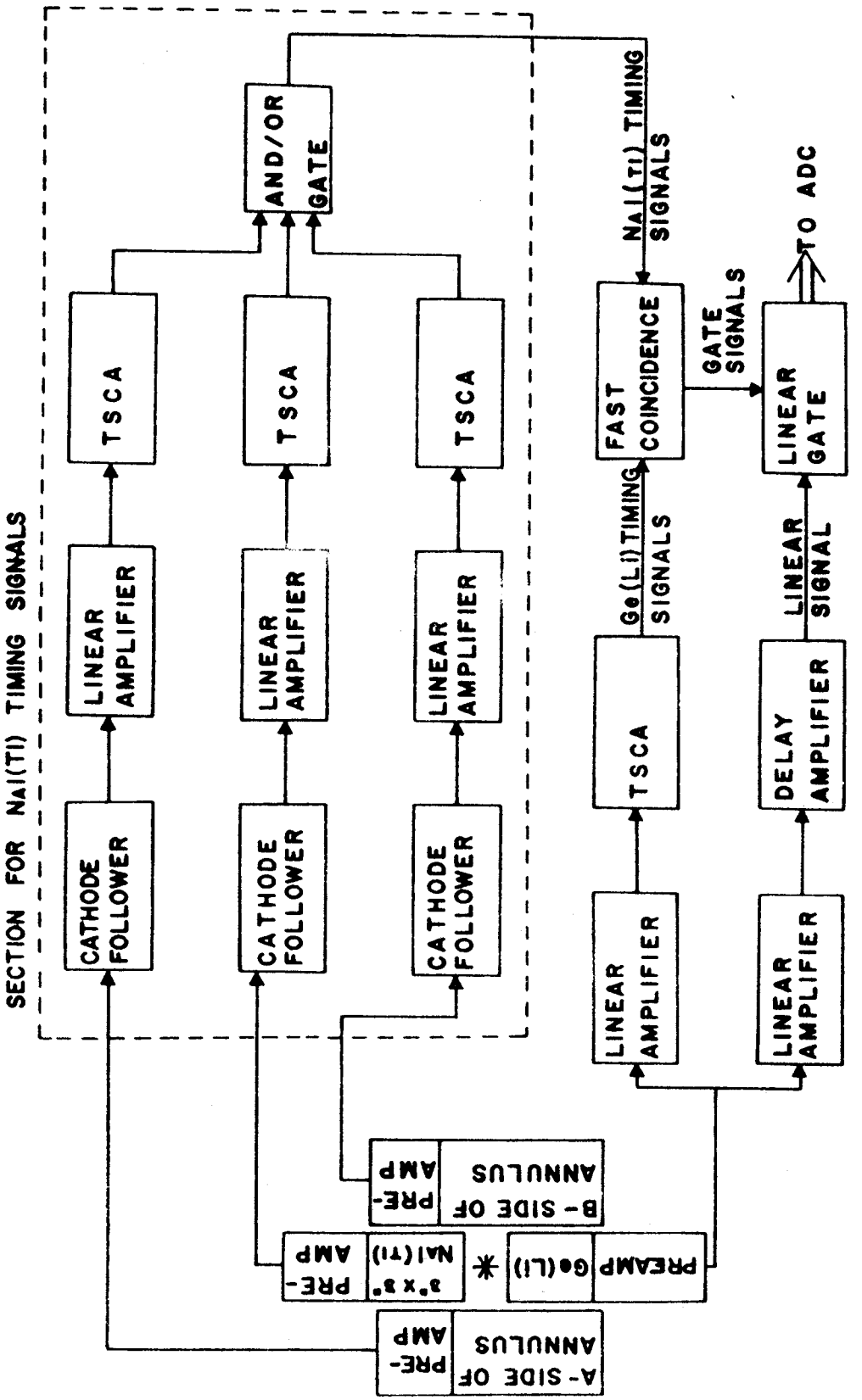

Fig. 2. Experimental setup for recording anti- and 511-511-γ coincidence spectra. For a 511-511-γ coincidence spectrum the TSCA's are adjusted such that the window falls on the 511-keV region and the linear gate is in normal mode. For an anticoincidence spectrum the TSCA's are wide open and the linear gate is in the "anti" mode.

detector. The output from the fast coincidence was used to trigger a linear gate operated in anticoincidence mode.

The 511-511-γ coincidence experiments required the two halves of the annulus to be operated independently with the 7.6×7.6 cm NaI(Tl) detector but with its associated electronics removed from the setup. The TSCA for each annulus half was set to gate on the 511-keV region. A triple coincidence among the annulus halves and the Ge(Li) timing signals was then required. As a result the AND/OR gate was bypassed. These along with operating the linear gate in "normal" mode are the only differences between the two coincidence systems.

2.1.2.B. Ge(Li)-Ge(Li) Megachannel Spectrometer

γ-γ coincidence spectroscopy was first developed in the early 1950's. The coincidence experiment was performed by placing a window on the output of one detector and using this signal to gate the output of the other detector. The result was a one-dimensional spectrum showing everything in coincidence with this window. However, because of the poor resolution of NaI(Tl) detectors, this window was rather wide and allowed coincidences with a wide region of Compton background and with peaks very close to the central peak. As a result it was possible to enhance peaks not in coincidence with the peak of interest.

With the advent of Ge(Li) detectors and their low efficiencies, a NaI(Tl) detector was retained more often than not as the gate detector in a coincidence system. Although the resolution in the resulting one-dimensional spectrum improved, the gate width was still much wider than a photopeak. As Ge(Li) detectors grew in efficiency and improved

in resolution, the use of two Ge(Li) detectors for a coincidence experiment became more feasible. Because of the better peak to Compton ratio, narrower photopeaks, etc., good coincidence data can be obtained with fewer counts per channel with Ge(Li) detectors than necessary with NaI(Tl) detectors! However, using one Ge(Li) detector to gate the other detector still produces only a one dimensional spectrum and requires many experiments to gate on all the peaks of interest. This problem of performing many experiments to obtain a complete set of coincidence spectra can be solved by storing the addresses produced by the ADC's in a list rather than using one to gate the other. This list of stored addresses is later digitally sorted to produce the desired coincidence spectra. With this system only one "mega" two-dimensional coincidence experiment is necessary to obtain the data that formerly took many simple two-dimensional coincidence experiments to obtain.

A system of this type with the code name EVENT was developed by D. Bayer (Ba71) at the MSU Cyclotron Laboratory. Figure 3 shows a block diagram of this system. An absorber was placed between the detectors to reduce the Compton scattering from one detector to the other. A further explanation of this problem is given in Section 4.1. The timing system and linear gates were used to allow only coincident signals from the linear amplifiers to be input to the ADC's. This is necessary since the resolving time of the ADC's is much greater than that of the fast coincidence circuit. The ADC's are operated in synchronous mode so that both would be controlled as one unit rather than as two separate ADC's. They are read through the interface to the XDS Sigma-7 by the task EVENT which runs under the JANUS (Ja69) time sharing monitor system. The

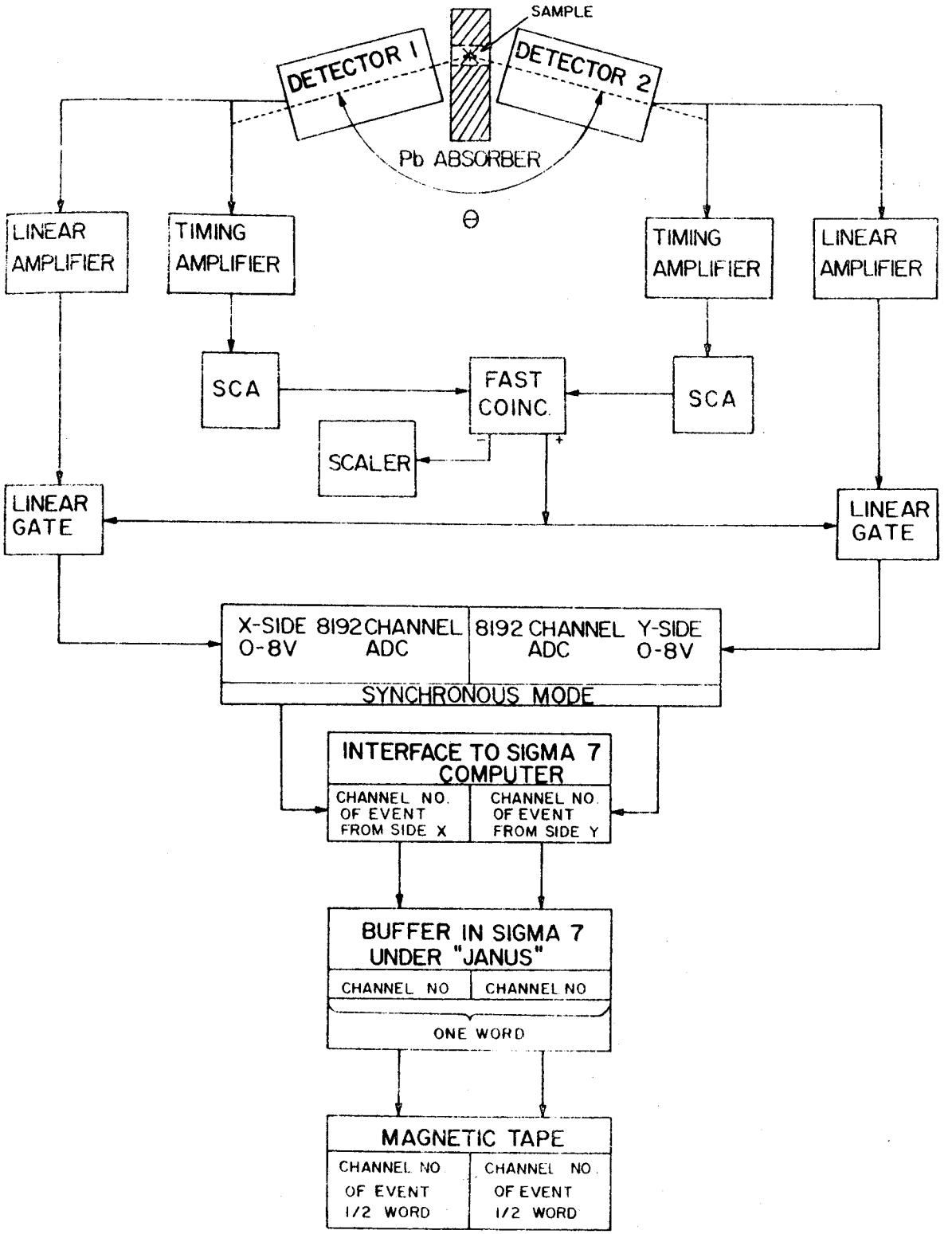

Fig. 3. Block diagram of the megachannel two-dimensional γ-γ coincidence system.

addresses are stored in two halves of a 32-bit computer word, each address in the least significant 13 bits of the half word. As a result, the 3 most significant bits may be used for routing, ADC designation, or some similar purpose. These computer words, each containing a coincidence event, were stored in a 240-word buffer, which when full was written onto magnetic tape while further events were stored in another similar buffer. The tape movement speed of the tape transport limits the system to ≈2000 events per second, although a typical coincidence rate is ≈20 events per second. A 2400-foot, 9-track magnetic tape will hold approximately 1.8 million events written in 60-word records. Recovery of the data written on magnetic tape was performed off-line by the program EVENT RECOVERY, which is described in Section 3.1.

This system allows an n-dimension coincidence experiment with a maximum of 8192 channels per dimension to be performed, since task EVENT is limited only by the number of ADC's available. Currently, four NS-629 ADC's are interfaced to the Sigma 7, thereby limiting the number of dimensions to four. These four ADC's need not necessarily be operated together but can also be operated as two independent two-dimensional coincidence experiments or any combination of single and multiparameter experiments at the same time (dependent only on ADC availability).

2.1.2.C. Ge(Li) - Time Spectrometer

For short-lived isotopes the determination of which γ rays decay with the same half-life becomes difficult. The method of taking many successive spectra during the decay of one or a few samples grows rapidly out of hand for short (less than a few minutes) half-lives because of the poor statistics of each spectrum. The result is a mountain of data which

must be added together to obtain statistically meaningful results.

To solve this problem a modification of a two-dimensional coincidence system was used. A block diagram of the system which is operated by the task TOOTSIE under the JANUS monitor system is shown in Figure 4. One side of the coincidence system is a Ge(Li) spectrometer, while the other side is a gated sawtooth ramp that was obtained from one of two different sources. Initially, SAWTOOTH A of a Textronics oscilloscope was used with its amplitude reduced by a potentiometer. However, the linearity of this source was poor, so it was replaced by an operational amplifier used as an integrator. In both cases, the slope of the ramp was set to reach the maximum ADC input voltage after several half-lives. The slowly rising DC level was converted to a pulse acceptable to the ADC by using an ORTEC linear gate stretcher operated in DC input mode. The output was gated by a TSCA such that both the time pulse and the linear signal were in coincidence. The time scales available from the operational amplifier range from $<<10^{-4}$ sec to $>>10^{4}$ sec.

The task TOOTSIE, written by D. Bayer of the MSU Cyclotron Laboratory and described elsewhere (Ba71), has two operational modes: *Setup* and *Run*. In *Setup* mode the task functions as a two-dimensional analyzer of maximum size 128×128 channels using the seven most significant bits of the ADC's. Bands can be drawn on this two-dimensional array, each band corresponding to a spectrum in *Run* mode. The maximum number of bands depends on the size of the spectra. For example, if a spectrum size of 4096 channels is chosen, five bands are the maximum number allowed. Once the bands are drawn the task can be changed to *Run* mode, in which each band becomes a spectrum of the designated size and the data are then taken as n one-dimensional spectra.

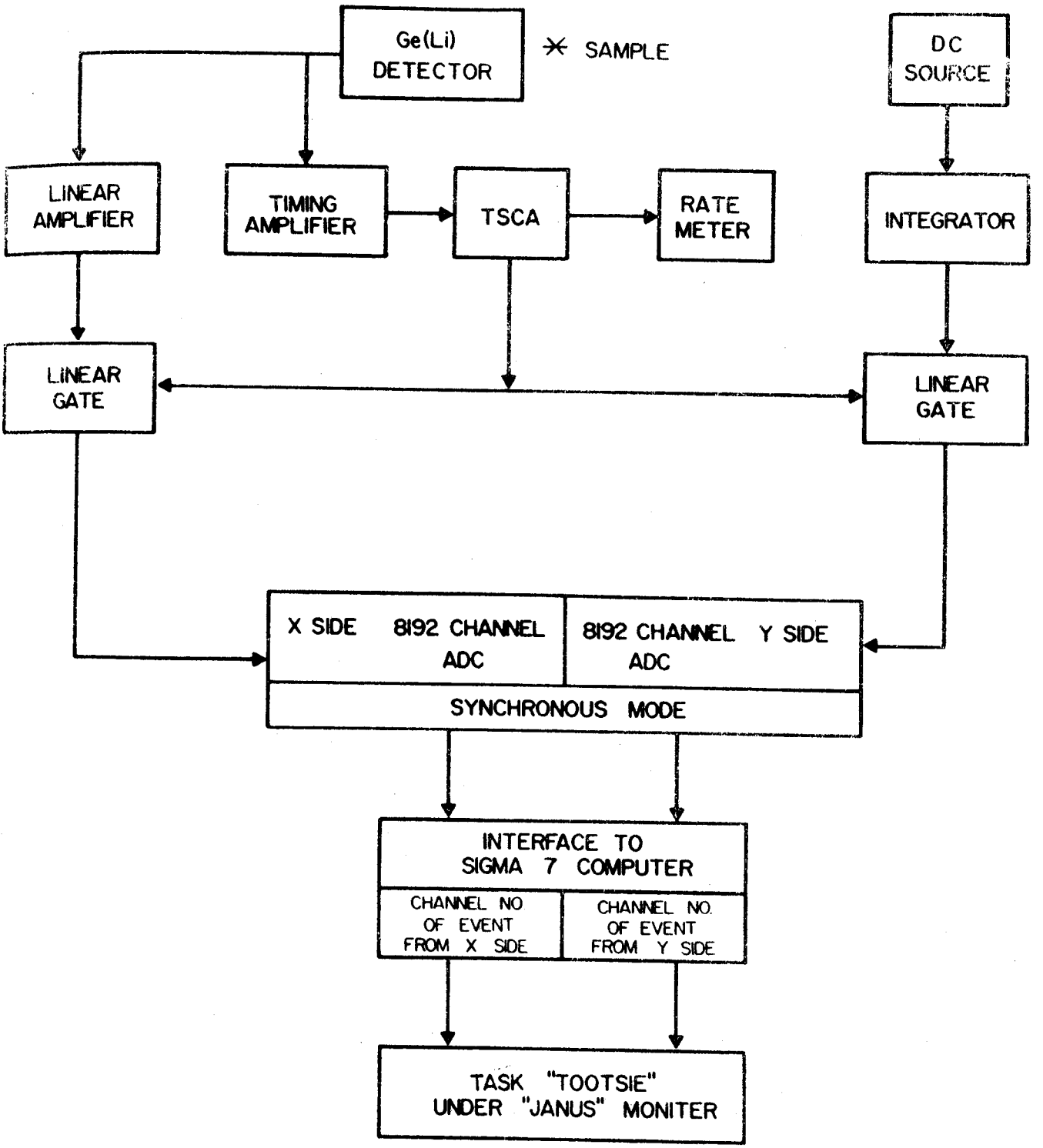

Fig. 4. Block diagram of the γ-time coincidence system.

Figure 5 shows the display produced by TOOTSIE operated in *Setup* mode. The display is a horizontal slice parallel to the energy-time plane, displaying all the locations having counts between the limits specified in the upper left corner. The vertical axis is the time axis and the horizontal axis is the energy axis. The numbers next to the arrows along the axis give the location of the arrows. These arrows are used to locate channel numbers and to define limits for expanding the display.

This display was produced by counting a ^{60}Co source. The solid area on the left portion of the area is the Compton tail with the two lines on the right being the two photopeaks. Discriminator cutoff in the linear gates and ADC's produces the dark areas along the left and lower sides of the display. The horizontal lines represent the lower and upper limits of five bands. The same line may be used as an upper limit of one band and the lower limit of the next band, since each band is defined as the region from the lower limit inclusive up to but not including the upper limit. These bands do not need to be of equal size and the limits can also be curves of any order polynomial up to 10. By using many bands of small size the half-life of the sample can be accurately measured, or by using a few bands of large size the determination of the parent isotope of each γ ray can be made. Operational control of the task and its display is performed by use of both sense switches and teletype input.

In Figure 6 the display of TOOTSIE in *Run* mode is shown. The upper spectrum is the first band and the lower spectrum is the fifth band of the decay of ^{63}Ga. Each spectrum represents a band of about 20 seconds time and has been expanded to show the region from $\simeq$550 keV to

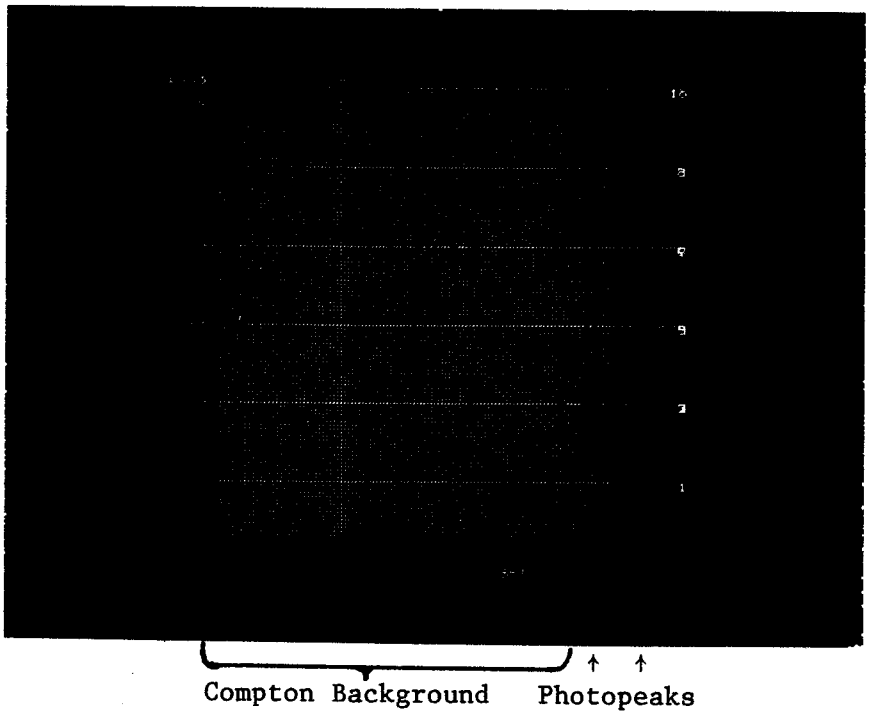

Fig. 5. Display produced by TOOTSIE in *Setup* mode.

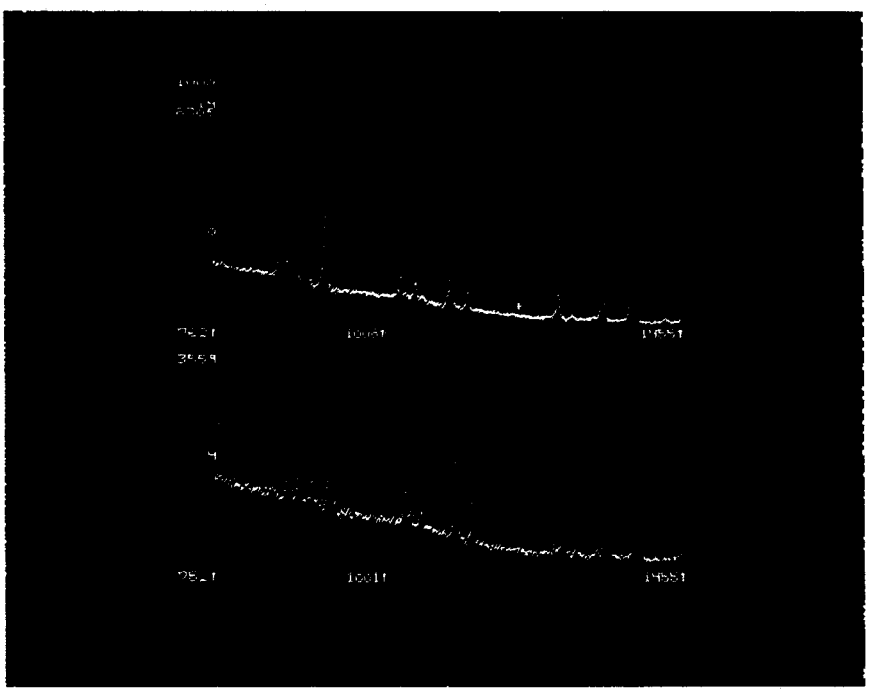

Fig. 6. Display produced by TOOTSIE in *Run* mode.

≈1000 keV. The numbers next to the arrows at each end of a spectrum are the limits of the expanded region. The number of counts in the highest channel of each spectrum is shown in the upper left corner of the spectrum. Below it is the number of the band, the bands being numbered from 0 to n-1, even though the limits in the *Setup* mode are numbered 1 to $2n$. The numbers in the upper left corner are the same as those in *Setup* mode.

2.1.3. Ge(Li) Detector Efficiency Curves

The photopeak efficiencies of Ge(Li) detectors are not constant with energy but generally decrease with increasing γ-ray energy. The exact behavior of this decrease is dependent on many factors such as the total active volume of the crystal, the ratio of depth to width of the active region, and the source to detector distance. Therefore, in order to obtain the relative intensities of the γ-rays emitted from a source, a photopeak efficiency curve for the particular detector and geometry used must be available.

Efficiency curves for the detectors used in the present study were determined by using a set of γ-ray sources, each of which emitted two or more γ-rays whose relative intensities are well known. These sources were chosen to provide data points over the widest energy range possible, and yet, having each source overlapping, at least at one point, with another. This allows the efficiency curves to be bootstrapped to higher and lower energies. A list of the γ-ray relative intensity standards used to obtain the efficiency curves is given in Table 3.

Previous to this work on the efficiency curves, the data were fit to a straight line on a log-log scale. However, systematic deviations

Table 3. γ-Ray Relative Intensity Standards

Isotope (Ref.)	Photon Energy (keV)	Relative Intensity	Isotope (Ref.)	Photon Energy (keV)	Relative Intensity	Isotope (Ref.)	Photon Energy (keV)	Relative Intensity
^{110m}Ag	446.78	3.5	^{56}Co	846.78	100.	^{182}Ta	65.72	30.0
(c)	620.24	2.7	(b)	1037.83	14.0	(a)	67.75	430.
	657.72	100.		1175.13	2.28		84.67	21.8
	677.56	11.5		1238.28	67.6		100.10	119.
	686.83	7.1		1360.22	4.33		113.66	17.7
	706.66	17.2		1771.49	15.7		116.40	4.30
	744.20	4.7		2015.36	3.08		152.44	71.0
	763.88	23.9		2034.92	7.89		156.39	27.2
	818.01	7.7		2598.58	16.9		179.39	31.7
	884.66	78.0		3010.20	1.00		198.30	15.3
	937.47	36.3		3202.30	3.04		222.11	79.8
	1384.22	27.6		3253.60	7.41		229.26	38.0
	1475.74	4.6		3273.25	1.75		264.07	37.6
	1504.91	14.7		3451.55	0.875		927.70	8.00
	1562.23	1.34		3548.05	0.180		959.11	4.40
							1001.66	24.3
^{140}La	109.60	0.22	^{192}Ir	136.35	0.15		1113.18	4.10
(a)	131.15	0.455	(a)	201.20	0.45		1121.19	370.
	241.91	0.555		205.81	3.30		1157.41	11.0
	266.53	0.510		295.94	29.2		1188.95	171.
	328.75	21.6		308.44	30.6		1221.31	289.
	432.54	2.95		316.49	85.8		1230.93	121.
	487.03	46.5		374.40	7.70		1257.34	16.0
	510.95	0.350		416.40	6.90		1273.67	6.90
	751.66	4.50		468.05	50.5		1289.07	14.7
	815.80	24.0		484.55	3.30		1342.60	2.80
	867.87	5.70		489.10	0.510		1373.80	2.40
	919.60	2.50		588.56	4.60		1387.20	0.810
	925.25	6.70		604.40	8.90		1410.00	0.470
	951.02	0.600		612.44	5.48		1453.00	0.330
	1085.30	1.05		884.50	0.170			
	1596.20	96.5				^{133}Ba	53.17	1.95
	2010.40	0.430	^{203}Hg	72	11.9	(a)	79.59	3.04
	2348.20	0.820	(e)	82	3.44		81.01	36.0
	2521.83	3.25		279.2	100.		160.62	0.760
	2547.70	0.090					276.29	7.50
			^{207}Bi	569.62	98.0		302.71	19.6
^{24}Na	1368.53	100.	(a)	1063.65	77.0		355.86	67.0
(a)	2754.14	100.		1770.18	6.4		383.70	9.40

Table 3. - Continued

^{177m}Lu	71.7	7.2	^{152}Eu	121.78	332.	^{160}Tb	86.79	209.
(d)	105.3	100.	(a)	244.70	72.0	(a)	197.04	65.0
	113.0	184.		344.27	314.		215.62	50.0
	128.5	131.		411.05	25.3		298.54	350.
	153.3	144.		443.89	33.0		309.49	11.0
	204.1	117.		688.80	91.0		337.30	5.40
	208.3	512.		778.85	152.		392.43	19.0
	228.4	310.		867.42	51.0		765.20	17.0
	281.8	118.		964.00	173.		879.31	400.
	327.7	152.		1085.80	100.		962.46	140.
	378.5	240.		1112.05	164.		966.17	344.
	413.6	135.		1212.90	17.0		1002.90	16.3
	418.5	172.		1299.20	19.0		1115.16	21.6
	466.0	20.		1407.92	243.		1177.98	206.
							1199.92	33.0
^{57}Co	122.05	85.3	^{46}Sc	889.30	100.		1251.30	1.70
(a)	136.46	8.40	(a)	1120.50	100.		1271.90	103.
							1312.17	40.0
^{60}Co	1173.23	100.	^{88}Y	898.02	92.0			
(a)	1332.51	100.	(a)	1836.13	100.			

(a) Gu69 (b) Ca71 (c) Ha69 (d) Be69a (e) Le66

of the data from a straight line suggested a third order fit of the form,

$$\log (\text{efficiency}) = A + B \log E + C (\log E)^2 + D (\log E)^3,$$

where A, B, C, and D are empirical constants and E is the energy in keV. (Gi69) A computer program was written for fitting the data to this equation. Actually, the data are divided into two overlapping sections, one with energies above ≈400 keV and one with energies below ≈400 keV. A curve for each section is obtained by calculating the curve for one isotope, then for a second isotope, normalizing the two curves for the best overall fit, and finally repeating for as many isotopes as used. The curves for the two sections are then normalized at 400 keV. The final curves are good to about 3% for energies greater than 400 keV, about 5% for 100 keV to 400 keV, and about 20% below 100 keV. The increasing error results from the fewer points available, the rapid drop in efficiency, and the increasing complexity of the function at lower energies.

The efficiency curve for our 10.4% Ge(Li) detector for a source at 10 inches is shown in Figure 7. This curve is for the detector without any absorbers. The shape of the curve can be changed, enhancing a particular energy region, by a judicious choice of absorbers. This is further described in Section 6.1.

2.2. β-Delayed α-Emission Spectrometer

In order to examine the possible β-delayed α emission of the Ga isotopes, a different system of sample preparation and counting was required. Because of the short range of α particles, the sample needed to be counted in a vacuum and preferably from a massless target. Also the short half-lives of the isotopes studied precluded any manual handling

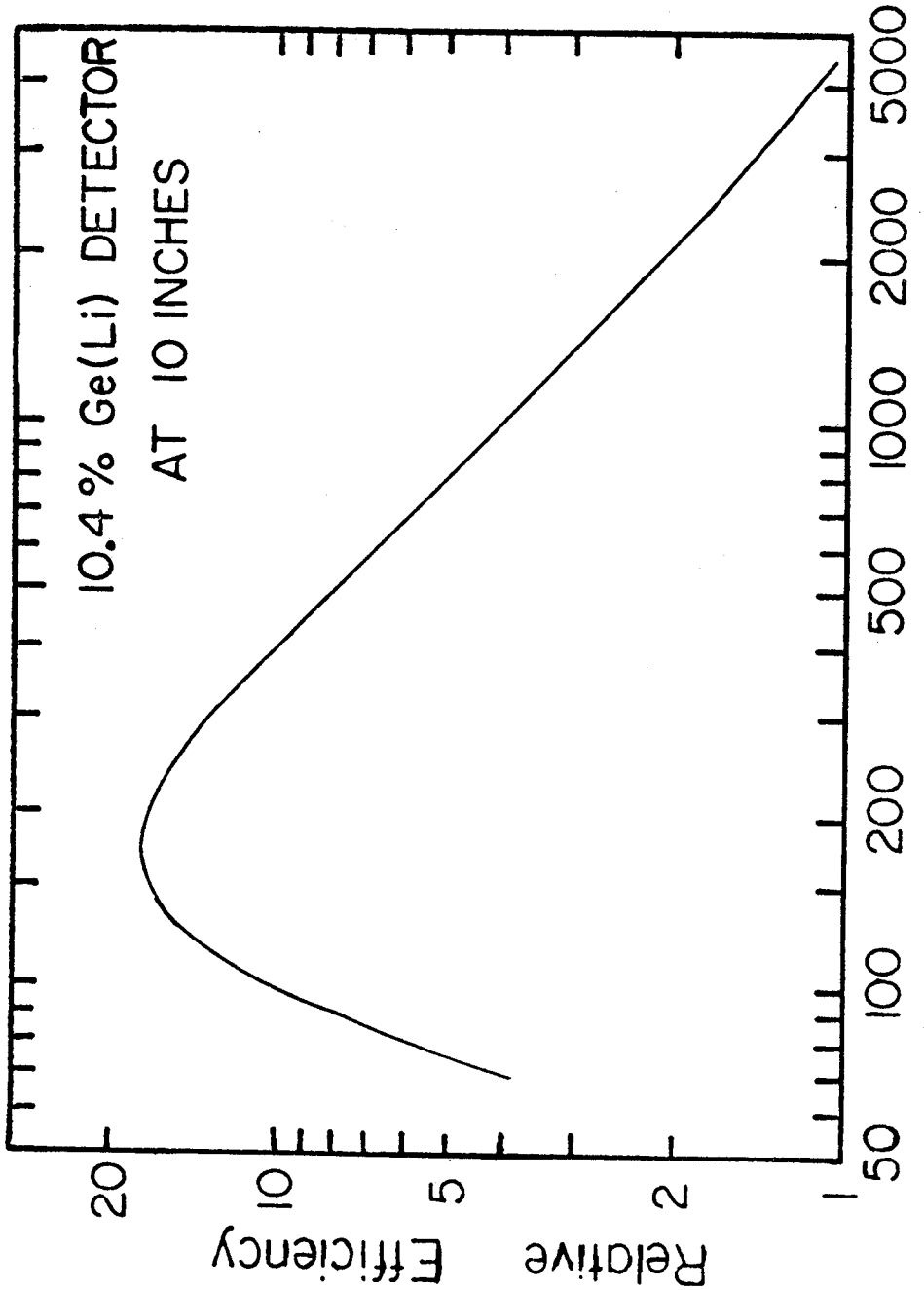

Fig. 7. Relative photopeak efficiency curve for the 10.4% efficient detector with the sources placed 10 inches in front of the detector.

of the samples. The He-jet thermalizer was utilized to transport the activated nuclei from the vicinity of activation to another location in vacuum. This eliminated the possibility of any prompt α's from the target being counted as well as produced a "massless" source for α particle counting. Any α particles were then counted using Si(Li) surface barrier detectors.

2.2.1. α-Particle Spectrometer

The α-particle used in this study consisted of a Si(Li) surface barrier detector and its bias supply, a charge sensitive FET preamplifier, a spectroscopy amplifier, an ADC, and some type of memory storage unit plus its associated readout. The Si(Li) barrier detectors used for the experiments were obtained from ORTEC. They had an active area of about 25 mm^2 and a sensitive thickness of about 100 microns. Their resolution for the 5.545-MeV α particles of ^{241}Am was about 16 keV. For these experiments the detectors were used with ORTEC model 125 preamplifiers. The rest of the spectrometer system utilized the same equipment as the γ-ray spectrometers described in Section 2.1.1.

2.2.2. He-Jet Thermalizer

In order to determine the existence of β-delayed α emission, a system was needed to transport the activated nuclei quickly into a vacuum chamber in a suitable form to count the α particles. This becomes rather difficult, since the half-lives of the nuclei under investigation were expected to be on the order of 1 second or less. A He-jet thermalizer built by K. Kosanke (Ko70) at the MSU Cyclotron Laboratory was utilized for this purpose. The system thermalizes the

recoils produced by the interactions of the cyclotron beam with the target in ≈1-2 atmospheres pressure of He. These recoils are collected with the He into a polyethylene capillary and transported at sonic velocities to the counting chamber. In the counting chamber, which is at $\approx 10^{-2}$ torr pressure, the He flow exiting the capillary diverges much more rapidly than the heavier recoils, thus allowing them to be collected on a surface placed near the exit of the capillary. This produces a "massless" source for counting with an α detector.

Figure 8 shows a view of the thermalizer box. The cyclotron beam enters from the left and passes through a water cooled collimator. Mounted to the rear of the collimator are several teflon blocks containing an ≈1" ϕ hole. The target foil is placed between the collimator and the first teflon block and if more targets are used, they are placed between the teflon blocks. The recoils are collected by He entering the rear of the teflon blocks and being drawn past the targets into the capillary which is placed in the first teflon block. The beam is stopped in the water-cooled Faraday cup to the right of the collection assembly, while the capillary exits through the rear of the box.

The recoil counting chamber is shown in Figure 9. The capillary enters the chamber through a port in lower right side of the figure. A Si(Li) surface barrier detector is in the cooled mounting and is connected to the coaxial cable connected to one of the feedthroughs in the upper right. A collector is placed between the detector and the port facing it. The port may be fitted with a thin plate so that the sample may be counted simultaneously with a Ge(Li) γ-ray

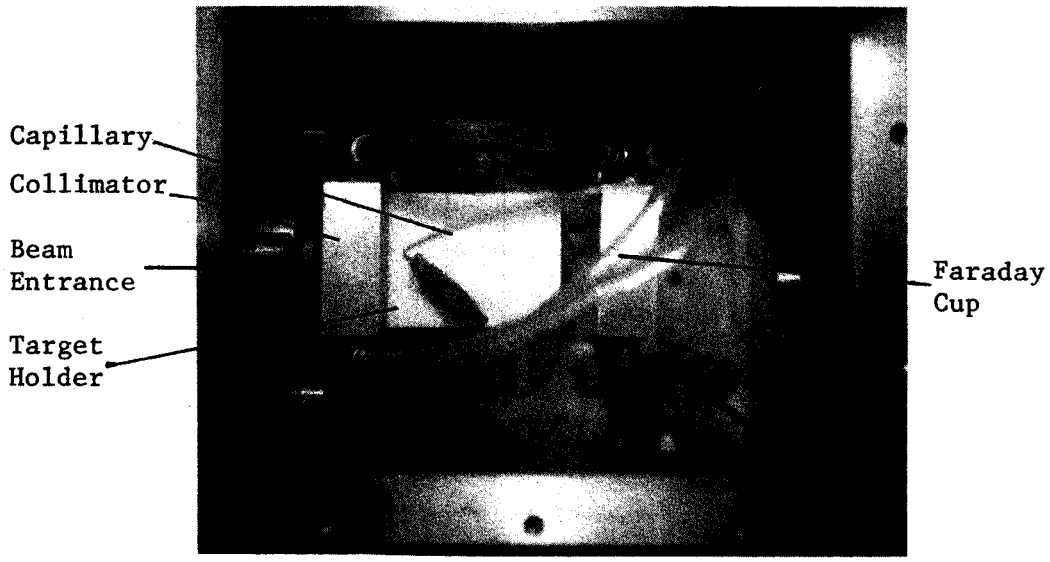

Fig. 8. Recoil thermalizer showing target holder-collector and Faraday cup.

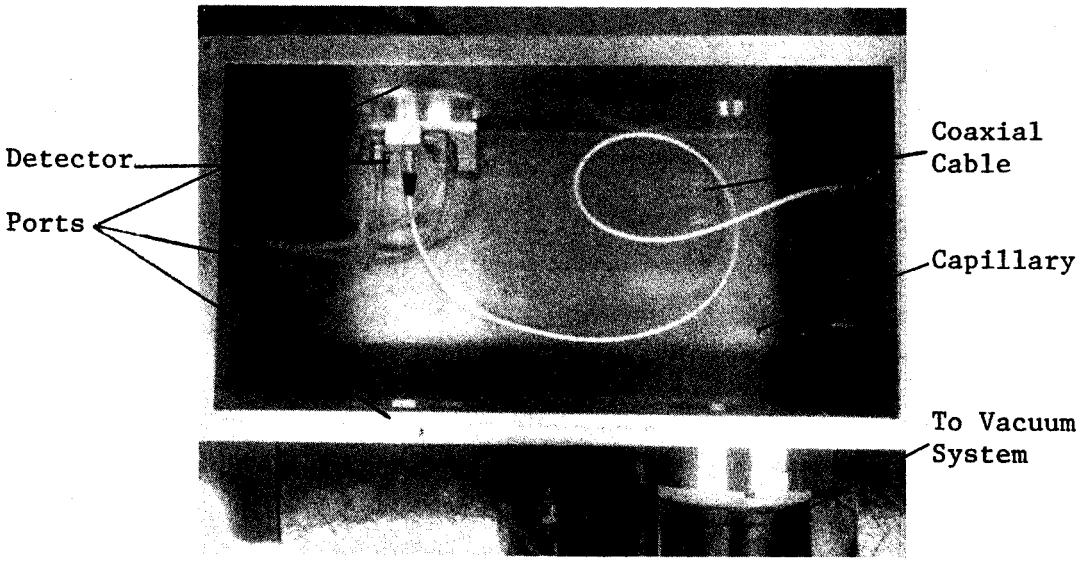

Fig. 9. Recoil counting chamber showing capillary and detector in cooled mount.

detector. The chamber is evacuated through the pipe located in the lower right corner.

2.3. Cu-Zn Chemical Separation

Some of the experiments using Cu targets required a chemical separation to insure that only the Zn isotopes produced and their daughters were present. Because of the 38.4-min half-life of ^{63}Zn, long involved procedures could not be used. The method utilized was found to be somewhat rapid, very simple, and efficient as compared to other methods.

A 1"×1"×0.01" target was dissolved in a solution containing 5 ml 30% H_2O_2, 10 ml 6*N* HCl, and 1 meq Zn^{++} carrier. The solution was evaporated to dryness and the residue taken up in a minimum volume of 2*N* HCl. This solution was then eluted through a column of Dowex 1×8 50-100 mesh anion-exchange resin that had been previously washed with 2*N* HCl. Following this eluent, the column was washed with 2*N* HCl until no trace of Cu could be observed. The resin was removed from the column, dried, and mounted for counting.

Chapter III

DATA ANALYSIS

Data analysis played a very important part in the development of the final decay schemes. Several programs have been used at MSU for the analysis of γ-ray singles and coincidence spectra. One program was used to sort through the data tapes from a megachannel coincidence experiment to produce several types of coincidence results. Some of the other programs were used to determine the energies and relative areas of the photopeaks observed. These results were then used by another program to determine the relative intensities of the γ-ray transitions. Finally, these results were used in the computation of the necessary values used in a decay scheme. Section 3.1. describes the program EVENT RECOVERY, which is utilized to sort through the multimillion coincidence events to obtain the desired coincidence spectra. The programs utilized for γ-ray energy and area determination are described in Section 3.2. In Section 3.3. the program which performed many of the decay scheme calculations is described.

3.1. EVENT RECOVERY Program

In Section 2.1.2.B. the task EVENT which was used to store the data from megachannel coincidence experiments was described. In the several years EVENT has been in use, several changes have been made in it. Some of the changes involved the three most significant bits of each data half word. Initially these bits were unused, but now they are used to designate the ADC producing the data address or to produce routing information. Also, the coincidence data may be used for γ-sum coincidence experiments as well as γ-γ coincidence experiments. Since task EVENT only stores the data, another program was therefore necessary to sort or recover the data in the desired modes. The program utilized for this sorting is called EVENT RECOVERY.

Since all the coincidence data are stored on magnetic tape without gating limitations, all the gating must be done by the recovery program. In order to perform this most efficiently, the program is a FORTRAN main routine, with most of the sorting being performed by a SYMBOL machine language subroutine. In this way, the data addresses may be stored in internal registers instead of core memory, thereby increasing greatly the rate of sorting the data. Basically, the program takes the two addresses of the coincidence event, places a digital gate on one address, and increments the location specified by the other address only if the first address falls within the digital gate.

However, in order to perform this gating, many items of information must be evaluated. For each gate to be performed, EVENT RECOVERY reads one control card, with a limit of ten control cards per pass of the data tapes. The limit results from the core size of the Sigma 7 and

the amount of swapping of core pages involved. A flow scheme of this program is shown in Figure 10. After reading the control cards for a pass of the data tapes, the program starts reading the tapes. If the end of a tape is encountered while reading, the program then determines if more data tapes are to be read. If no tapes are left to be read, the data are punched out and more control cards are read. If there are tapes left to be read, the program calls for new tape and then continues reading data when the tape is mounted. When an event is read, the sum of the two addresses is computed and stored in a register for later use. With the two addresses and the sum address stored in registers, the program now checks the parameters on each control card: which of the three axes, x, y, or *sum*, is to be displayed, whether there are any limitations on the *sum* address, and which axis if any is to be gated. If the gated axis address falls within the background limits, a weighted amount is subtracted from the display spectrum, whereas if the gated axis address fall within the peak limits, the address in the display spectrum is incremented by one count. This process is repeated for this coincidence event until all the control cards have been checked. When all the cards have been checked, the process is repeated for each succeeded coincidence event until the last tape has been read. A complete listing of this program is found in the Appendix *A*. A four-dimensional version of this program is being developed for experiments using more than two parameters, such as γ-γ resolving time experiments.

3.2. γ-Ray Energy and Intensity Determination

The centroids and areas of the photopeaks in a spectrum were found by subtracting various order interpolated backgrounds from the

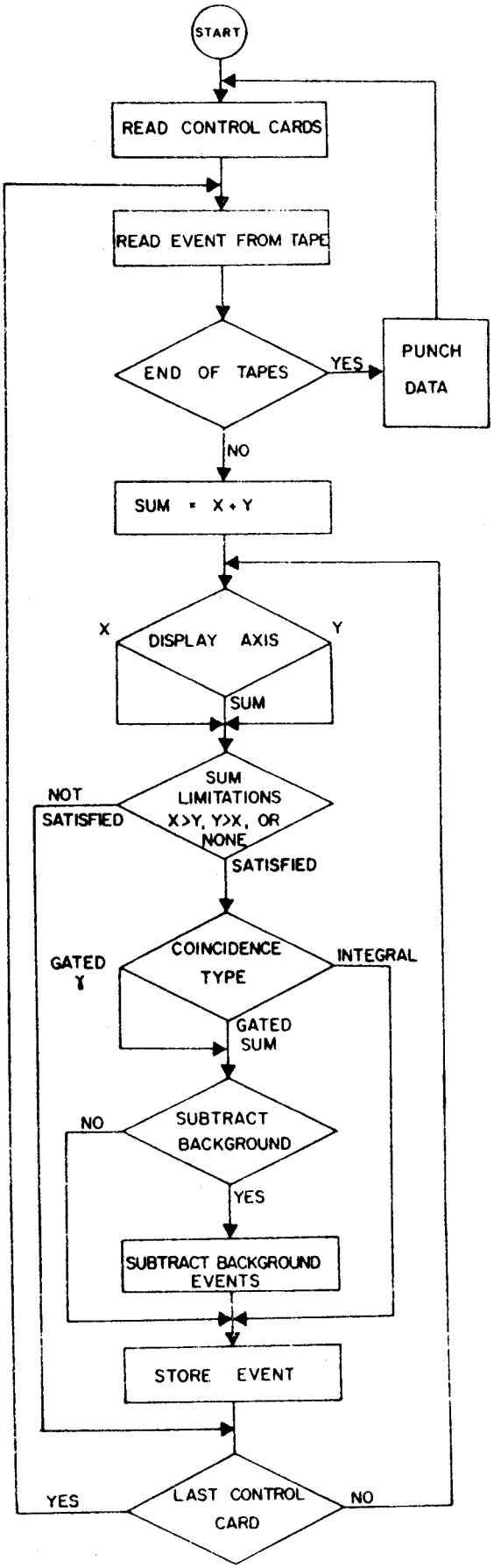

Fig. 10. Flow diagram of EVENT RECOVERY program.

data. These computations were performed with the aid of two spectrum analysis routines used at the MSU Cyclotron Laboratory: MOIRAE and SAMPO.

3.2.1. MOIRAE Spectrum Analysis Routine

MOIRAE is a machine language task under the JANUS monitor that utilizes a Fairchild 737A live-display oscilloscope and sense switches to perform the spectrum analysis. MOIRAE was developed by R. Au and G. Berzens at the MSU Cyclotron Laboratory. A modified version of this task called MOD7 was developed by D. Bayer, also at the Cyclotron Laboratory. The primary difference between the two is that MOD7 utilizes a Textronics 611 storage oscilloscope for its display. The following description will be of MOIRAE but for the most part applies also to MOD7. The primary purpose of MOD7 is to alleviate the large amount of computer time used to drive the live display.

All the analysis performed by MOIRAE is controlled by instructions to the computer via interfaced sense switches arranged below the display oscilloscope as shown in Figure 11. Once the data have been read in from the card reader or transferred from a data acquisition task, the switches control the type of display, log or linear, expansion and shifting of the axes, various computational routines, and the outputs of the results. Figure 12 shows a closeup of the switches with labels for the routines they control.

A display of the ≈1300 keV to ≈1500 keV region of the ^{63}Zn spectrum is shown in Figure 13. The information across the top of the display gives the number of counts in and the channel location of the long pointer, the run number, the subroutine presently in use, and the order, up through 9th, of the background fit being used. If a log display had been used instead of this linear display, the number of cycles

Fig. 11. MOIRAE display oscilloscope and sense switches.

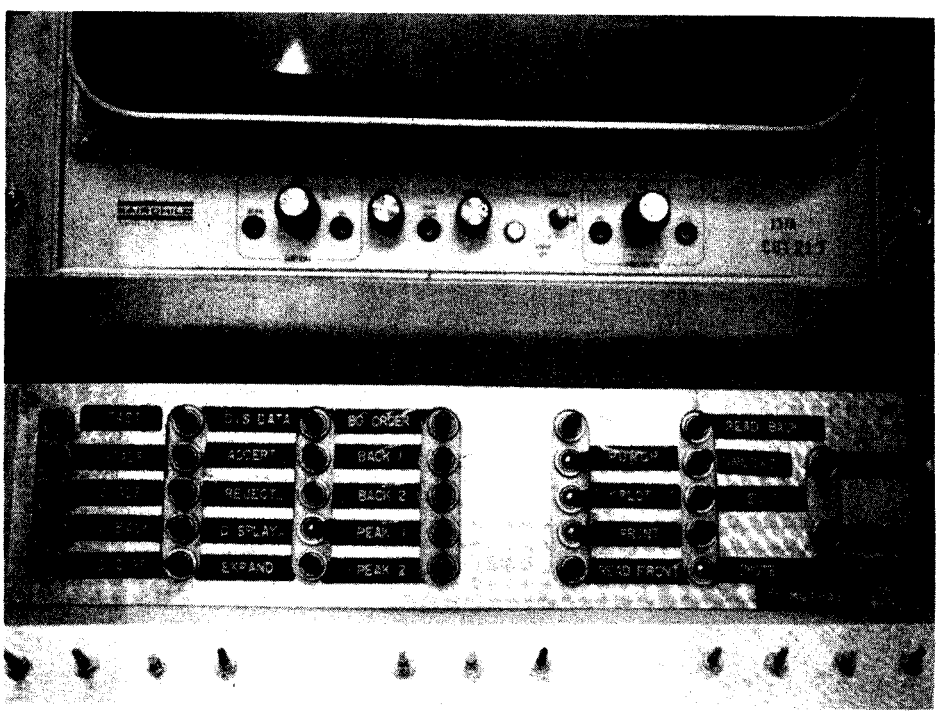

Fig. 12. Closeup of MOIRAE sense switches.

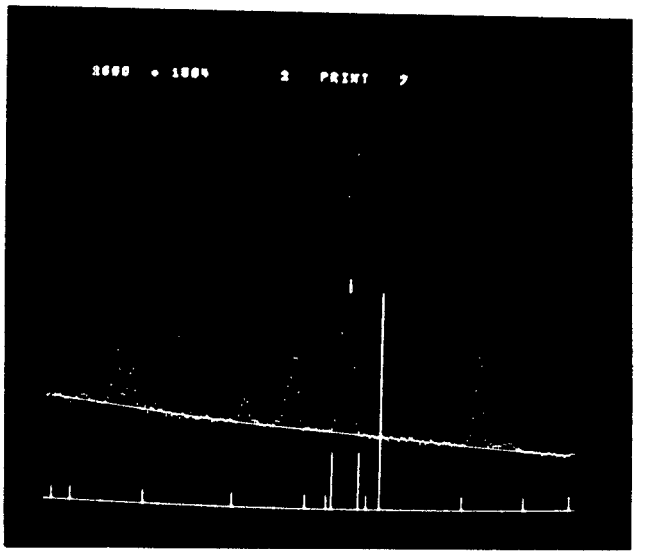

Fig. 13. MOIRAE oscilloscope display of a portion of the ^{63}Zn γ-ray spectrum with a seventh order background fit.

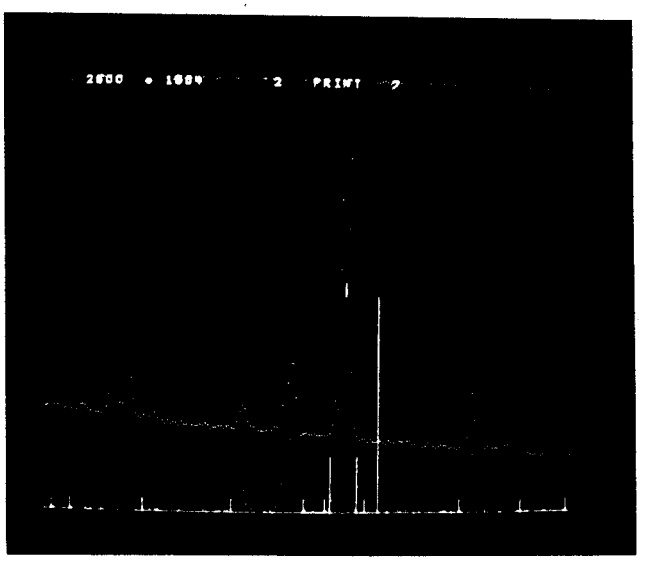

Fig. 14. Display of peaks after calculated seventh order background has been subtracted.

would be displayed to the left of the run number. The background displayed with the data was determined by fitting all the points between each pair of short lines (BACK 2) inclusive to a 7th order polynomial. The sense switches were used to move the tall pointer to the position of the points used for the limits of the background regions, with the short lines indicating the points that have been accepted. Instead of using several regions for the fitting of the background, a set of individual points (BACK 1) may be used.

The two tall lines indicate the points selected as the limits of the 1412-keV peak, with the short mark indicating the centroid of the peak. Either the full raw peak (PEAK 1) or the portion of the peak with counts greater than one-third the maximum (PEAK 2) may be used to calculate the centroid. In both cases the task then finds the centroid, area, sum of the raw data and background, and the square root of that sum. This information may be punched on cards, printed, and/or plotted on a Calcomp plotter. Figure 14 displays the difference between the background and the data displayed in Figure 13 in addition to the data. The points at the top of the display indicate those channels with fewer counts than the fitted background.

In order to convert the centroids and areas produced by MOIRAE into energies and relative intensities, the program MOIRAE $E(I)$ is used. This FORTRAN program written by myself and D. Beery uses the card output from MOIRAE for its data. The centroids of several strong γ-rays in the spectrum are used to perform a least-squares fit to a quadratic energy calibration curve. This curve is then used to calculate the energies of all the peaks in the spectrum. Using these energies and a detector

efficiency curve calculated by the method described in Section 2.4., the relative area for each peak is calculated. The energies and relative intensities as well as all the input information are then printed. A listing of this program is found in Appendix *B*.

The advantages of MOIRAE include the immediate operator control over such parameters as background order, background points, and intervals and peak end points. This control is especially helpful for regions with complex or unusual background such as Compton edges. The disadvantages also become rather obvious. One is its inability to strip unresolved peak multiplets. Since no standard peak shape is used, another strong disadvantage is that, although the operator has visual control of the analysis, the analysis of one γ-ray spectrum may take 2 to 3 hours.

Some of the disadvantages of MOIRAE are also of the subjective type. Because the determination of the background and the peak limits are under operator control, the choice of what background order and what collection of data points produce a good background fit can be difficult. Also, the choice of how large a region to fit the background over and then what peak limits to use may be very difficult to make, especially if the peak has tailing. For an ideal peak of high intensity situated on a smooth background, a good low order fit is easy. However, for several closely spaced peaks, a peak on a Compton edge, or a peak in a region of poor background, what is the best background? In general, an ideal fit would be a linear background approximation; however, it seems reasonable that any single polynomial curve may be used as long as the background is fit smoothly and approximates the desired background shape

under each of the peaks included in the interval. A change in the background shape changes the peak control only slightly while producing a much larger effect on the area.

3.2.2. SAMPO Spectrum Analysis Routine

SAMPO is a FORTRAN program written and modified by J. Routti and S. Prussin (Ro69) at the University of California, Berkeley, and modified for use on the MSU XDS Sigma 7 by C. Morgan. It can be controlled either via storage scope sense switches and teletype or by FORTRAN control cards. This program utilizes the photopeak method analysis, with each experimental peak being fit to a Gaussian function having exponential tails. The mathematical evaluation involves initial shape calibrations using strong well-resolved peaks well-spaced over the region to be analyzed. The shape parameters are stored and a linear interpolation is used to obtain the parameters for any other peaks under consideration. Once the shape parameters have been calculated for a given spectrum, for subsequent runs they may be reread directly into the program from FORTRAN control cards, thereby saving computational time. After a shape calibration has been established, an energy calibration curve using these and/or other peaks may be calculated at the operator's discretion either by linear interpolation or by a linear or higher order least-squares polynomial fit. Similarly, efficiency calibrations may be performed using a number of well-spaced peaks and their relative efficiencies.

The analysis by SAMPO of the data may be performed in two modes, "automatic" or "manual". In "automatic" mode, SAMPO searches out all the statistically meaningful peaks based on the calculated shape parameters, evaluates suitable fitting intervals, and fits the peaks

using the shape, energy, and efficiency calibration data. For peaks that fall below the minimum statistical limit for the automatic search, for multiplets that are not clearly resolved, or for any other peaks or regions of interest the manual mode may be used. In this mode, the fitting intervals and the peak locations are input and the program then fits these peaks similarly to the automatic mode. The program may operate entirely in manual mode if desired.

Figure 15 shows a portion of the program's output for the 1392-keV doublet from ^{63}Zn decay. The plot displays the data, the calculated fit, and the calculated background. Above the plot are the upper and lower limits of the plot, and below the plot is the legend. The channel number, standard deviation of the difference between the data and the calculated fit, and the calculated background are printed to the left of the plot, while the data and calculated fit are found at the right. Below the plot is given the sum of the difference between the data and the calculated background and the sum of the difference between the calculated fit and the calculated background. For each peak fit, the program returns the centroid and its error, the energy and the error due to the calibration curve and the overall error, the fit peak area and its error, the fit peak relative intensity, the error due to the efficiency curve, and the total error.

Since its inclusion into the data analysis program in this laboratory, SAMPO has proven invaluable in the time saved stripping multiplets. An example of its ability to strip multiplets including unresolved ones is shown in Figure 15. The deviation from the average energy over three separate ^{63}Zn runs was less than 0.4 keV for the

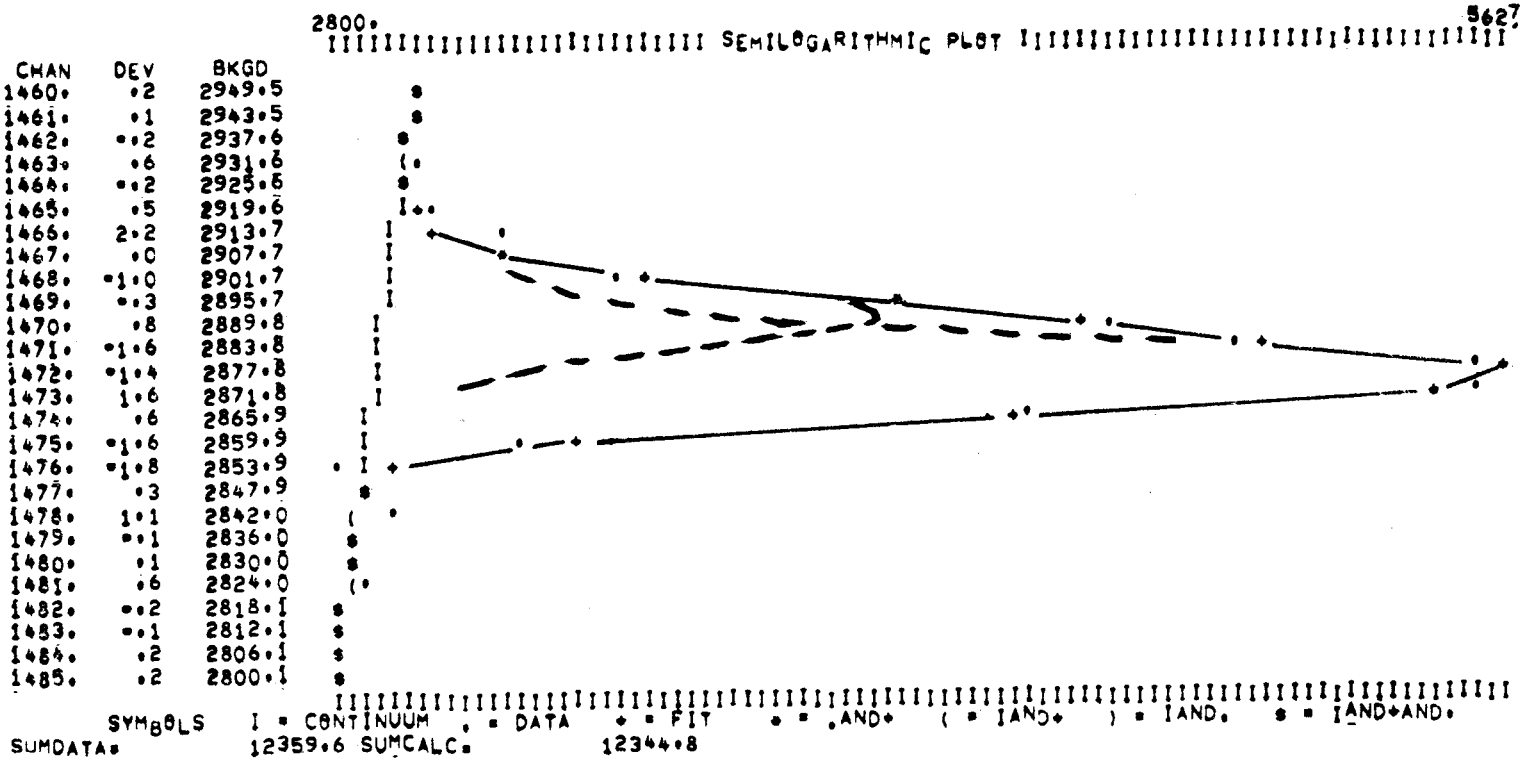

RESULTS FROM THE ABOVE FIT, BE CRITICAL WITH THE ERROR ESTIMATES
REJECT IF CHISQUARE = 22.2079 OR SIGMA = 1.081 IS UNACCEPTABLE, CHECK PLOT FOR MISSING PEAKS

PEAK CHANNEL	FIT-ERROR (CHAN)	ENERGY (KEV)	CALIB-ERR (KEV)	ENERGY-ERR (KEV)	PEAK AREA (COUNTS)	FIT-ERR (PCT)	INTENSITY (COUNTS)	CALIB-ERR (PCT)	INT-ERR (PCT)
1469.6960	.0815	1389.6333	.1950	.2108	3177.6	4.7974	3177.6	.0000	4.7974
1472.4519	.0034	1392.3391	.1956	.1956	9165.1	1.7305	9165.1	.0000	1.7305

Fig. 15. Photograph of line printer output of spectrum analysis routine SAMPO showing its fit of the 1389-1392-keV doublet from ^{63}Zn decay. Lines have been drawn to show the doublet and its individual components.

1389.5 keV peak and less than 0.25 keV for the 1392.3 keV peak, while the deviation from the average intensity for the 1389.5 keV peak was less than 10% and the stronger 1392.3 keV was less than 6%. In general, the range of values for the energy and especially the intensity of a peak from several runs is less for SAMPO than for MOIRAE.

Another advantage of SAMPO is the relative amount of time necessary to obtain results. Much less time is involved in using SAMPO even if many regions have to be fitted in manual mode than in a MOIRAE analysis. In return for these advantages, SAMPO has some disadvantages that might require fitting many peaks in manual mode. Primary among these is the low order (2nd) background fit and the associated small limits of the fitting region. The result of this is very poor background fits in regions of poor statistics or near Compton edges, requiring these peaks to be refit in manual mode.

SAMPO may be operated with and controlled by a storage oscilloscope and sense switches. This allows the user an opportunity to examine each fit before it is finalized. If the fit is not good, the limits of the region may be changed or perhaps the number of peaks to fit and their centroids may be changed; however, the background remains the second order fit. While this produces better fits to the data, this procedure also consumes more of the user's time, thus returning to the disadvantages of MOIRAE.

3.2.3. γ-Ray Energy and Intensity Calculation

After several sets of data have been analyzed by the methods described above, the results must be evaluated to obtain the final γ-ray energies and intensities. The γ-ray energies were calculated by SAMPO or MOIRAE $E(I)$ by a least-squares quadratic calibration equation

using the centroids of well-known standard γ rays and then computing the energies of "unknown" γ rays from their centroids and the standard curve. These calibration curves were computed from "internal" energy calibration spectra taken by simultaneously counting the unknown and standard calibration sources. The energies of the weaker peaks were then calculated by using the strong, calibrated peaks as internal secondary standards for computing the energy calibration curve. The final results in this work were obtained by averaging the results from 3 to 6 runs for each isotope.

Choosing the standard calibration sources is an important factor in the γ-ray energy calibration. Ideally, the standards are chosen to "bracket" the unknown peaks closely and contain only the γ rays used in the calibration, since a spectral distribution may obscure photons of interest. This, however, must be tempered with the need for many good calibration points in order to establish a reliable calibration curve.

The γ-ray relative efficiencies were calculated by using detector efficiency curves for the energy range from $\approx$100 to $\approx$3000 keV. These efficiency curves were produced using the program DETECTOR EFFICIENCY described in Section 2.1.3. and were incorporated into the program MOIRAE $E(I)$ described in Section 3.2.1. In this work, the relative areas from 3 to 6 runs for each isotope were averaged and then the final relative intensities were calculated from these areas using the program MOIRAE $E(I)$.

3.3. Decay Scheme Construction

A nuclear decay scheme represents one result of the investigation of a radioactive nucleus. Placing the γ transition in a

consistent decay scheme may be a difficult process, since as the number of interlevel transitions and the number of states increases the more complex the decay scheme becomes. With the aid of sums of γ-ray energies and the results of anti-, megachannel, prompt, delayed, and 511-511-γ coincidence experiments, the placement of these transitions becomes easier. In addition, the results from charged particle reactions and particle-γ excitation experiments may provide a good level scheme in which to place transitions. However, since each decay is different, some of these methods may not be able to be used. Even with the help of these aids, the process still requires much inspiration and perspiration.

Once a tentative decay scheme has been determined, many parameters are still to be evaluated. Using the total β decay energy and the relative β feedings to each level as determined by the relative intensity feeding to and from each level, the log ft for the β transition to each level can be calculated using the values calculated by several authors (Mo51, Br55, Zw54, Wa59), and collected in reference (Le66). Since this becomes tedious if many levels are present, a program was written by D. Beery (Be69) to perform these calculations. This program, DECAY SCHEME, uses the values from the tables and performs the many repetitive operations required to obtain the log ft for the β transition to each level.

The spin and parities of these levels may be assigned with the aid of several factors. The various selection rules governing β and γ decay often limit the spin to a few values integrally spaced and also somewhat limit the parity assignment. In addition, the results of charged particle reactions and γ-ray angular correlation experiments narrow these assignments often to only one value for spin and parity.

the higher the energy of the excited state, the less available the data and the wider the limits on spin and parity assignments.

With the placing of spin and parity assignments, the long task of producing a nuclear decay scheme is completed. With this completion, however, the difficult and rewarding task of interpreting the results is only beginning.

CHAPTER IV

EXTENSIONS OF Ge(Li)-Ge(Li) MEGACHANNEL COINCIDENCE SYSTEM

The Ge(Li)-Ge(Li) megachannel coincidence system described in Section 2.1.2.B. has been used at this laboratory to study various decay schemes. In the course of these experiments, unexpected peaks were observed. After examining these (misshaped) peaks, it was determined that they occurred from Compton scattered γ rays from one detector being observed in the other detector. The γ-γ coincidence results also provided a system with which to reexamine the γ-sum coincidence experiments and their results. In Section 4.1. the results of the examination of Compton scattering in a Ge(Li)-Ge(Li) coincidence system are presented. In section 4.2. the results of the γ-sum coincidence system are described and its possibilities are discussed.

4.1. Compton Scattering Problems In Ge(Li)-Ge(Li) Coincidence Gamma-Ray Spectrometers (Gi71)

In γ-γ coincidence spectrometry Compton scattering is often regarded as a benign nuisance, its worst effects being a wasteful increase in the number of spurious coincident events and an effective obscuring of the weaker peaks. When the gate and full-energy peak widths approach each other in magnitude, however, more insidious effects can set in, such as the generation of "artificial full-energy peaks". Thus, in the days when NaI(Tl)-NaI(Tl) coincidence spectrometers were standard, a number of such false γ rays found their way into the literature and a number of precautionary papers appeared to discuss ways of recognizing and avoiding such effects (Be55).

With the advent of Ge(Li) detectors with their low efficiencies, a NaI(Tl) detector was retained more often than not as the gate detector in a coincidence system, and, because now the gates were much wider than even the widest photopeaks, such problems largely disappeared. But now that larger Ge(Li) detectors are available and Ge(Li)-Ge(Li) coincidence spectrometers are coming into general use, misleading Compton-generated γ rays are again making their appearance. The problem is especially acute for experiments with short-lived radioactivities for which repeated bombardments and/or source preparations are required in order to accumulate enough data to make the results statistically significant. The highest count rates possible are desired to minimize the number of necessary bombardments, and this often leads to the use of close 180° geometry, which is very efficient but somewhat unfavorable with respect to Compton scattering.

The basic problem that can arise from the ability to gate on a region only a few keV wide in a Ge(Li)-Ge(Li) coincidence experiment is quite simple in concept. Each tiny region in a Compton distribution from one detector has a one-to-one correspondence, both with respect to energy and with respect to angle, with a specific region in the Compton distribution resulting from scattering from that detector into a second detector. And, at a fixed angle, if the gate from the first detector be made small enough, the corresponding coincident region from the second detector could also be quite small or narrow, narrow to the point of having the width of full-energy peak. In a simple spectrum these are easy to spot, but in a complex spectrum one may confuse them with full-energy peaks if he is not wary of them. In some instances the spurious peaks may well fall at the very same energies as a real γ ray itself. Herein lies perhaps the greatest danger of all, for one could easily be misled by false coincidence results into placing the γ ray into an incorrect position in a decay scheme. Thus, when we found ourselves on the verge of coming up with such "new" full-energy peaks in the ^{63}Zn experiment, we decided to make a thorough study of the effects of Compton scattering and narrow gates. This section describes the interesting results and the methods that can be used to suppress these unwanted additions to the coincidence spectrum.

4.1.1. Experimental Apparatus

Sources were counted with the megachannel coincidence system described in Section 2.1.2.B. utilizing the 2.5% efficient and 2.0% efficient Ge(Li) detectors.

Figure 16 shows the relative positioning of the detectors. Since both detectors were mounted on right-angle dipstick cryostats, it was possible to adjust their relative angular positions to almost any angle. For some of the experiments a 1.27-cm thick graded Pb collimator was placed between the detectors. A small biconical hole, ≈0.64-cmϕ, was drilled in an absorber and the source was placed at the center of this hole so that γ rays from the source itself would not be absorbed. The source was normally placed such that it was 3.8±0.2 cm from each detector and on a line with the axis of each detector. The various angles were measured from detector axis to detector axis, with the collimator, if used, bisecting the angle as closely as possible.

4.1.2. ^{63}Zn Results: A Complex Spectrum

In Figure 17 a portion of the spectra obtained from a two-dimensional γ-γ coincidence experiment on 38-min ^{63}Zn is shown. The detector angle was 150° and an absorber was placed between the detectors but only up to the source. The integral or "any" coincidence spectra taken with the 2.5% and 2.0% detectors are shown at the top in parts *A* and *D*, respectively. In these the various gates have been denoted. The only remarks that need be made here about the decay scheme are that the intense 669.71- and 962.14-keV γ's are ground state transitions from the first and second excited stated in ^{63}Cu and that the weak 449.8-keV γ feeds the second excited state. Further results are given in Chapter 5 of this thesis.

As part of the examination of the coincidence data, a very narrow gate as indicated by the bar *B* was set on the weak 449.8-keV peak, and the result is shown in part *B*. Since the 962.14-keV peak is

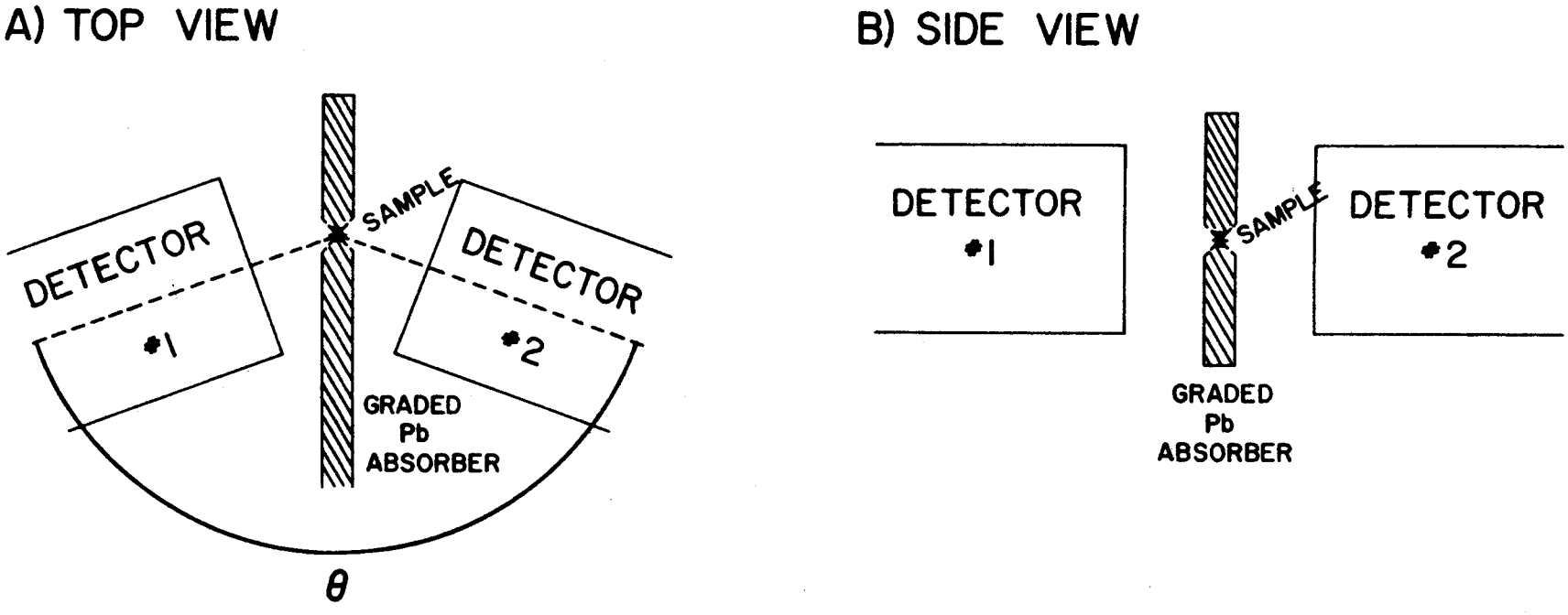

Fig. 16. Relative positioning of the Ge(Li) detectors for the Compton scattering coincidence experiments.

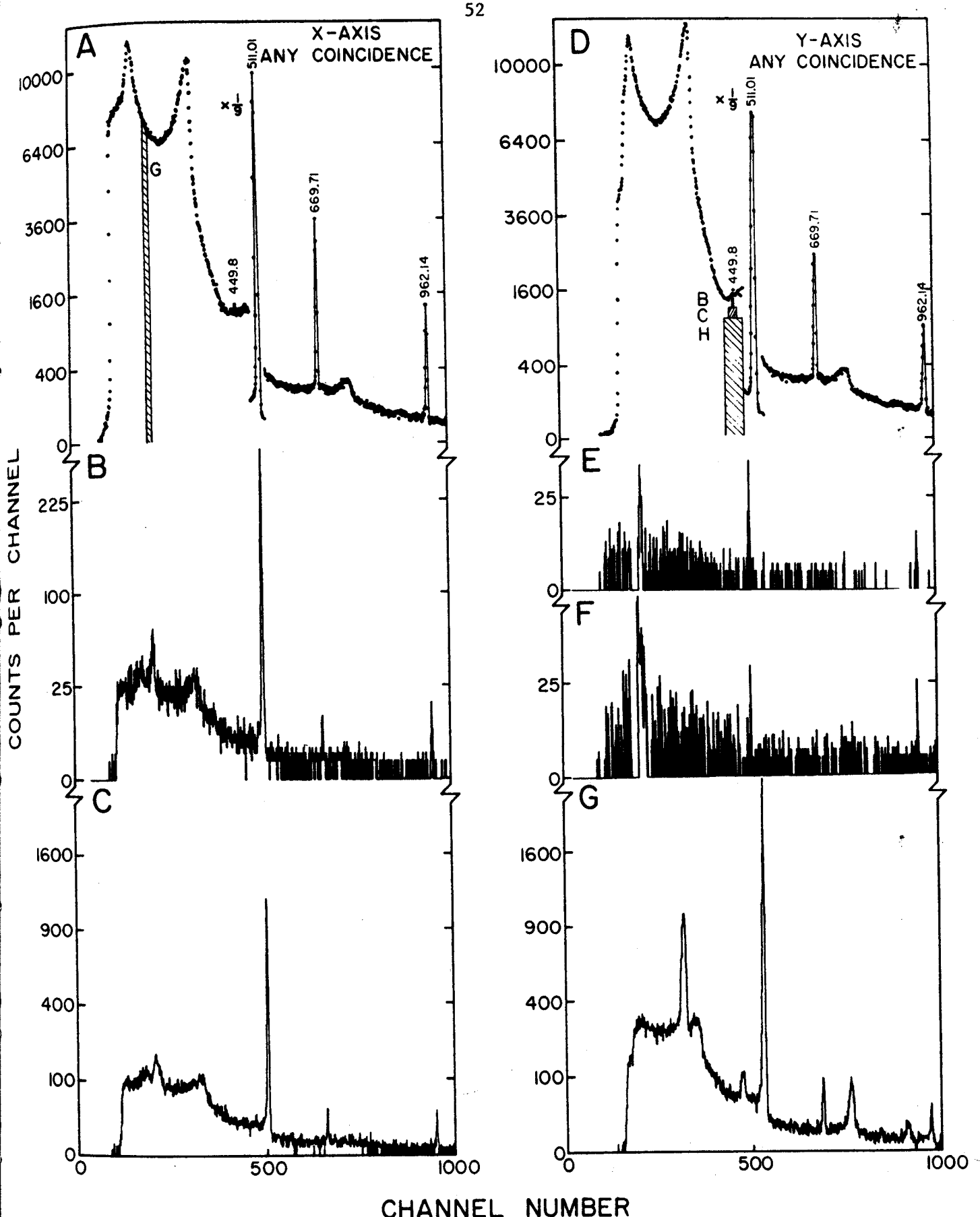

Fig. 17. Coincidence spectra for ^{63}Zn. The integral coincidence spectra are shown in *A* and *D*. Gates were set on the spectrum in *D* as indicated by the bars, with *E* and *F*, same as *B* and *C* except that the background indicated by bar *H* has been subtracted. Spectrum *G* was produced by gating on the spurious "220-keV" peak.

more intense in this spectrum than the 669.71-keV peak but is much weaker in the singles and any coincidence spectra, the 962.14-keV γ is shown to be in coincidence with the 449.8-keV γ. A new peak also appears at 220 keV. There was never any sign of this peak in the singles spectra, so further gates were used.

Part *C* shows the results of a gate on the 449.8-keV peak with a width four times that of *B*. Here the entire spectrum increases in intensity, but the peak at 220 keV has also increased greatly in width and is now much wider than the three known photopeaks.

In parts *E* and *F* the results of background subtraction are shown. The background used was the region denoted by the bar *H* but excluding the regions in gates *B* and *C*, respectively. Region *H* is 50 keV wide and centered on the 449.8-keV peak. In spectra *E* and *F* the 669.71-keV peak has disappeared, confirming our previous conclusion, but the $\gamma^{\pm}$ and 962.14-keV peaks are weakly though definitely present. The 220-keV "peak", however, has increased greatly with respect to these and the regions on either side of it have gone to zero. This shows clearly that the Compton distribution in the gates was not only in coincidence with other regions of the spectrum in general, but also with this region in particular.

By gating on the 220-keV "peak", as shown in spectrum *G*, new peaks appear at 290, 740, 895, and 1180 keV in addition to the one at 450 keV. These energies are 220 keV less than the strong $\gamma^{\pm}$, 669.71-, 962.14-, 1115- (^{65}Zn contaminant), and 1414.1-keV peaks, corresponding to Compton-scattered γ rays from one detector being captured in the other detector.

4.1.3. Angular Dependence

In order to insure that the effects observed came strictly from Compton scattering between the detectors, further studies were performed with a ^{137}Cs source.

The effects of variations in the angle between the detectors on Compton scattering can be seen in Figure 18. The full-energy chance-coincidence peak is noticeably narrower than the large Compton edge and backscatter peaks. As the detectors are moved from 90° geometry toward the unfavorable 180° geometry, the increase in the Compton edge and backscatter peaks is very apparent, indicating that the primary direction of the Compton-scattered photons is back toward the source of the incident radiation. Table 4 gives the total, chance, and true coincidence rates.

Calculations of these angular effects are well known. With E_γ as the energy of the incoming photon, E'_γ that of the scattered photon, E_0 the electron rest energy, and θ the scattering angle of the photon, one obtains

$$E_o \left(\frac{E_\gamma - E'_\gamma}{E'_\gamma} \right) = 1 - \cos \theta$$

which has a maximum at $\theta = 180°$; E'_γ is related to E_γ and E_o by

$$E'_\gamma = \frac{E_o E_\gamma}{2E_\gamma + E_o} .$$

For ^{137}Cs, $E'_\gamma = 184.4$ keV, which is the energy of the backscatter peak observed at all angles; in these close geometries the angular

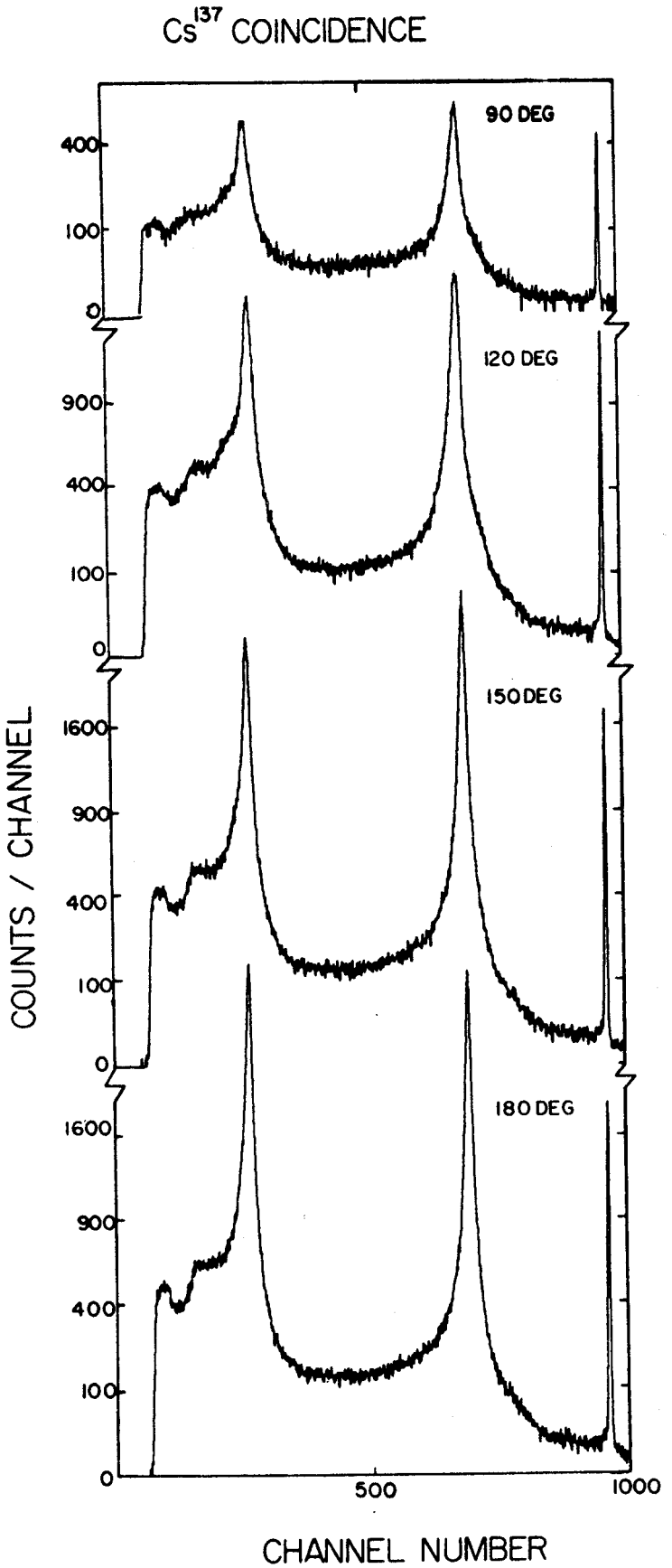

Fig. 18. ^{137}Cs Compton-scattering coincidence spectra showing the effects of the angle between detectors.

Table 4

^{137}Cs Coincidence Counting Rates as a Function of Detector Angle and Absorber Usage.

Angle	Absorber	Total cps	Random cps ($R_1 R_2 \tau$)	Net cps
90°	no	2.74	2.55	0.19
90°	yes	1.51	1.33	0.18
120°	no	9.84	1.85	7.99
150°	no	10.95	2.21	8.74
180°	no	12.08	1.61	10.47
180°	yes	3.21	2.45	0.76

acceptance of the detectors is large enough to wash out most of the predicted angular dependence.

When a graded Pb collimator, as shown in Figure 16, is placed between the detectors, we see the effects illustrated in Figure 19. At 90° the huge Compton edge and backscatter peaks have been almost removed. At 180°, while not removed, they have been decreased to an almost reasonable level. This points up the fact that such collimators are all but essential for serious Ge(Li)-Ge(Li) coincidence experiments, but even they cannot insure completely valid results at close 180° geometry. These results are also included in Table 4.

4.1.4. Gate Widths

Figure 20 shows the effects of varying gate width on the coincident backscatter and Compton edge peaks. The display spectrum (from the 2.5% detector) is shown in part *A*, while the gates (from the 2.0% detector) are shown in part *F*. In parts *B* through *E* the effects of the various widths of gates on the backscatter peaks are shown. The gates correspond to the regions denoted in part *F*. For the narrowest gate (in *B*) the Compton edge peak is about twice the width of the photopeak, and by decreasing the gate width even further, it could undoubtedly be made the same width as the photopeak. As the gate width is increased, the Compton edge peak broadens somewhat but does not increase in height. This is rather graphic evidence for the one-to-one correspondence between portions of the spectra resulting from Compton scattering between detectors.

A similar effect is seen by gating on the Compton edge and looking at the resulting spectra, *G* through *J*. Notice the dip that

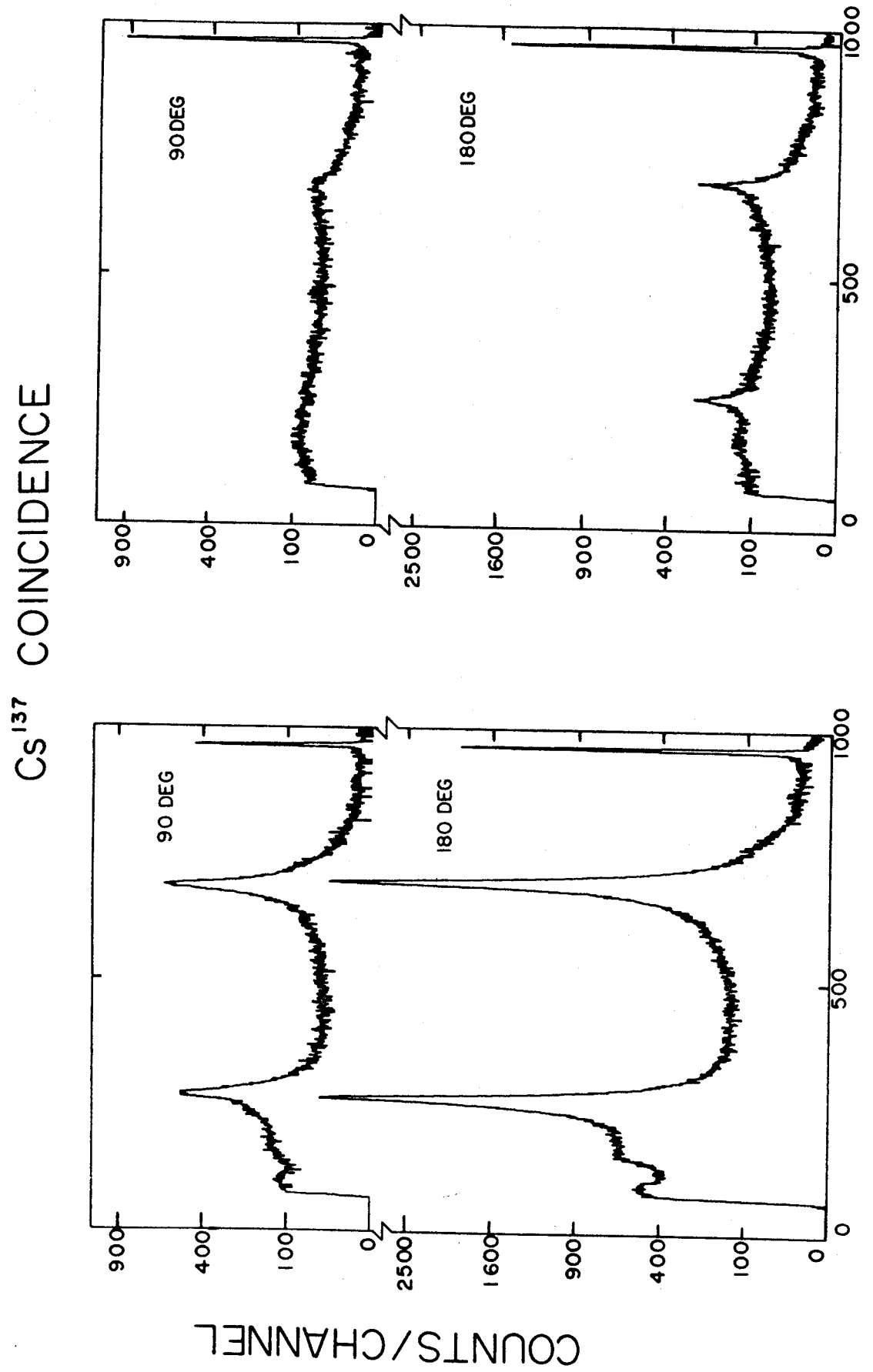

Fig. 19. ^{137}Cs Compton scattering coincidence spectra showing the effects of placing an absorber between the detectors. The spectra on the left were taken without an absorber; those on the right, with a 1.27-cm thick graded Pb absorber placed as shown in Fig. 16.

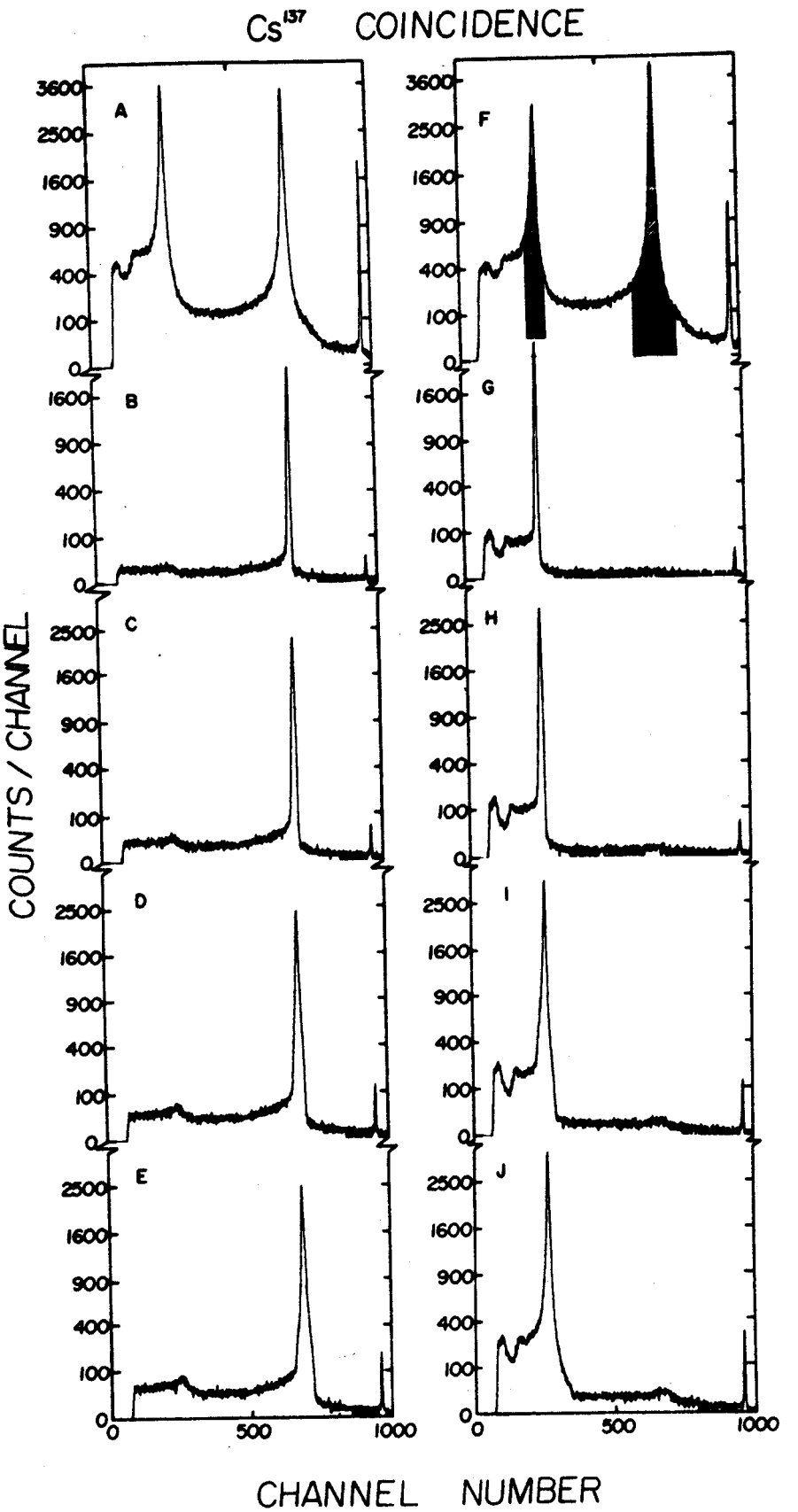

Fig. 20. ^{137}Cs Compton-scattering coincidence spectra showing the effects of varying gate width. The two integral coincidence spectra are shown at the top in *A* and *F*, and the gate widths are indicated in *F*.

appears in the spectrum below the backscatter peak. This is discussed in the next section, where gates are applied on different regions of the Compton distribution.

In Figure 21 a plot of the full width at half and tenth maximum vs the gate width is shown. Gating on the backscatter peak and on the Compton edge produced identical results, so both are included in the points on the graph.

The flattening out of the FWHM curve could be reproduced fairly well by a very simple calculation. Two Gaussian-shaped peaks were used, a wider one for the gate (G) and a narrower one for the displayed peak (P), this because customarily (but not always) one gates on the spectrum with the poorer resolution. For these Gaussians the experimental FWHM for our two detectors as found from the worst integral coincidence spectrum, the one at 180° with no absorber, were used.

Each channel in G then corresponded to a complete peak P, the amplitude depending on the height of the channel in G. Thus, a particular gate width in G was represented by a sum of peaks P having shifted centroids and differing amplitudes. The results showed that, for this idealized case, the limiting value of the FWHM is twice that of the display peak in its integral coincidence spectrum. This limiting value is reached at a gate width twice that of the FWHM of G, the same as was found experimentally in Figure 21. However, the calculated limiting value is about half that observed experimentally.

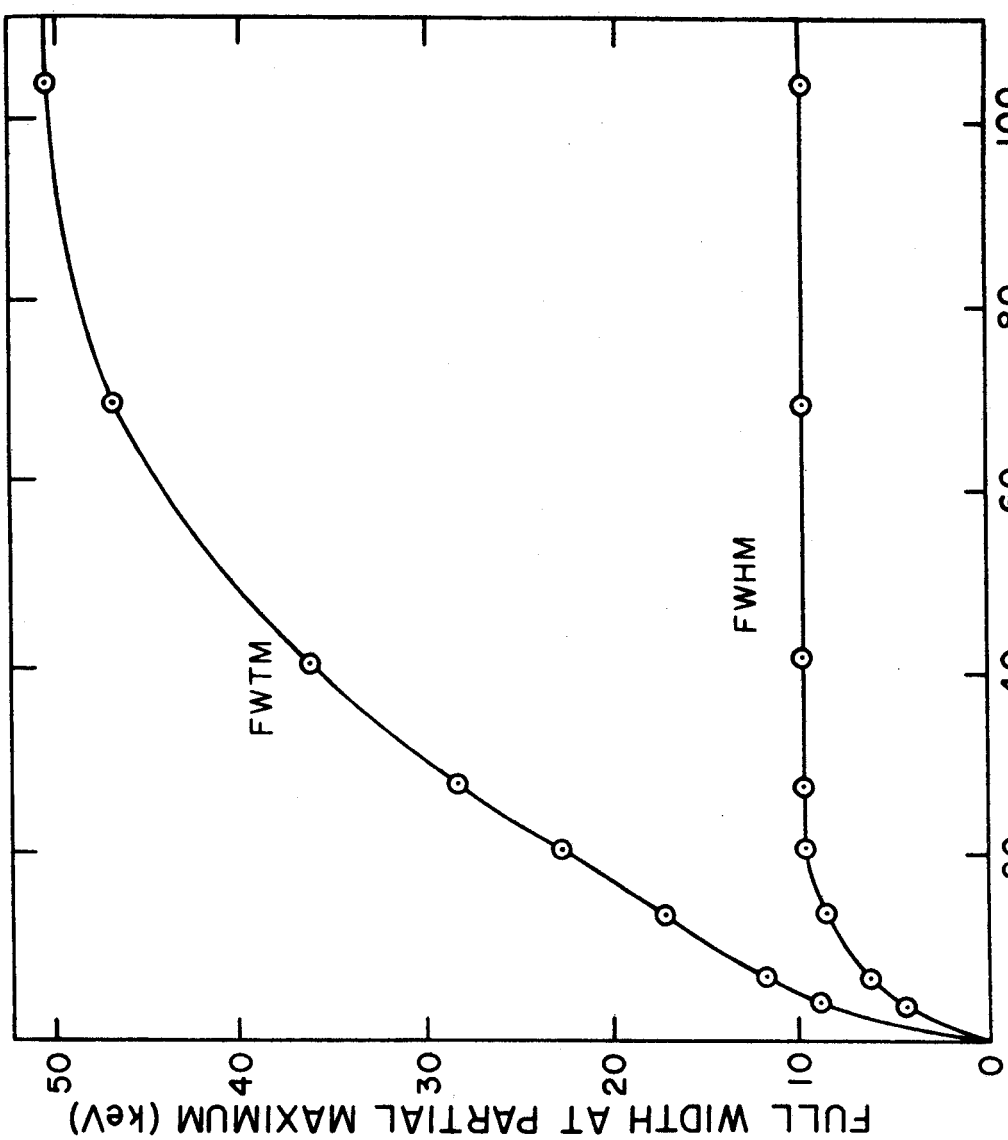

Fig. 21. Plot of display peak widths for ^{137}Cs as a function of the gate widths shown in Fig. 20.

4.1.5. Gate Positions

In Figure 22 gates have been set on various regions of interest in the coincidence spectrum resulting from 180° geometry without using an absorber. Parts *A* and *F* show the 2.5% and 2.0% detector integral coincidence spectra, respectively. All gates were set as indicated in part *F*.

Gates *B*, *C*, and *D* study the region with energies less than the backscatter peak. In part *B* the large Compton edge and the full-energy photopeak are seen on top of a rather typical Compton background. Part *C* shows the Compton edge broadening and with lower intensity and another broad, weak peak at about channel 820. By the time gate *D* is reached, the edge has again narrowed and the new peak has increased in intensity and has moved to a lower energy. The distance of this shift is the same as and in the opposite direction of the movement of the gate from *C* to *D*. Other gates show that as the gate is moved toward the backscatter peak, the new peak moves toward the Compton edge. In all cases the sum of the energy of the new peak and that of the gate equals that of the photopeak. That, plus the fact that the new peak appears in the Compton-forbidden region between the edge and the photopeak, indicates that this is the result of multiple Compton scattering. It arises when a photon is emitted from the source, then is Compton scattered in the first detector, rescattered in the second detector, and finally captured completely in the first detector. As a result, the Compton valley for the backscatter occurs at *C* instead of adjacent to the backscatter peak, at *D*.

Gate *E* is the center of the backscatter peak, and it is, as expected, mostly in coincidence with the Compton edge. In part *G*, in

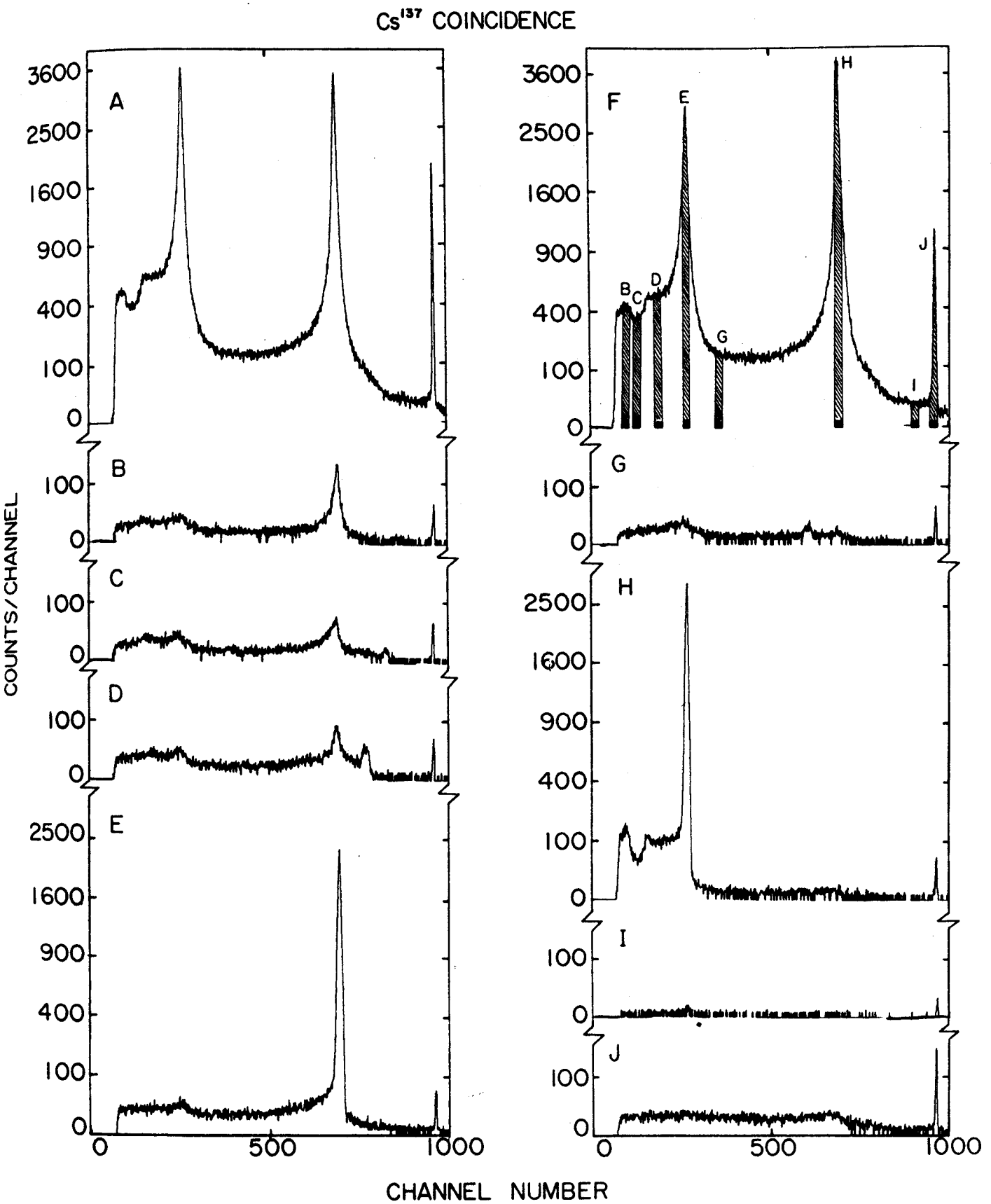

Fig. 22. ^{137}Cs Compton-scattering coincidence spectra showing the effects of gating at different positions. The display integral coincidence spectrum is shown in *A*, while the gate integral coincidence spectrum is shown in *F*. The other spectra correspond to their respective gates as indicated in *F*.

addition to the weak backscatter and Compton edge peaks and the full-energy peak, a broad peak is present at about channel 600. The centroid of this peak when added to that of gate *G* again equals the full-energy peak. This also is a Compton scattered photon in coincidence with a captured Compton scattered photon.

The backscatter peak plus the lower energy region are found in coincidence with gate *H*. In this gate the drop in the Compton background is even more prominent and is strong evidence for the double Compton scattering.

The gate *I* on the valley between the Compton edge and the photopeak shows the photopeak, a Compton background, and a weak peak at the backscatter position. Evidently these are mostly chance coincidences. Finally, in part *J* a coincidence spectrum where the gate was on the photopeak is shown. This appears as a normal ^{137}Cs spectrum, resulting entirely from chance coincidences.

4.1.6. Conclusions

Large, high-resolution Ge(Li) detectors present many exciting new possibilities for nuclear research; yet, along with all their advantages, several problems appear. Potentially one of the most troublesome is the Compton scattering between detectors in a coincidence experiment, which has been illustrated and discussed here. In many cases it is possible to use a 90° geometry with a large graded Pb absorber between the detectors to eliminate the problem, but when working with short half-lives, more care must be used. An absorber of the type described in Section 4.1.1. has been found useful, and using a geometry of 150° or so instead of 180° can be helpful. Most of all, however, one must simply be aware of the problems that now exist

with such coincidence experiments. For without consideration of Compton scattering, newly found coincidence peaks may unknowingly be considered to arise from γ transitions in the nucleus under study, when in fact they are only Compton scattered photons.

4.2. Ge(Li)-Ge(Li) Sum Coincidence Spectrometer (Gi71a)

During the 1950's when γ-ray coincidence spectroscopy came into its own with NaI(Tl) detectors and the newly developed fast electronics, a number of modifications and improvements on the straightforward γ-γ coincidence experiments were made. Most of these were designed to improve the poor peak-to-Compton ratios and the poor resolution of the NaI(Tl) detectors. Among these improvements was the "sum-coincidence" method introduced by Hoogenboom (Ho58) in 1958 In this method the coincident pulses from two NaI(Tl) detectors were passed through a summing network, producing a "sum-coincidence" spectrum. A single-channel analyzer was used to set a window on a sum peak in this spectrum, and this window was then used to gate the output of one of the NaI(Tl) detectors.

Some major advantages of the sum-coincidence technique were readily apparent:

a) Attention was focused on the cascade de-excitation of nuclear states themselves rather than on individual γ rays. Thus, in principal one could work his way up a level scheme, setting the sum-window gates on the energies corresponding to each state in turn and observing the various (two component) cascades that de-excite this state.

b) The method does improve the peak-to-Compton ratio in the gate, thereby helping to eliminate some of the ambiguities caused by the underlying Compton backgrounds from stray, unwanted peaks.

c) The resolution of the NaI(Tl) detectors was effectively improved, especially at higher energies, for it was shown (Ho58) that

$$\Gamma_{S_1} = \Gamma_1 \sqrt{\Gamma_2^2 + \Gamma_3^2} \Big/ \sqrt{\Gamma_1^2 + \Gamma_2^2 + \Gamma_3^2} \quad ,$$

where the Γ's are the energy widths of the various γ-ray peaks in a cascade (Γ_1 and Γ_2), of the sum-coincidence peak (Γ_S), and of the γ-ray peak appearing in the sum-gated spectrum (Γ_{S1}). For γ-rays of equal energy this improvement in resolution approached a factor of $\sqrt{2}$, which could make a considerable difference in NaI(Tl) spectra.

Despite these advantages, the sum-coincidence technique never really became popular. Probable reasons for this can be seen fairly easily by considering its major disadvantages:

a) The method was cumbersome. Some insight into the nature of a decay scheme was needed before sum-window gates could be set intelligently. As a result, often as much or more time was spent in running sum-coincidence experiments as in running standard γ - γ coincidence experiments.

b) In order to achieve the improvement in resolution -- indeed, in order to prevent the actual broadening of the sum

peaks or their becoming split into several components -- the gains and energy zeros of the two detectors had to be matched as closely as possible. This, of course, could be a very tedious procedure.

c) The gates on the sum-coincidence peaks had to be set very carefully in order to avoid distortions in the peaks appearing in the final spectra. This introduced an added degree of uncertainty in determining γ-ray intensities and energies and made any stripping of peaks in complex spectra very difficult.

d) False peaks could be generated from the underlying Compton background. Because of the poor detector resolution involved, these peaks were difficult to distinguish from those originating from bona fide γ-rays.

The necessity of having prior knowledge concerning a decay scheme before being able to set gates intelligently was emphasized in an adaptation of the sum-coincidence method called the "integral-bias" summing spectrometer (Ka62). Here one set of lower-level discriminators (the "integral bias") or windows on the outputs of the individual detectors and used these to gate the sum spectrum itself. The appearance of a particular sum peak in a sum spectrum gated by, say, windows m and n thus indicated that its components lay in energy regions m and n in the respective singles spectra. In principle, with this method a clever setting of three or four gates could furnish all the coincidence information needed to unravel a reasonably complex decay scheme. In

practice, however, one almost never succeeded in setting the windows "cleverly" before he already knew the specific locations of states in a major portion of the decay scheme.

The main application, then, of the sum-coincidence methods was for neutron-capture γ rays (Dr60), where any technique that might simplify the spectra was welcomed. They have also found occasional uses in total absorption spectroscopy (Ka62a), directional correlation experiments (Ha68), and some g-factor measurements (Bo68). And with the advent of Ge(Li) detectors the sum-coincidence methods might reasonably be expected to become quite obsolescent, for their operational difficulties appear to outweigh their advantages rather quickly. The problem of matching the gains of the detectors, for example, becomes all the more difficult and critical. A recent paper by Kantele and Suominen (Ka70), does extend the "integral-bias" sum-coincidence method to Ge(Li)-Ge(Li) systems, but in all fairness it must be concluded that their results show it to be more of a curiosity than a viable laboratory technique.

Recently, however, a variant of the sum-coincidence method has been used in our laboratory, using Ge(Li)-Ge(Li) detector systems, and has been found to be quite useful in helping to clarify complex spectra and decay schemes. Its usefulness depends critically on the fact that the sum-coincidence method is used only for off-line, after-the-fact analysis of the recorded data from two-dimensional "megachannel" γ-γ coincidence experiments. The spectra are obtained later by sorting the two-dimensional data with the program EVENT RECOVERY which is described in Section 3.1.

During the sorting process, the sums can easily be calculated so little or no additional experimental effort is required to add the sum-coincidence method to the other methods of analysis. Also, since the data are available in *digital* rather than analog form, the computer can be made to perform some of the routine tasks that made the older sum-coincidence techniques so unwieldy. For example, it can correct for the energy calibration of the detectors after the experiment has been completed, making it no longer necessary to match the detector gains exactly. Or, since a record is available of which events originated from which detectors, one can immediately obtain meaningful sum spectra even without bothering to convert from channel number to energy, providing that the gains were only moderately mismatched (cf. Sec. 4.2.2.)

In other words, having a complete digital record of the data from a Ge(Li)-Ge(Li) γ-γ coincidence experiment on hand and then performing sum-coincidence analyses on these data makes the sum-coincidence method a worthy supplement and complement to the standard γ-γ coincidence analyses, especially for very complex spectra. Its various advantages and disadvantages are discussed and some results from its use on a moderately complex spectrum (^{63}Zn) and a very complex spectrum (^{205}Bi) (Ko71) are presented.

4.2.1. Experimental Methods

Our sum-coincidence experimental set-up differs very little in concept from a standard two-dimensional γ-γ "megachannel" coincidence

experiment. This is shown dramatically in Figure 23 where the only difference is the addition of a summing network to a γ-γ coincidence block diagram in order to obtain the sum-coincidence block diagram -- and this summing network is simply a modification of the off-line recovery program. It should be pointed out that all of the data presented had been taken prior to the decision to try a sum-coincidence analysis. The experimental methods used to record these data were developed strictly to optimize the γ-γ coincidence results; yet the data could be analyzed quite successfully by sum-coincidence methods.

A description of the two-dimensional megachannel coincidence system used to obtain the data is given in Section 2.1.2.B. The detectors used to obtain the ^{63}Zn spectra were the 2.5% efficient and the 2.0% efficient Ge(Li) detectors. The 2.5% detector was also used to obtain the ^{205}Bi spectra, along with the 3.6% efficient, Ge(Li) detector.

The EVENT RECOVERY program was used to perform sum-coincidence gating as well as the normal γ-γ coincidence gating. The additional limitation on the sum of $X>Y$ or $X<Y$ was performed because the gains of the detectors were not perfectly matched. In this way two peaks appearing for the same sum were prevented from appearing without having to go through the procedure of converting the addresses to γ-ray energies.

4.2.2. Analysis of a Moderately Simple Spectrum: ^{63}Zn

As an example of the power of the sum-coincidence method to reduce a large background under weak peaks, some results obtained on the decay of 38-min ^{63}Zn are presented. In Figure 24 portions of the spectra obtained from a two-dimensional γ-γ coincidence experiment are

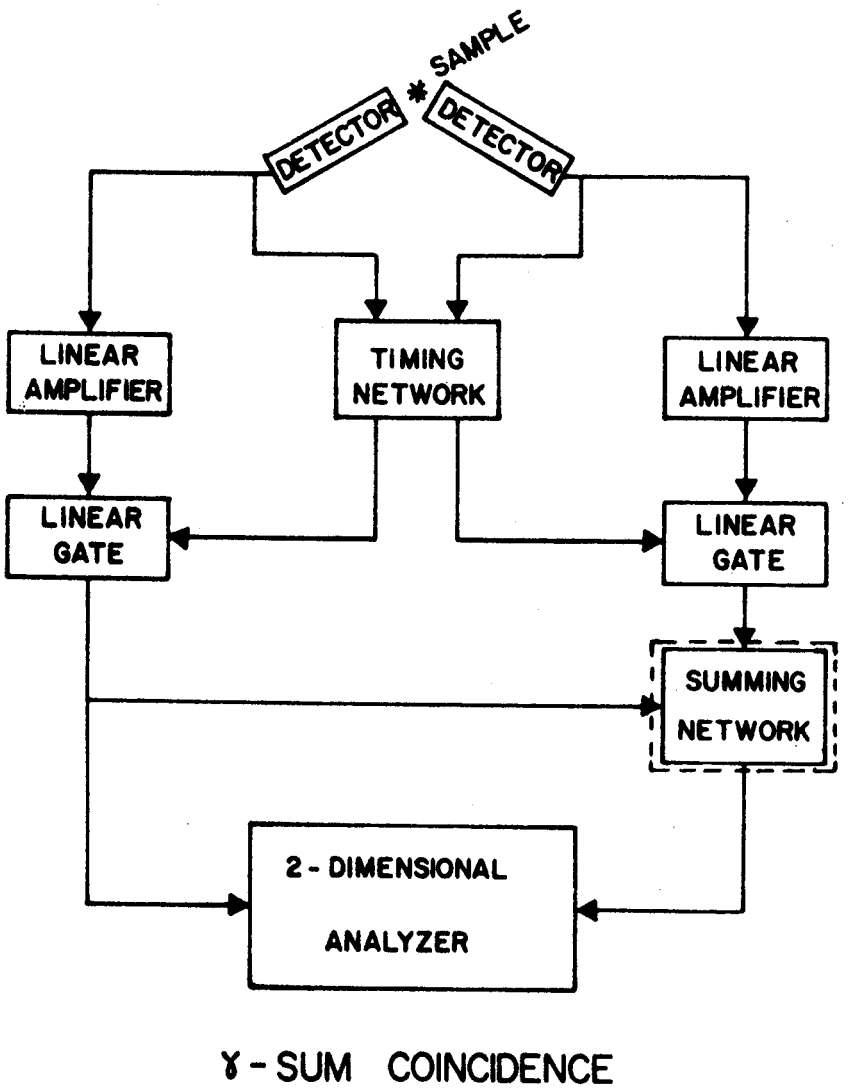

Fig. 23. Block diagram of the sum-coincidence experiment. The addition of the "summing network" is the only way in which this differs from a standard two-dimensional megachannel coincidence experiment, and the "summing network" is merely an addition to the offline computer recovery program.

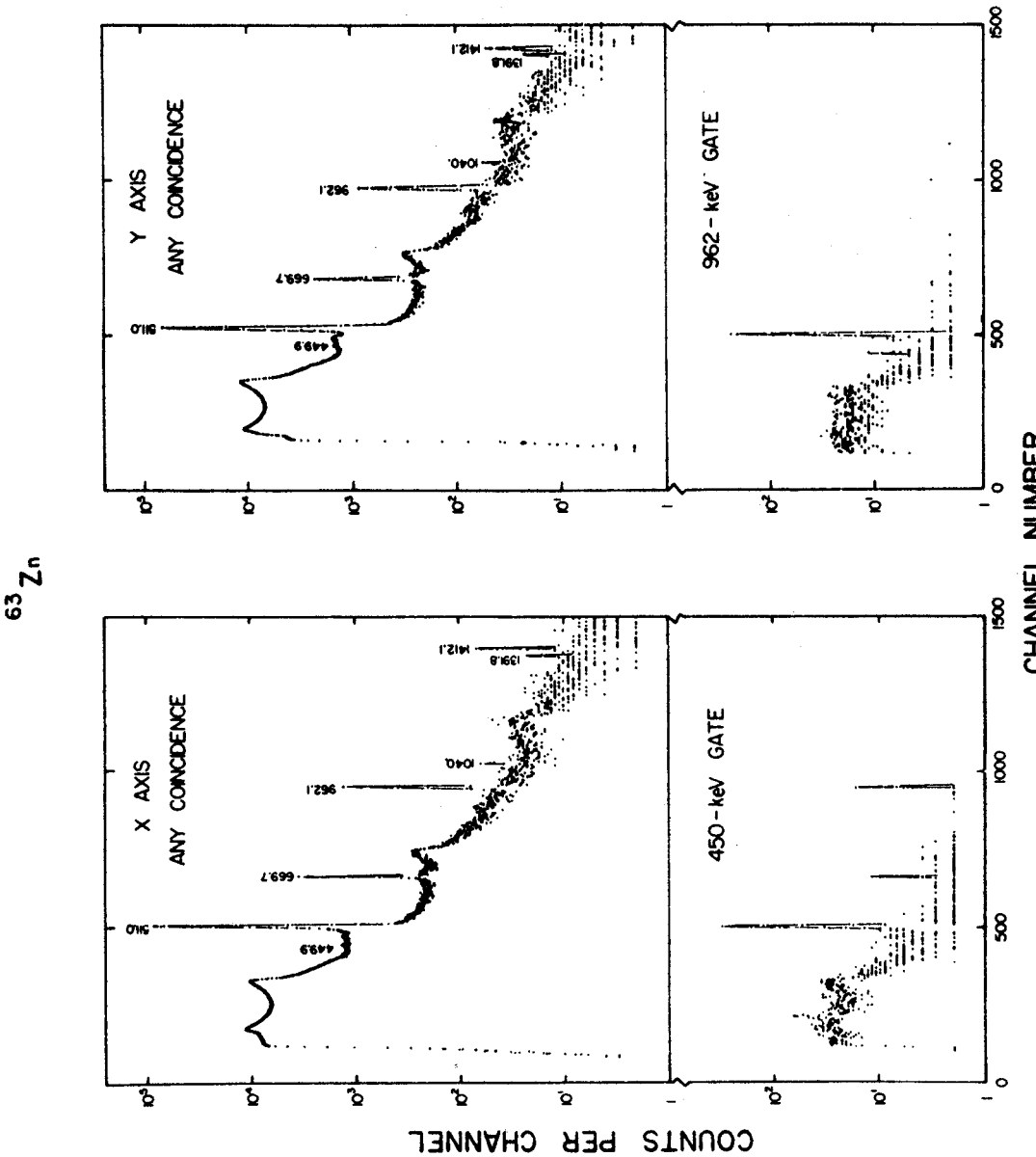

Fig. 24. Coincidence spectra for ^{63}Zn. The integral or "any" coincidence spectra are shown at the top and the lower spectra are gated slices.

shown. The integral or "any" coincidence spectra, which were obtained by adding up all the listed events recorded by the 2.5% and the 2.0% detectors singly, are shown at the top as *X* and *Y*, respectively. All that need be said about the decay scheme, which is described in Chapter 5, is that the first and second excited states of ^{63}Cu lie at 669.7 and 962.1 keV, both decay exclusively to the ground state, and the weak 449.9-keV γ feeds the 962.1-keV state from a state 1412.1 keV. The 669.7-, 962.1-, and 1412.1-keV states are all strongly β^+ fed. The cascade nature of the 449.9-keV γ is demonstrated by the gated spectra appearing in the lower half of Figure 24. Placing a gate on the 450-keV region causes an enhancement of the 962.1-keV γ over the 669.7-keV γ, although the latter is more intense in most of the other spectra. Also, placing a gate on the 962-keV region results in an enhancement of the 449.9-keV γ. It can be seen, however, that the background interference from the $\gamma^{\pm}$ (in true coincidence with 962.1-keV γ) is quite severe in this last spectrum.

The spectrum resulting from summing each pair of *X* and *Y* addresses together is shown in Figure 25. Two types of peaks appear in this spectrum, sum peaks, as indicated, and Compton scattered peaks. The Compton scattered peaks are those that result from a Compton scattered photon from one detector being captured by the second detector. The peaks at 511.0, 669.7, 962.1, and 1115.4 keV are examples of this type. The peak at 1412.1 keV is mostly a sum peak but contains a Compton scattered component.

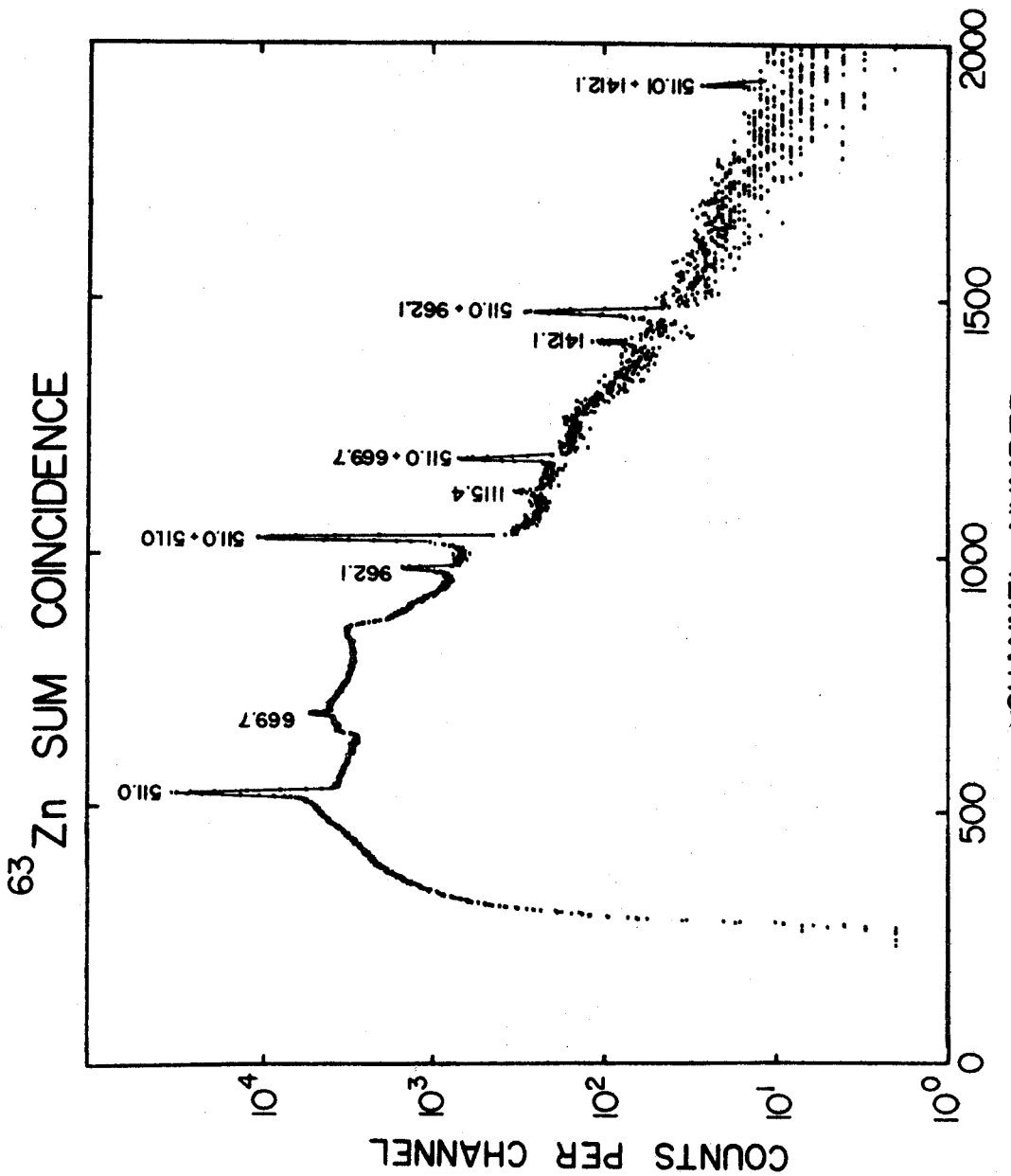

Fig. 25. Total sum-coincidence spectrum for ^{63}Zn. This spectrum was obtained by summing the addresses of each coincidence event in the integral coincidence spectra of Fig. 24.

Figure 26 shows examples of gating on each type of peak. At the top is shown the X and Y components of all sums with $Y>X$. The result is that the Y axis shows a relatively normal integral coincidence spectrum, although skewed toward higher energies, while the X axis shows a spectrum whose intensity is greatly reduced at the higher energies. Gating on the 669.7-keV peak (a Compton scattered peak) as displayed in Figure 25, the following results appear: A sharp peak appears at 511 keV in the Y-axis spectrum, and it appears to be in coincidence with a peak at ≈160 keV in the X-axis spectrum. What is appearing is a true coincidence between the 511-keV photopeak from one detector with that portion of the $\gamma\pm$ Compton distribution from the other detector that is required to add up to the 670-keV gate. The peak at ≈160 keV is narrow only because the gate on the 670-keV region was also quite narrow.

In the 670-keV gated spectra three broader peaks also appear. The Compton edge from the 669.7-keV γ in the Y spectrum is in coincidence with the backscatter peak from the same γ ray in the X spectrum. And the broad Gaussian-looking peak that is split between the X and Y spectra represents those portions of the Compton continuum from the $\gamma^{\pm}$ in each detector that, in true coincidence, add up to ≈670 keV.

The spectra gated on the 511+670-keV sum start to show the advantages of the sum-coincidence method. First, notice the welcome reduction in the Compton background in these spectra. Then notice the clean appearance of the 669.7-keV photopeak in the Y spectrum and the 511.0-keV photopeak in the X spectrum. The 962.1-keV peak (weak) in the Y

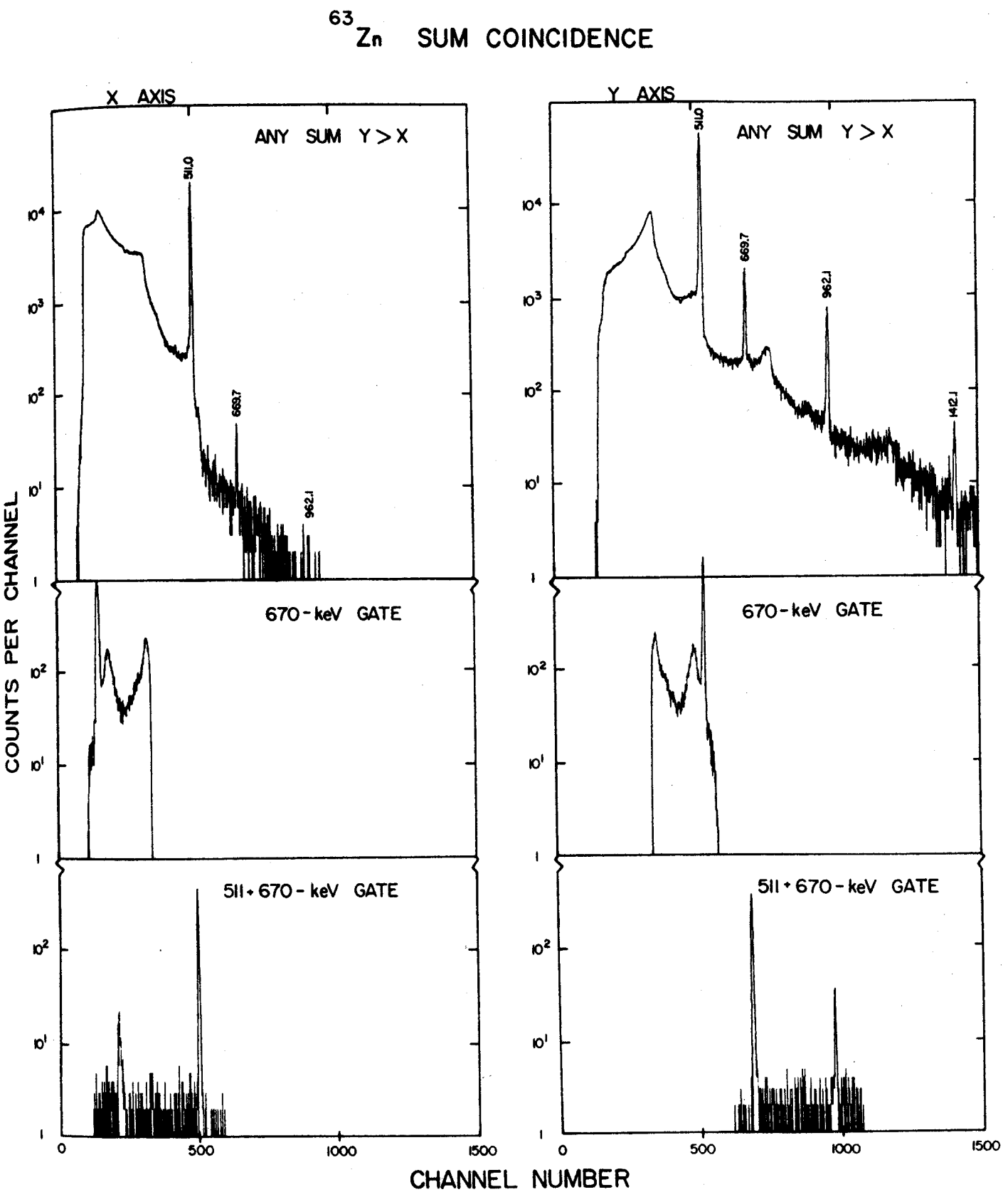

Fig. 26. Sum-coincidence spectra for ^{63}Zn. All of the spectra shown were taken with the limitation $Y>X$, and the X-axis spectra are displayed on the left opposite their corresponding Y-axis spectra.

spectrum arises from chance coincidences, as does the backscatter peak from the 669.7-keV γ in the *X* spectrum.

In Figure 27 the results of gating on the 1412-keV sum peak are shown. The 449.8- and 962.1-keV peaks are very strongly enhanced, demonstrating conclusively that they are a cascade adding up to 1412 keV. The 511.0- and 669.7-keV peaks are present because of being in coincidence with the underlying Compton background. The fact that there is a 1412.1-keV ground-state transition is evidenced by the Compton edge of this transition appearing in coincidence with its backscatter peak. Subtracting a weighted background from each side of the sum peak improves the peak-to-Compton ratios further and removes some of the 511.0- and 669.7-keV peaks. Perhaps the strongest statement that can be made in favor of the sum-coincidence technique is "compare the 449.8-keV peak in the lower part of Figure 27 with the same peak in the 962-keV gated spectrum in Figure 24." The reader is reminded that both spectra were extracted from the same set of magnetic tapes.

4.2.3. Analysis of a Complex Spectrum: ^{205}Bi

(in conjunction with K. Kosanke)

A second example of how the sum-coincidence method can aid in resolving a weak, closely spaced triplet peak in the complex spectrum is the results from the decay of 14.6-d ^{205}Bi. The ^{205}Bi singles spectrum presented in Figure 28 with its myriad of weak peaks, illustrates the complexity of the decay -- a total of 99 γ rays have been identified as belonging to this decay. The peak of interest here is the weak peak near 1002 keV. Figure 29, which shows only that small portion of the decay scheme (Ko71) necessary for the present discussion,

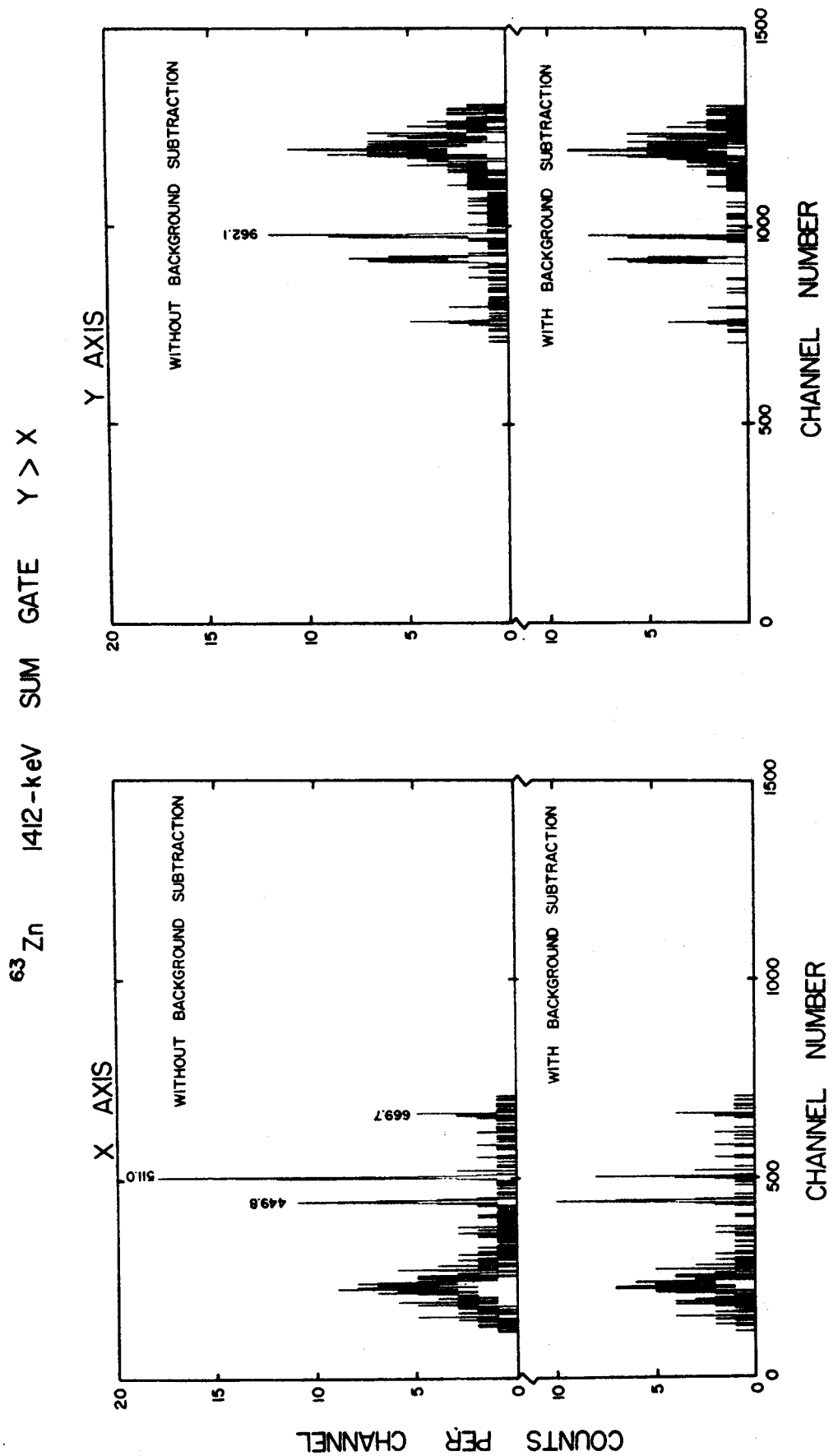

Fig. 27. Sum-coincidence spectra for ^{63}Zn with the sum gate set on the 1412.1-keV sum peak.

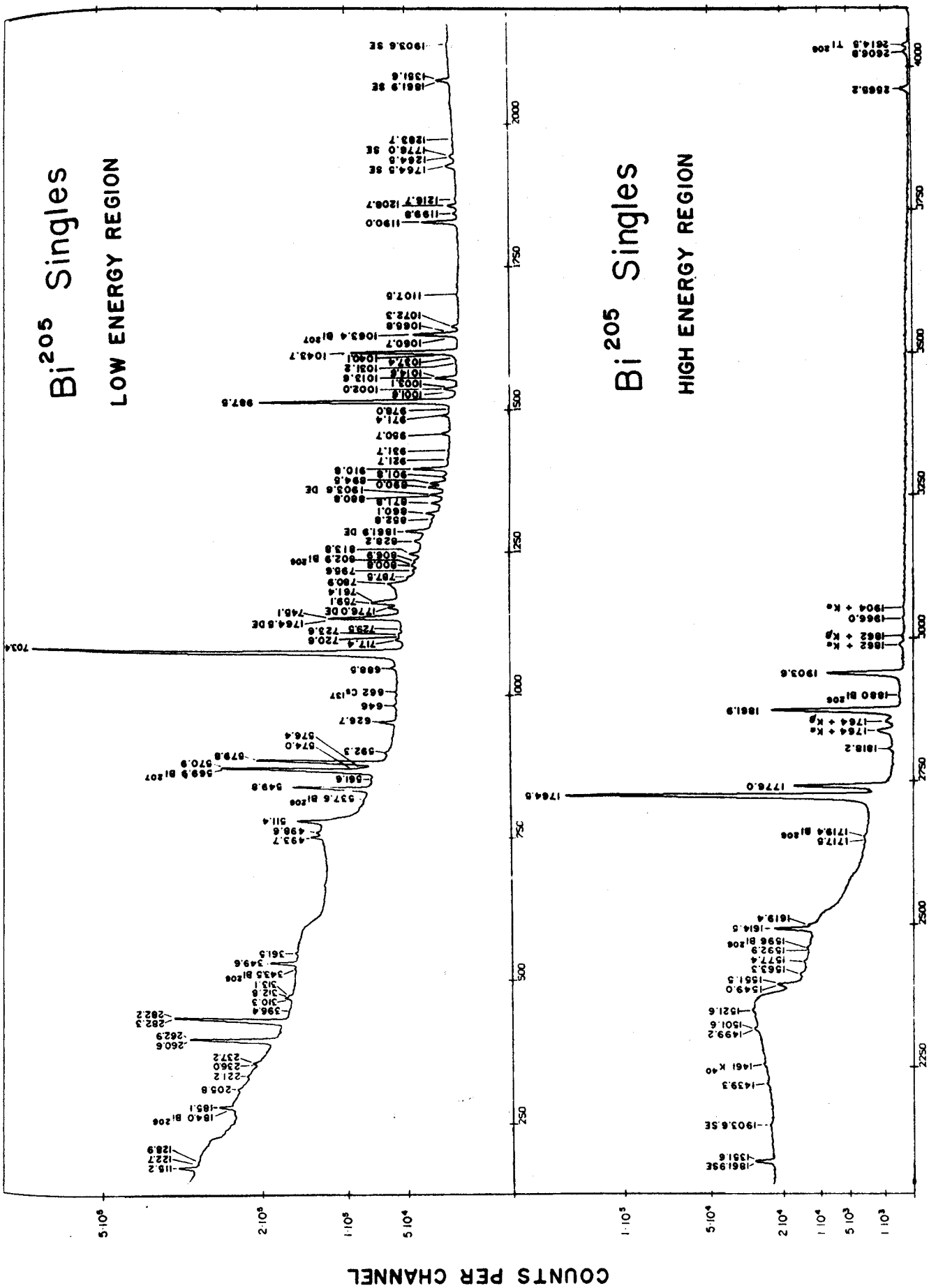

Fig. 28. ^{205}Bi singles γ-ray spectrum taken with a 7 cc Ge(Li) detector.

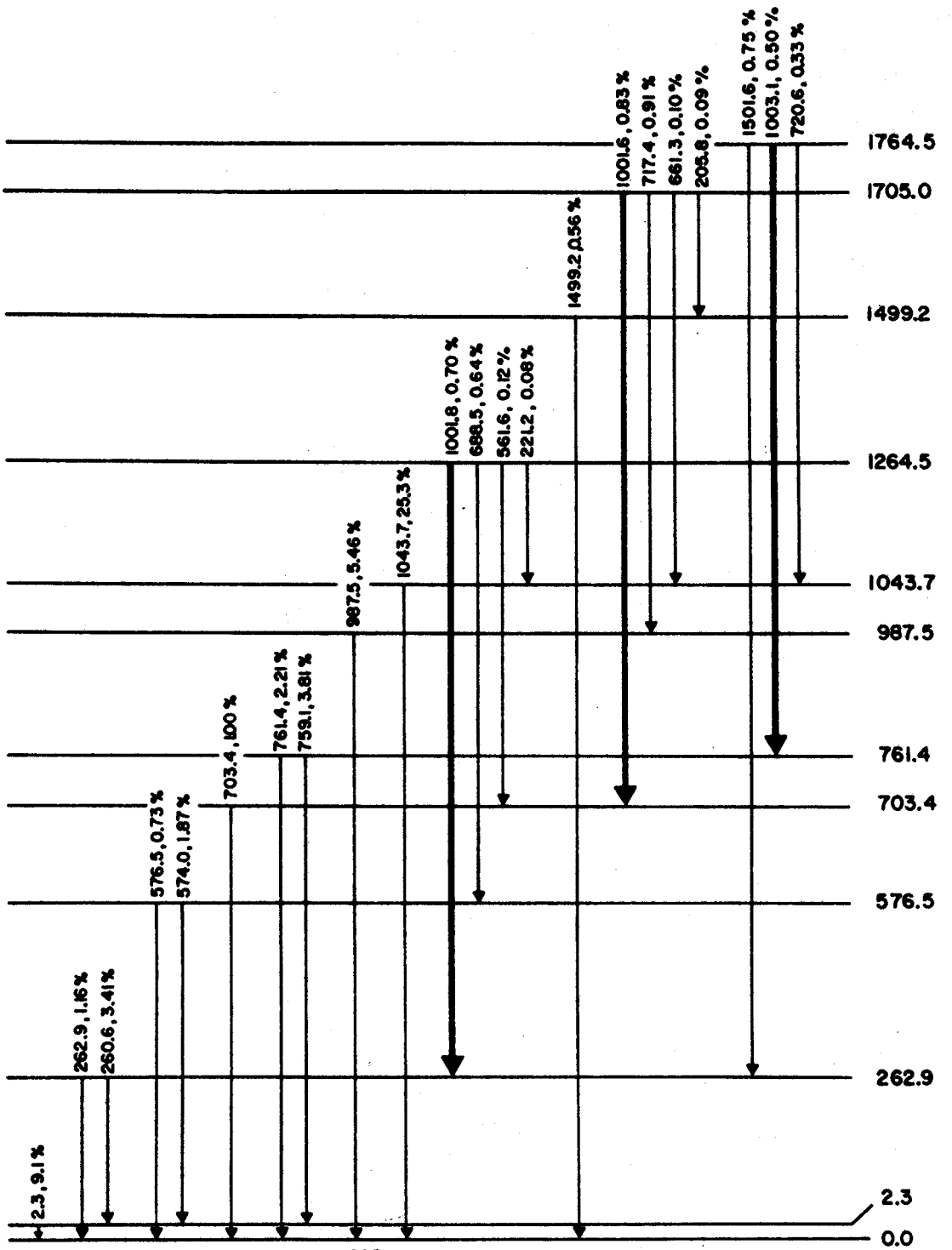

Fig. 29. A small portion of the ^{205}Bi decay scheme showing those states and transitions of interest to the present discussion. The three components of the ≈1002-keV triplet are drawn as larger arrows to aid the eye in locating them.

indicates the reason for selecting this peak. All of the previous studies of this decay (Ru71) concluded that the 1002-keV peak represents a single γ-ray that feeds the 262.9-keV state. And although a slight broadening of the 1002-keV peak was noted, even the best Ge(Li) detectors did not have the ability to resolve the peak even partially. In our studies, however, considerable Ge(Li)-Ge(Li) γ-γ coincidence data suggested a triplet with the placements indicated in Figure 29.

To substantiate the tentative placements of the transitions in the ≈1002-keV triplet, sum-coincidence gates were set on the regions corresponding to the 1264.5-, 1705.0-, and 1764.5-keV states. The integral or "any" sum spectrum is shown in Figure 30. There are relatively few clearcut sum peaks in this spectrum, considering the wealth of cascade γ-rays resulting from ^{205}Bi decay. In fact, examining the positions of the three sum-coincidence gates does not lead to much initial optimism. The position of the 1264.5-keV gate shows no sign of an obvious sum peak -- all that is present is a Compton-type background. At the location of the 1705.0-keV gate there is only a weak peak. Only at the location of the 1764.5-keV gate is the sum peak obviously present.

The spectra resulting from these three sum-coincidence gates is shown in Figure 31. Only the composite spectra from the *Y* axis (the 3.6% detector) is displayed, with the small arrows indicating where *X*>*Y* ends and *Y*>*X* begins. Even though the sum peaks were small in Figure 30, the gated spectra in Figure 31 show many well-defined peaks. A closer examination of each of these indicates that only a few are in coincidence with other γ rays, while most of them result from Compton scattering.

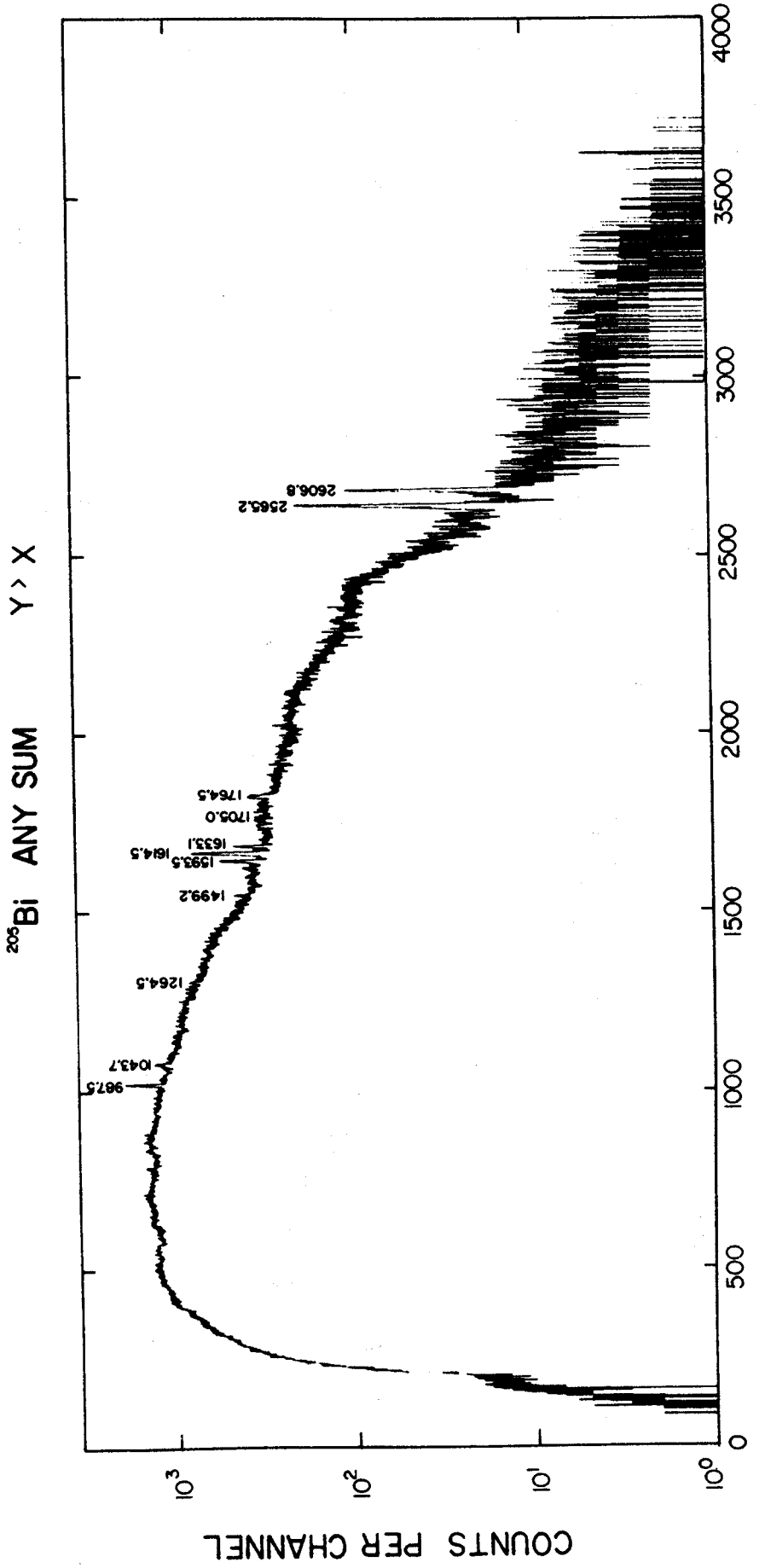

Fig. 30. Total or "any" sum-coincidence spectrum for ^{205}Bi.

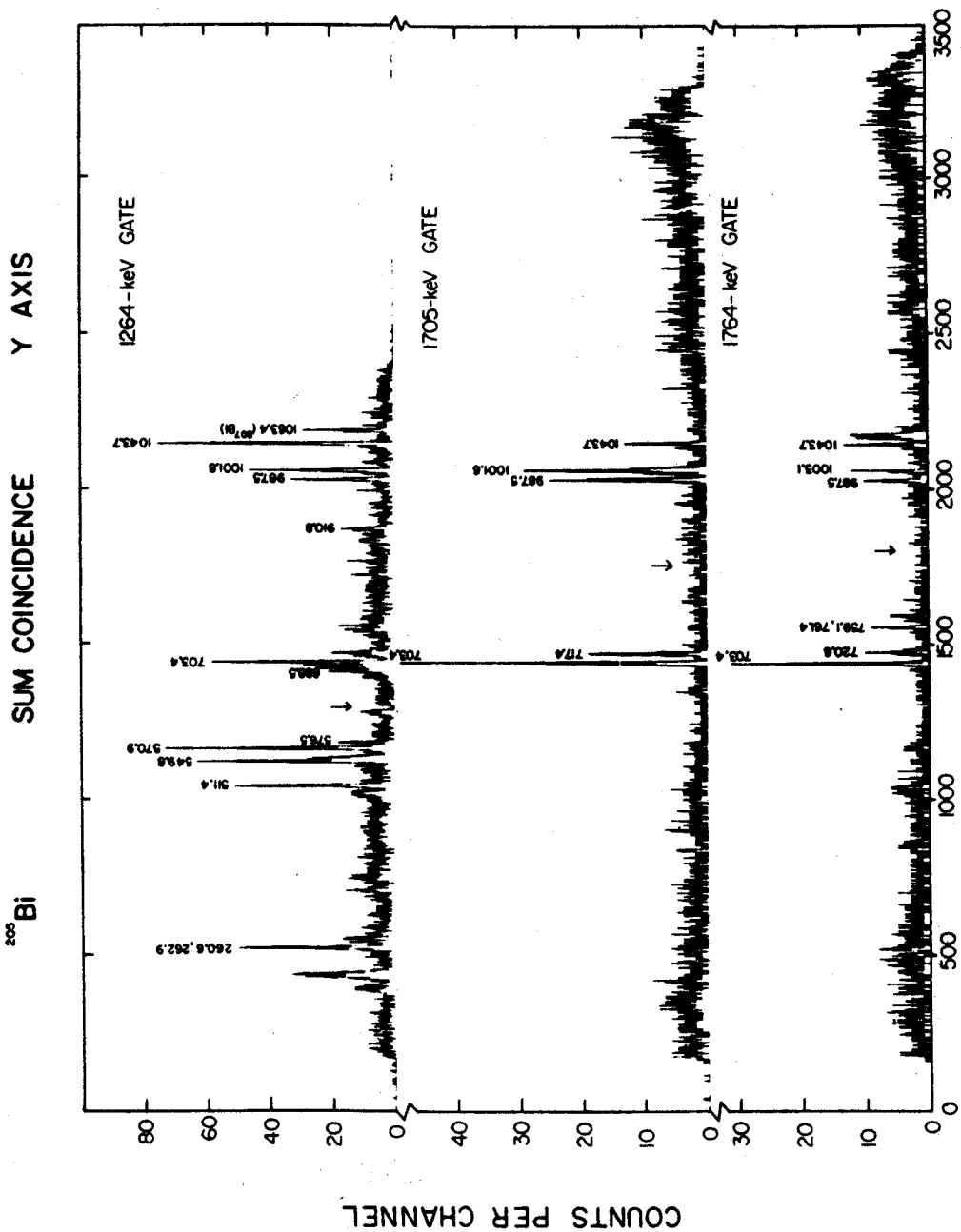

Fig. 31. Sum-coincidence spectra for ^{205}Bi showing the results of gating on the 1264-, 1705-, and 1764-keV sum peaks. These are all Y-axis spectra. The small arrows show where the condition $Y<X$ stops and $Y>X$ begins.

In the top spectrum, resulting from a gate on the 1264-keV region, the 1001.8-keV γ is shown definitely to be in coincidence with the 260.6-262.9-keV doublet. Also present is the 576.5-keV and 685.5-keV coincidence pair. Both the 561.6- and the 221.2-keV γ's are too weak to stand out from the background in this spectrum. Also present in the spectrum are strong γ rays such as those at 549.8, 570.9, 703.4, and 1043.7 keV, which are present because of chance coincidences and because of Compton scattering, as discussed in Section 4.1. The other peaks in the spectrum are caused almost solely by Compton scattering, as was verified by increasing the gate widths and observing the resulting changes in the intensities and shapes of these peaks.

The middle spectrum, resulting from a gate on the 1705-keV region, is considerably simpler. The 1001.6-keV and 703.4-keV coincident pair is definitely established, and so is the 717.4-keV and 987.5-keV pair. Both the 661.3- and the 205.8-keV γ's are too weak to stand out in this spectrum.

A few more peaks are present in the bottom spectrum, gated on the 1764-keV region. The 1003.1-keV and 759.1-761.4-keV and the 720.6-keV 1043.7-keV coincident pairs are readily observed. Also present are the 703.4- and 987.5-keV γ's, here only in coincidence with the Compton background in the gate, for their intensities are much lower than in the 1705-keV spectrum. In the spectrum drawn at the bottom of Figure 31, the 1501.6-keV and 262.9-keV coincident pair is not seen even though it is moderately intense. However, when using a wider gate width (≈20 keV), this pair was easily seen. This result points out one of the problems that has not been completely solved here --

that of unmatched gains for the two detectors. These peaks were far enough away in energy from the other two coincident pairs that their sum peak produced simply by adding channel numbers was excluded from the narrow sum gate based on the other two pairs. In this instance the apparent difference in sum energy was almost 10 keV. Thus, although one can and does use detectors without perfectly matched gains, he must be on the lookout for this sort of sum-peak "jitter". That is, unless he is willing to convert the spectra from channel numbers to γ-ray energies before setting the sum-coincidence gates, a somewhat tedious procedure but one that can be performed readily by the computer.

Accordingly, the presence of the 260.6-262.9- & 1001.8-keV, the 703.4- & 1001.6-keV, and the 759.1-761.4 & 1003.1-keV pairs in the sum gates set both confirm the existence of the $\approx$1002-keV peak as a triplet and also the placements of its components. Perhaps it is worth noting that the sum-coincidence method also added a confirmation of the new state at 1705.0 keV and by removing ambiguities in the γ-γ coincidence results has allowed the definite placement of the 720.6-keV transition, the center member of a quite weak 717.4-720.6-723.6-keV triplet.

4.2.4. Conclusion

It has been shown that the sum-coincidence technique as applied to the digitally-stored data from a two-dimensional Ge(Li)-Ge(Li) γ-γ "megachannel" coincidence experiments is a viable and useful tool for the nuclear spectroscopy laboratory. When thus applied, using sum-coincidence gates to complement the standard γ-γ coincidence gates in the off-line sorting of the spectra, the sum-

coincidence method is quite useful for pulling weak peaks out of a strong Compton background. The analysis of spectra must be made carefully and cautiously, however, for the spectra resulting from sum-coincidence gates are not quite so easily interpreted as those resulting from standard γ-γ coincidence gates. This is particularly true when there is significant Compton scattering between the detectors. Nevertheless, when used to supplement and complement these γ-γ coincidence experiments and *not as a stand-alone technique*, the sum-coincidence method should find considerable use in high-resolution γ-ray spectroscopy.

CHAPTER V

DECAY OF ^{63}Zn

5.1. Introduction

The first report of the decay of ^{63}Zn was by Bothe et al. (Bo37) in 1937, who produced it by the ^{64}Zn$(n,2n)^{63}$Zn reaction. Since then it has been studied by many groups. Most of the γ-ray work has been performed by stripping γ-ray spectra obtained from NaI(Tl) detectors and comparing the results to the more precisely measured levels obtained from charged particle reactions. Since the advent of Ge(Li) detectors, several authors (Ho66, De67, Bo69) reported γ-ray spectra obtained with Ge(Li) detectors a few cubic centimeters in size, each reporting more and more precisely measured γ transitions than the previous authors. Kiuru et al. (Ki70) presented results obtained using a relatively large Ge(Li) detector that are in good agreement with previous results. The only coincidence results reported on ^{63}Zn are from a NaI(Tl)-Ge(Li) coincidence experiment performed by Borchert (Bo69).

Many charged particle scattering reactions have also been performed to study the excited states of ^{63}Cu. Since ^{63}Cu is stable as are many of its neighbors, a large variety of reactions have been performed. Some of the reactions performed were ^{63}Cu(p,p') (Ma57), ^{62}Ni(τ,d) (B165), ^{64}Zn(t,α) (Ba67), ^{62}Ni(α,t) (Ro68), and ^{62}Ni(d,n) (Ma71). A comparison of the results from the different reactions and the γ-ray studies is shown in Figure 32.

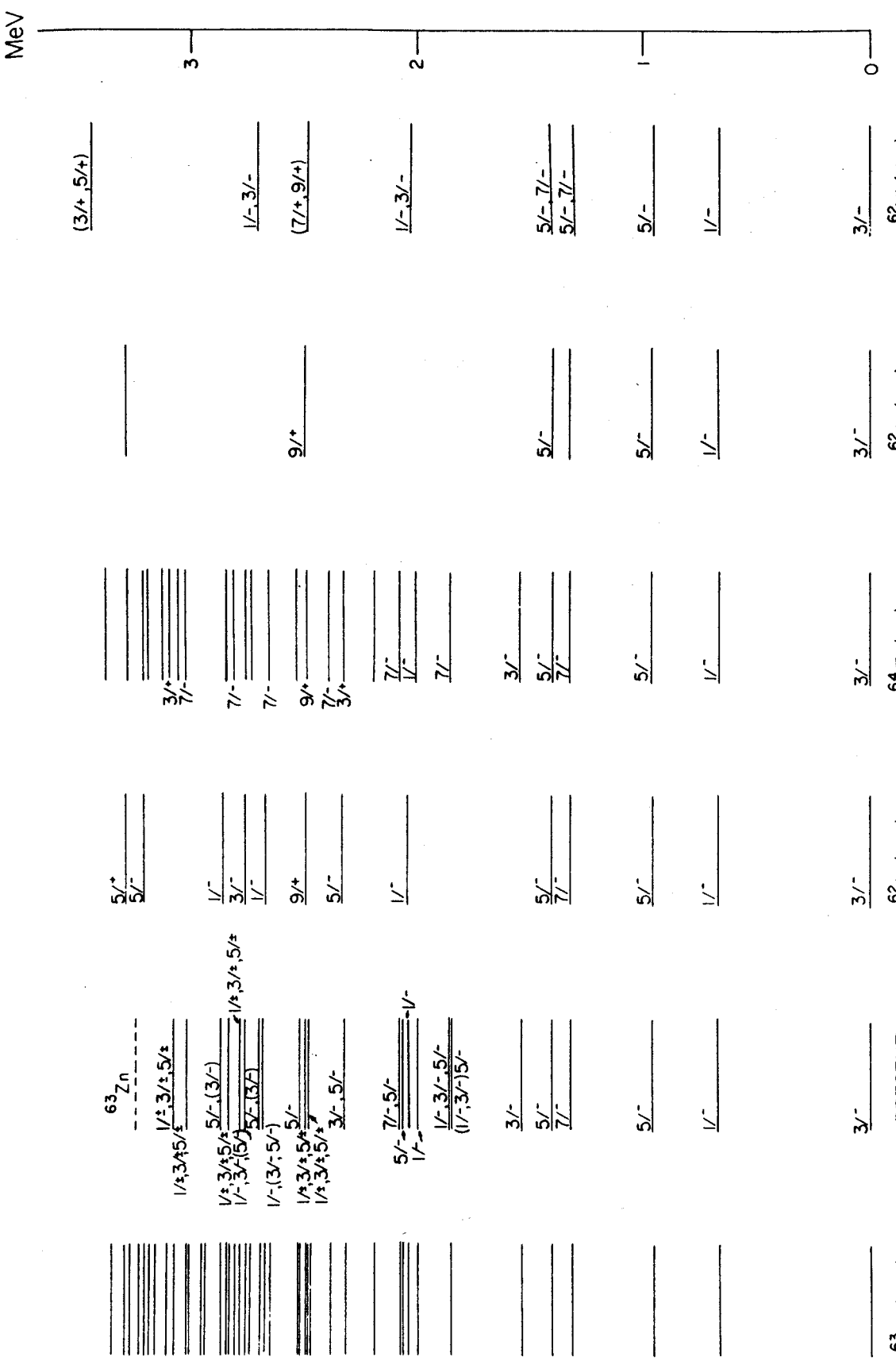

Fig. 32. A summary of various reactions used to study excited states in ^{63}Cu.

5.2. Source Preparation

The ^{63}Zn sources were prepared by bombarding natural Cu foils (69.09% ^{63}Cu, 30.91% ^{65}Cu) with protons from the Michigan State University Sector-Focused Cyclotron; these protons were degraded from higher energies to 12 MeV by the use of Al absorbers to induce the ^{63}Cu(p,n)^{63}Zn reaction. Typically, 10-mil Cu foils were bombarded for ≈3 minutes with a typical beam current of ≈2 μA. The sources were allowed to decay for several minutes before being counted for several half-lives. More source was added with the passage of time to retain a relatively constant counting rate. To insure that only radiations from ^{63}Zn were observed the γ-ray spectrum was confirmed by counting sources that had been chemically separated according to the procedure in Section 2.3.

5.3. Experimental Results

5.3.1. γ-Ray Singles Results

Energies and intensities of ^{63}Zn γ rays were determined using the 10.4% efficient Ge(Li) detector. The energies of the prominent γ rays were measured by counting ^{63}Zn sources simultaneously with ^{110m}Ag and ^{56}Co. The energies of most of the weaker ^{63}Zn γ rays were then determined by using the energies of the prominent ^{63}Zn γ rays as secondary standards. The centroids and areas of the photopeaks were determined using the computer program SAMPO.

A typical γ-ray spectrum is shown in Figure 33. Forty-four γ transitions were assigned to the ^{63}Zn decay, and their energies and intensities are listed in Table 5 along with those of other authors (Ho66, De67, Bo69, Ki70). Also included in the table are the levels observed in the (p,p') reaction (Ma57). The uncertainties in the energies listed in

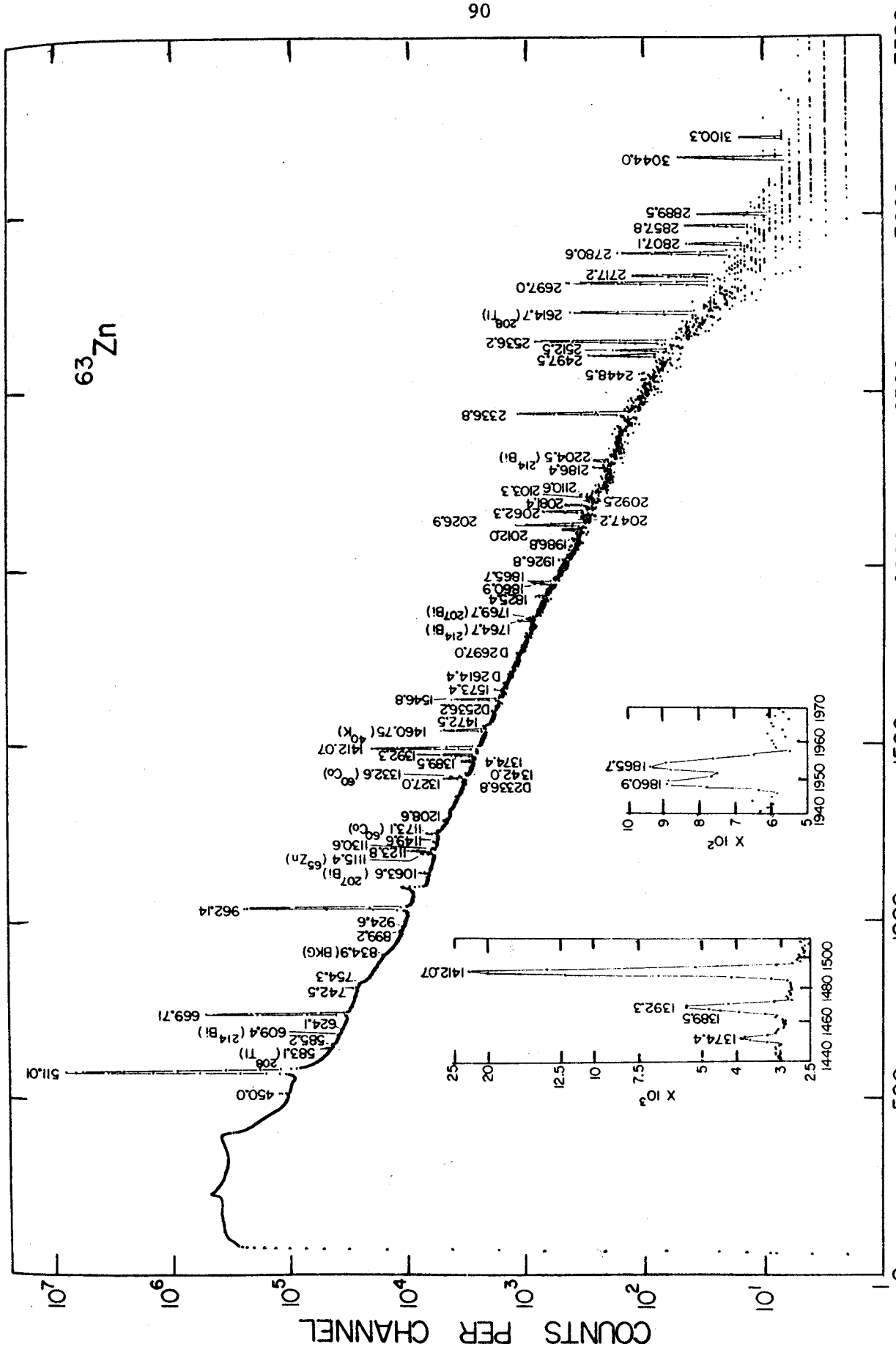

Fig. 33. ^{63}Zn γ-ray spectrum. The insets show the regions at 1392 keV and 1865 keV in more detail.

Table 5. Energies and Relative γ-Ray Intensities from the Decay of ^{63}Zn

Present Work		Holmberg, Spring & Lundán		DeFrenne et al.		Borchert		Kiuru & Holmberg		Mazari et al.
E	I	E	I^a	E	I^a	E	I^a	E	I^a	E
----	----	----	----	----	----	364.5±2.0	0.2±0.1	----	----	----
450.0 ±0.2	2.7 ±0.2	----	----	----	----	450.0±0.5	3.0±0.5	449.8 ±1.0	2 ±1	----
511.0	2188	511	≡1600	511	≡2110	511.0	≡2190	511.0 ±0.2	≡2060	----
585.2 ±0.5	0.22±0.10	----	----	----	----	----	----	----	----	----
624.1 ±0.6	0.18±0.05	----	----	----	----	----	----	----	----	----
669.71±0.1	≡100	670±1	100	668±1	100±5	669.6±0.2	100 ±3.9	699.75±0.2	100±2	668±5
----	----	----	----	----	----	684.7±1.7	0.45±0.16	----	----	----
742.5 ±0.5	0.76±0.13	----	----	----	----	742.5±0.5	0.86±0.13	742.0 ±1.0	0.7±0.4	----
754.4 ±0.7	0.33±0.15	----	----	----	----	----	----	----	----	----
899.2 ±0.6	0.16±0.06	900±20	weak	----	----	----	----	----	----	----
924.6 ±0.6	0.13±0.06	----	----	----	----	923.5±1.0	0.25±0.09	----	----	----
962.14±0.1	79.8 ±3.2	962±2	84.0	961±1	79±5	961.9±0.2	78.8±2.2	962.1 ±0.2	80±2	961±5
----	----	----	----	----	----	1087 ±2	0.32±0.11	----	----	----
1123.8 ±0.6	1.3 ±0.2	----	----	----	----	1123.7±0.3	1.5 ±0.3	1123.6 ±1.0	1.6±0.4	----
1130.6 ±0.5	0.13±0.04	----	----	----	----	----	----	----	----	----
1149.6 ±0.3	0.21±0.05	----	----	----	----	1150 ±2	0.30±0.05	----	----	----
----	----	----	----	----	----	1168 ±3	0.20±0.04	----	----	----
----	----	----	----	----	----	1189 ±3	0.2 ±0.1	----	----	----
1208.6 ±0.8	0.17±0.06	----	----	----	----	1208 ±2	0.15±0.04	1209.1±1.0	0.3±0.1	----
1327.0 ±0.4	0.84±0.06	----	----	1327±4	0.7±0.4	1326.4±0.3	0.98±0.12	1327.1 ±1.0	0.8±0.2	1327±5
----	----	----	----	----	----	----	----	1340.0 ±1.0	0.6±0.2	----
1374.4 ±0.3	0.41±0.06	----	----	----	----	1374.3±0.3	0.48±0.09	1374.4 ±1.0	0.4±0.2	----
1389.5 ±0.6	0.44±0.09	----	----	1390±4	1.8±0.5					----
1392.3 ±0.5	1.24±0.12	----	----			1391.5±0.4	1.8±0.1	1392.1 ±1.0	1.8±0.3	----
1412.07±0.2	9.3 ±0.4	1411±2	4.8	1412±1	10. ±0.8	1411.9±0.2	8.8±0.3	1412.1 ±1.0	9.6±1.0	1412±5
1546.8 ±0.6	1.6 ±0.1	1550±10	2.2	1548±1	1.5±0.2	1546.9±0.2	1.4±0.2	1546.6 ±1.0	1.8±0.3	1547±5
1573.4 ±0.5	0.19±0.07	----	----	1573±4	0.2±0.1	1574.0±2.0	0.14±0.04	1573.3 ±1.0	0.25±0.1	----
----	----	1650±20	0.72	1700±4	0.3±0.1	----	----	----	----	----
1825.4 ±0.6	0.11±0.04	1800±10	weak	1822±4	0.2±0.1	1816.9±1.0	0.031±0.003	1825.6 ±1.0	<0.09	----

Table 5 - Continued

Present Work		Holmberg, Spring & Lundán		DeFrenne et al.		Borchert		Kiuru & Holmberg		Mazari et al.
E	I	E	I^a	E	I^a	E	I^a	E	I^a	E
1860.9 ±0.6	0.24±0.05	----	----	----	----	1865.2±0.3	0.38±0.03	1863.4±1.0	0.36±0.21	1862±5
1865.7 ±0.6	0.26±0.05	----	----	----	----					
1926.8 ±0.8	0.082±0.025	----	----	----	----	1926.4±2.0	0.07±0.01	----	----	----
2012.0 ±0.5	0.14±0.03	----	----	----	----	2012.0±0.5	0.12±0.02	2010.9±1.0	0.15±0.05	2012±5
2026.9 ±0.3	0.78±0.05	----	----	----	----	2027.2±0.5	0.66±0.11	2026.7±1.0	0.8±0.2	----
2047.2 ±0.8	0.041±0.14	----	----	----	----	2048.6±1.5	0.08±0.01	----	----	----
2062.3 ±0.5	0.41±0.06	----	----	2059±4	0.4±0.1	2062.0±0.8	0.35±0.08	2062.7±1.0	0.4±0.4	2063±5
2081.4 ±0.7	0.21±0.05	2080±10	1.2	2082±5	0.3±0.2	2082.0±0.5	0.16±0.04	2082.1±1.0	0.2±0.1	2082±5
2092.5 ±0.8	0.057±0.025	----	----	----	----	----	----	----	----	2093±5
2103.3 ±1.2	0.069±0.030	----	----	----	----	2103.2±3.0	0.03±0.02	----	----	----
2110.6 ±0.6	0.087±0.022	----	----	----	----	----	----	----	----	----
----	----	2180±20	0.80	----	----	----	----	----	----	2210±6
2336.8 ±0.3	0.99±0.08	2350±20	1.3	2337±2	0.84±0.08	2336.5±0.2	1.0±0.07	2336.7±1.0	0.9±0.2	2337±6
----	----	----	----	2394±4	0.11±0.05	----	----	----	----	2405±6
2497.5 ±0.6	0.25±0.03	----	----	2497±4	0.16±0.05	2497.7±0.4	0.25±0.02	2497.1±1.0	0.3±0.2	2497±6
2512.5 ±0.5	0.12±0.03	----	----	2516±4	<0.08	2512.0±0.5	0.14±0.02	2512.1±1.0	0.09±0.05	2504±6
----	----	----	----	----	----	----	----	----	----	2510±6
2536.2 ±0.4	0.80±0.05	2540±10	0.6	2535±2	0.7±0.2	2535.9±0.2	0.84±0.04	2536.2±1.0	0.9±0.2	2535±6
----	----	----	----	----	----	----	----	----	----	2543±10
----	----	----	----	----	----	----	----	----	----	2673±8
2697.0 ±0.4	0.48±0.04	2700±20	weak	2694±2	0.3±0.1	2696.7±0.2	0.47±0.09	2696.7±1.0	0.5±0.2	2694±8
2717.2 ±0.5	0.14±0.012	----	----	----	----	2717.0±0.5	0.13±0.02	2716.8±1.0	0.16±0.05	2716±8
----	----	----	----	2767±4	0.09±0.05	----	----	----	----	2761±8
2780.6 ±0.3	0.18±0.015	2770±10	0.4	2781±4	0.11±0.05	2780.1±2.0	0.20±0.02	2780.1±1.0	0.19±0.05	2778±8
2807.1 ±0.6	0.039±0.007	----	----	2805±4	0.05±0.02	2806.5±0.4	0.030±0.007	2807 ±2	0.05±0.02	2805±8
----	----	----	----	----	----	----	----	----	----	2831±8
2857.8 ±0.7	0.032±0.006	----	----	2856±4	0.03±0.01	2857.4±1.0	0.036±0.008	2856 ±2	0.04±0.02	2856±8
----	----	----	----	----	----	----	----	----	----	2869±8
----	----	----	----	2880±4	0.026±0.011	2882.1±2.0	0.011±0.003	----	----	----
2889.5 ±0.5	0.026±0.003	----	----	----	----	2891.1±1.5	0.026±0.005	2890 ±2	0.03±0.01	2888±8
----	----	----	----	----	----	----	----	----	----	2958±8
----	----	----	----	----	----	----	----	----	----	2974±8
----	----	----	----	3032±6	<0.04	----	----	----	----	3032±8
3044.0 ±0.7	0.058±0.010	----	----	3042±6	<0.04	3044.9±1.0	0.055±0.011	3044 ±2	0.06±0.01	3042±8
----	----	----	----	----	----	3090.8±2.0	0.004±0.002	----	----	----
3100.3 ±1.0	0.009±0.004	----	----	----	----	3100.9±0.7	0.009±0.002	3101 ±2	0.02±0.01	3099±8

a. Intensities renormalized relative to the 669.71-keV γ retaining the original number of significant figures.

Table 5 are based on the uncertainties in the energy standards, the heights of the peaks above the background, and the reproducibility of the calculated energies of the different spectra. The relative intensities listed are averaged from several spectra, and their uncertainties are based on the reproducibilities of the intensities and the uncertainties in our experimentally-determined efficiencies for the detector. They are in general 50% greater than the largest deviation of a value from the average of several runs. The γ-ray intensities of the other authors were renormalized to the 669.71-keV γ while retaining the original number of significant figures.

A comparison of the present results with those of other authors, especially Borchert (Bo69) and Kiuru et al. (Ki70), shows good agreement among the authors. The results of Holmberg et al. (Ho66) and DeFrenne et al. (De67) will not be further discussed since their results have significantly fewer peaks than the others, even though their results are in generally good agreement with the others. Borchert reports seven transitions not observed here or by Kiuru and Holmberg, while Kiuru and Holmberg report only one transition not observed by other authors. In the present work, nine transitions were reported that were not observed by other authors, while five others were observed only by Borchert.

Shown in one inset in Figure 33 is the 1360-1420-keV region of the ^{63}Zn spectrum. Notice here the broadening of the photopeak at $\simeq$1390 keV in comparison to the photopeaks on either side. This broadening on the low energy side is better shown in Figure 15. Because even our best detector could not resolve the 1389.5- and the 1392.3-keV components of the doublet, the program SAMPO was used to strip it, and the results are included in Table 5. The other inset shows the two resolved peaks at

1860.9 and 1865.7 keV. These are both full energy γ rays, and neither one of them is the double escape peak of the 2889.5-keV γ, since both are much stronger than any double escape appearing in the spectrum.

5.3.2. Ge(Li)-Ge(Li) Megachannel Coincidence Results

The decay of ^{63}Zn was also examined using the two-dimensional Ge(Li)-Ge(Li) megachannel coincidence system described in Section 2.1.2.B. For this experiment, the 2.5% efficient and 2.0% efficient Ge(Li) detectors were used as the *x* and *y* detectors respectively. The angle between detectors was ≈150 degrees. In Figure 34 some of the results are shown, where Figures 34*A* and 34*E* are the *x* and *y* integral or "any" coincidence spectra, respectively. Table 6 gives the γ-γ coincidence results, in addition to those of the other coincidence experiments.

Figure 34*B* shows the results of gating on the 450-keV peak. This gate produces a 962-keV peak greatly enhanced with respect to the 670-keV peak even though the 670-keV peak is stronger in both the singles and integral coincidence spectra. Therefore, the 962-keV γ is clearly in coincidence with the 450-keV γ. Also observed is a peak at 220 keV which results from a Compton scattered γ-ray from one detector being captured in the other. This was discussed further in Section 4.1.

The next gate, 511 keV, is shown in Figure 34*C*. The γ-rays appearing in this spectrum indicate the states that are β^+ fed. Feeding to other states is too weak to be seen in this spectrum. Further results on β^+ feeding to states are given in Section 5.3.4.

Gating on the 670-keV peak, Figure 34*D*, shows only the 511-keV γ from the β^+ feeding. Although there is a continuum at energies above 511 keV, no γ transition to the 670-keV level is strong enough to be observed.

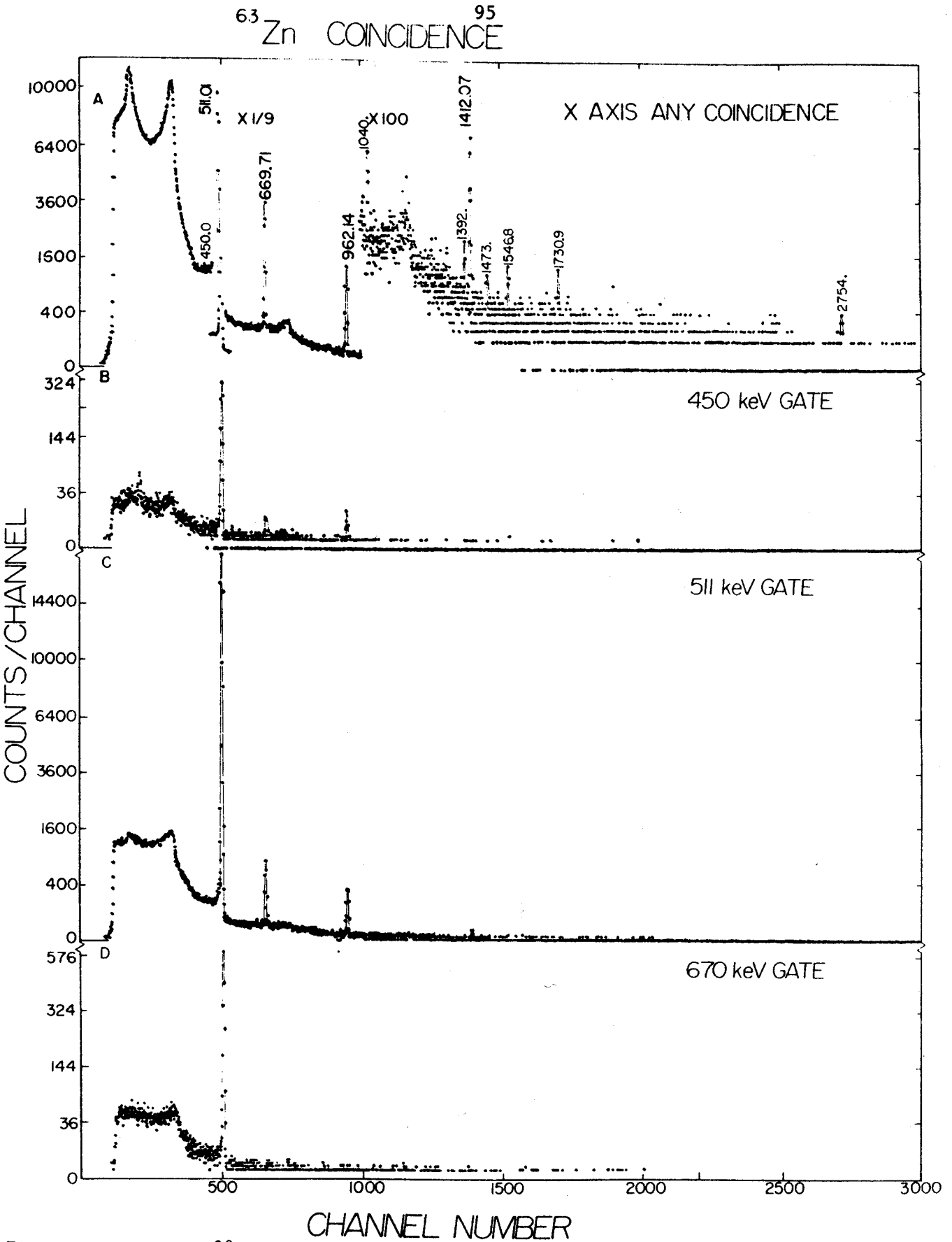

Fig. 34 (Part 1). ^{63}Zn γ-γ megachannel coincidence spectra. In the top of this Figure and of Part 2 are shown the integral coincidence spectra, and in the lower portions are shown the various selected gates.

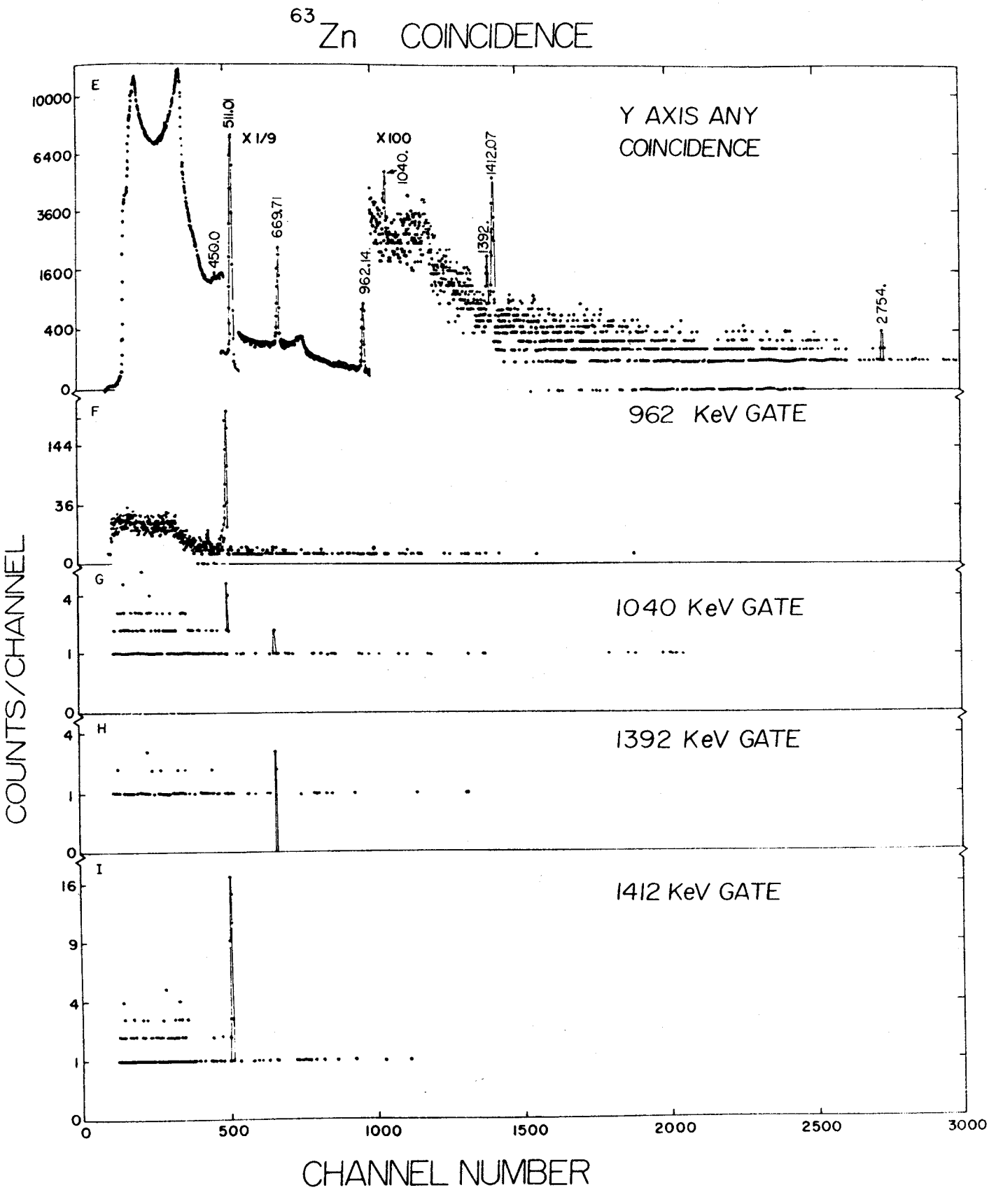
63Zn COINCIDENCE
E
Y AXIS ANY
COINCIDENCE
511.0
X 1/9
X100
1040.
1412.07
669.71
450.0
962.14
1392.
2754.
F
962 KeV GATE
G
1040 KeV GATE
H
1392 KeV GATE
I
1412 KeV GATE
COUNTS/CHANNEL
CHANNEL NUMBER

Fig. 34 (Part 2).

Table 6 Intensities of ^{63}Zn γ rays in Coincidence Experiments

E_γ (keV)	Relative Intensities									
	Singles	Anticoincidence	511-511-γ	450-keV gate	511-keV gate	670-keV gate	962-keV gate	1039-keV gate	1392-keV gate	1412-keV gate
450.0	2.7	1.72	---	---	---	---	9.2	---	---	---
511.0	≡2188	---	31.3	2952	2814	≡2188	≡2188	310	---	≡2188
585.2	0.22	---	---	---	---	---	---	---	---	---
624.1	0.18	---	---	---	---	---	---	---	---	---
669.71	≡100	≡100	≡100	≡100	≡100	---	---	≡100	≡100	---
742.5	0.76	0.56	---	---	---	---	---	---	---	---
754.4	0.33	---	---	---	---	---	---	---	---	---
899.2	0.16	---	---	---	---	---	---	---	---	---
924.6	0.13	---	---	---	---	---	---	---	---	---
962.14	79.8	88.4	69.7	212	72.0	---	---	---	---	---
1123.8	1.3	1.2	---	---	---	---	---	---	---	---
1130.6	0.13	---	---	---	---	---	---	---	---	---
1149.6	0.21	0.30	---	---	---	---	---	---	---	---
1208.6	0.17	---	---	---	---	---	---	---	---	---
1327.0	0.84	0.76	---	---	---	---	---	---	---	---
1374.4	0.41	0.44	---	---	---	---	---	---	---	---
1389.5	0.44	1.57	---	---	---	---	---	---	---	---
1392.3	1.24		---	---	---	---	---	---	---	---
1412.07	9.3	12.5	4.5	---	5.8	---	---	---	---	---
1546.8	1.6	1.8	0.45	---	---	---	---	---	---	---
1573.4	0.19	0.23	---	---	---	---	---	---	---	---
1825.4	0.11	0.21	---	---	---	---	---	---	---	---
1860.9	0.24	0.22	---	---	---	---	---	---	---	---
1865.7	0.26	0.23	---	---	---	---	---	---	---	---
1926.8	0.082	0.28	---	---	---	---	---	---	---	---
2012.0	0.14	0.14	---	---	---	---	---	---	---	---
2026.9	0.78	0.67	---	---	---	---	---	---	---	---
2047.2	0.041	0.038	---	---	---	---	---	---	---	---
2062.3	0.41	0.81	---	---	---	---	---	---	---	---
2081.4	0.20	0.19	---	---	---	---	---	---	---	---
2092.5	0.057	0.043	---	---	---	---	---	---	---	---
2103.5	0.069	0.062	---	---	---	---	---	---	---	---
2110.6	0.087	0.080	---	---	---	---	---	---	---	---
2336.8	0.99	1.8	---	---	---	---	---	---	---	---
2497.5	0.25	0.46	---	---	---	---	---	---	---	---
2512.5	0.12	0.20	---	---	---	---	---	---	---	---
2536.2	0.80	1.5	---	---	---	---	---	---	---	---
2697.0	0.48	0.87	---	---	---	---	---	---	---	---
2717.2	0.14	0.25	---	---	---	---	---	---	---	---
2780.6	0.18	0.34	---	---	---	---	---	---	---	---
2807.1	0.039	0.091	---	---	---	---	---	---	---	---
2857.8	0.032	0.071	---	---	---	---	---	---	---	---
2889.5	0.026	0.057	---	---	---	---	---	---	---	---
3044.0	0.058	0.098	---	---	---	---	---	---	---	---
3100.3	0.009	0.016	---	---	---	---	---	---	---	---

Figure 34*F* displays the results of gating on the 962-keV peak. Here the 450-keV γ is greatly enhanced with respect to the 511-keV γ, indicating again the 450-keV γ is in coincidence with the 962-keV γ.

Gating on the 1040-kev γ shows, in Figure 34*G*, a spectrum similar to the singles spectrum, but greatly reduced. The appearance of the 1040-keV γ in the singles spectrum is debatable, since it would appear on a Compton edge. It also does not fit anywhere in the decay scheme and is probably a strong background peak that is in chance coincidence with the strong peaks in ^{63}Zn.

The gate on the 1392-keV peak, Figure 34*H*, shows a coincidence with only one γ, the one at 670 keV. This confirms the placement of it as feeding from the 2062-keV level to the 670-keV level.

Finally, Figure 34*I* shows the results of gating on the 1412-keV peak. Only the 511-keV γ from the β^+ feeding appears. No other feeding to this level is strong enough to be seen.

Gating on the remaining peaks in the x and y integral coincidence spectra show very little if anything. The 1472-keV gates show possible coincidences with 270- and 511-keV γ's. The 1547-keV gate shows only random coincidences and no firm indication of its β^+ feeding. All the counts in this gate were below 550 keV. The other gates are similar in that all the counts appear below 1000 keV. No channel in any of these gates has more than one count in it, and the channels with counts are randomly spaced. The peak at 2754 keV in the integral coincidence spectra could be from ^{24}Na in room background and the Pb collimator.

5.3.3 Anticoincidence Results

An anticoincidence experiment was performed using a 20.3×20.3-cm NaI(Tl) split annulus, a 7.6×7.6-cm NaI(Tl) detector, and the 10.4%

efficient Ge(Li) detector, with the latter two detectors placed in opposite ends of the annulus tunnel. The γ rays observed by the Ge(Li) detector were counted only when there were no γ rays observed in any of the NaI(Tl) detectors. A description of the system and the electronics was given in Section 2.1.2.A. A spectrum obtained using this system is shown in Figure 35, and the results are included in Table 6.

Most of the ground state transitions observed in this experiment were enhanced over their singles intensities. One of those not enhanced is the 1327-keV γ. This is because the 1327-keV state has no β feeding because of the large difference in spin between it and the ^{63}Zn parent. As a result this state is fed completely by γ transitions from higher-lying states.

Other ground-state transitions not enhanced were at 1861, 1866, 2012, 2081, and 2092 keV. All these transitions were weak in the singles and were very weak in the anticoincidnece results. Of special interest are the 1861- and 1865-keV γ peaks. It was expected that one of the peaks would be enhanced over the other to indicate which is a ground-state transition from a state at the same energy and which is a possible cascade transition. However, even though neither was enhanced, the relative intensities of the two to each other remained near that of the singles spectrum, indicating both transitions are of the same type, either ground state or cascade. Since other weak ground-state transitions of similar energies showed similar enhancements to this pair, these two peaks both appear to be ground-state transitions.

5.3.4. 511-511-keV-γ Triple Coincidence Results

A 511-keV-511-keV-any γ triple coincidence experiment was performed using the 20.3×20.3-cm NaI(Tl) split annulus and the 2.5% efficient

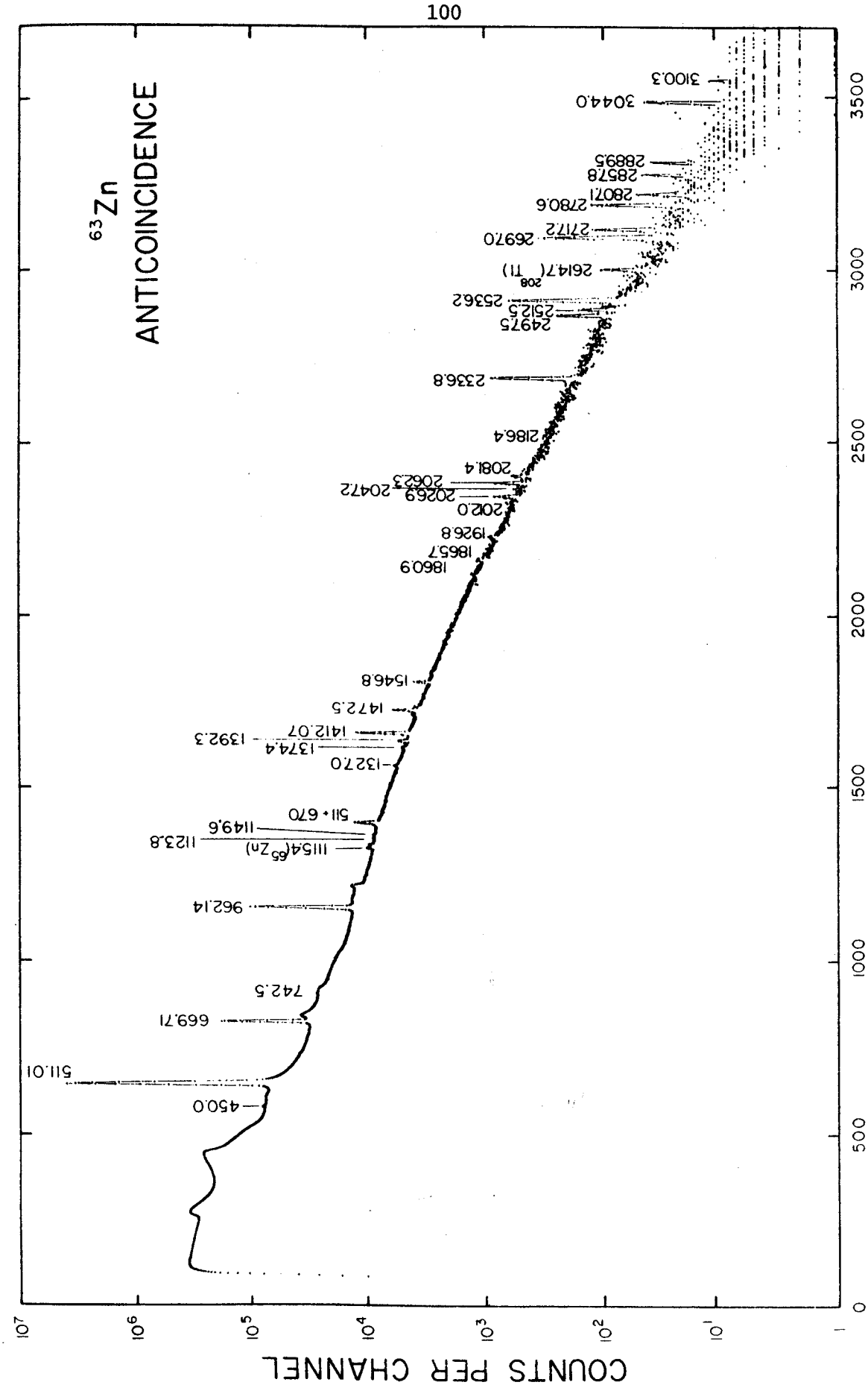

Fig. 35. An anticoincidence spectrum from the decay of ^{63}Zn.

Ge(Li) detector. The two halves of the annulus were operated separately and each was gated on the 511-keV region. A triple coincidence was required between the two annulus halves and the Ge(Li) detector in order to count the γ-ray observed by the Ge(Li) detector. A further description was given in Section 2.1.2.A. A spectrum obtained from this experiment is shown in Figure 36, and the results are included in Table 6.

The experimental results show β^+ feeding to the 670-, 962-, 1412-, and 1547-keV states. An upper limit of 0.02% has been placed on the β^+ feeding to the 1327-keV state. All states above 1547 keV are fed too weakly to be observed in this spectrum. A comparision of the measured β^+ feeding to the states to those predicted from calculated ε_K/β^+ ratios (Le66) is given in Table 7. The experimental values were normalized to the predicted ε_K/β^+ ratio for the ground state and the ratio of the 670-keV γ intensity to the 511-keV intensity as measured by Borchert (Bo69). The differences between the experimental and theoretical values for the first two excited states is small, but it is very large for the other two β^+-fed states. This is another case where the apparently allowed β decay is "hindered" as indicated by the lower than predicted β^+ feeding. A further discussion of the nature of these levels is given in Section 5.6.

5.4. Decay Scheme

Figure 37 shows the decay scheme deduced from our experiments. Transition and excited-state energies are in keV, with the adopted energies for the levels being a weighted average of several experimental runs. The Q_ε of 3364 keV was obtained from $^{63}Cu(p,n)$ measurements by Birstein et al. (Bi66). The total transition intensities, in percent of total ^{63}Zn decay, are given in the decay scheme. Since all the internal

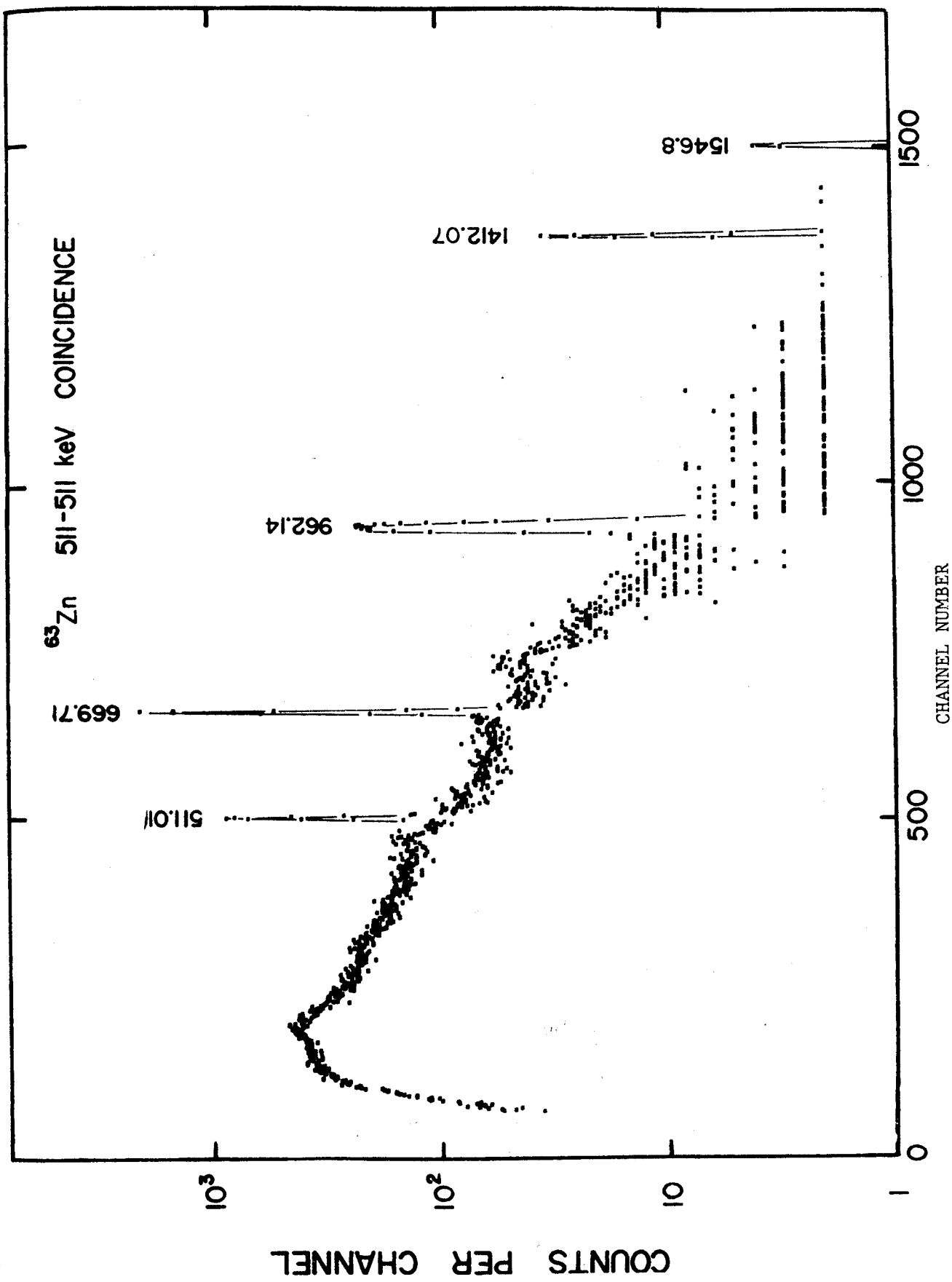

Fig. 36. A 511-511-γ triple coincidence spectrum obtained using the NaI(Tl) annulus and the 2.5% efficient Ge(Li) detector.

Table 7.

Comparison of Experimental and Theoretical β^+ Feedings for ^{63}Zn.

Level (keV)	β^+ Feeding		ε_K/β^+	
	Experimental	Theoretical	Experimental	Theoretical
670	7.54%	7.32%	0.0942	0.127
962	5.23%	5.23%	0.232	0.232
1412	0.33%	0.52%	1.91	0.840
1546	0.032%	0.055%	3.19	1.41

Theoretical results are from Le66.

conversion coefficients would be less than 0.5% of the transition intensity, they were ignored. From the measured relative β^+ feedings, the I_{670}/I_{β^+} ratio measured by Borchert (Bo69), and the theoretical ε_K/β^+ ratio for the ground state, the total intensity of the 670-keV γ was calculated. The total feeding intensities for decay to each state were then calculated based on the transition intensities relative to the 670-keV γ. These total feeding are given in the decay scheme to the right of the energy levels with the exponents given in parentheses. Log ft values based on them appear in italics at the extreme right of the levels. A comparison of these results with those of charged particle scattering reactions was shown in Figure 32. Three weak γ rays were not placed.

5.5. Spin and Parity Assignments

Ground State

The ground state of stable ^{63}Cu is assigned $I^\pi=3/2^-$ on the basis of the results of many charged particle scattering experiments as well as those of many other types of experiments, e.g., atomic beams, etc. The log ft for the feeding to this state is 5.4, which agrees well with an allowed decay from the $3/2^-$ ground state of the ^{63}Zn parent.

669.71-, 962.14-, and 1327.0-keV States

These states have been observed many times in scattering reactions and have been assigned $I^\pi=1/2^-$, $5/2^-$, and $7/2^-$, respectively. The log ft's for the first two excited states are well within the range of allowed β decay. This is expected from the scattering results. No decay is observed to the 1327-keV state, this in keeping with it being a second-forbidden decay, which would have a log ft in the range 10-14. A detailed comparison with results predicted by a number of calculations for these states is given in Section 5.6.

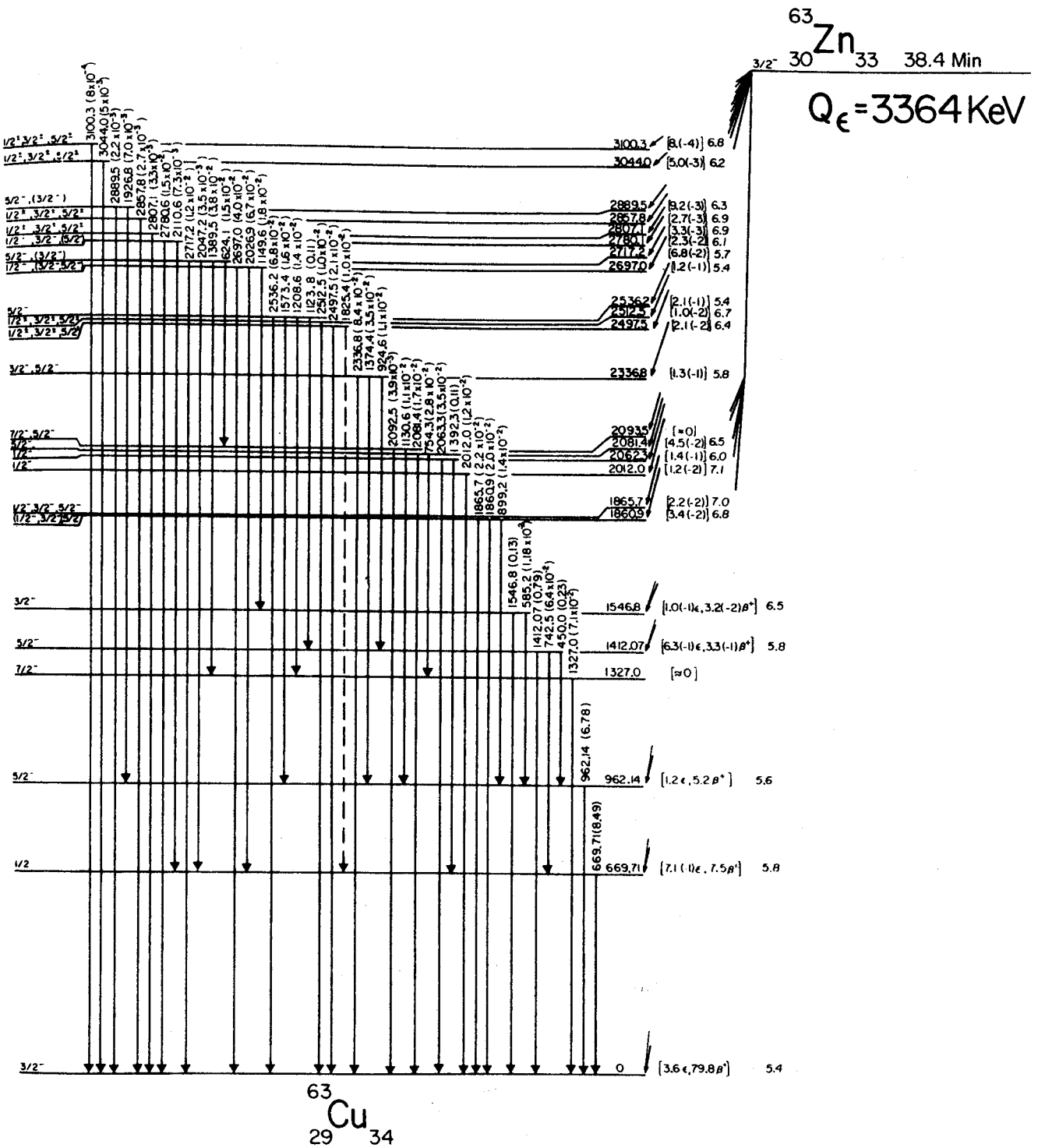

Fig. 37. Proposed decay scheme for ^{63}Zn.

1412.07-keV State

The results of many scattering experiments suggest $I^{\pi}=5/2^{-}$ for this state. The log ft of 5.6 which falls in the range of an allowed transition supports this assignment. Although the evidence is not conclusive, this assignment is supported by the existence of the strong 450-keV transition to the 962-keV ($5/2^{-}$) state, a weak 742-keV transition to the 670-keV ($1/2^{-}$) state, and a very strong transition to the ground state ($3/2^{-}$).

1546.8-keV State

decay to this state has a log ft of 6.5 suggesting an allowed decay or a fast first-forbidden transition. Since the only positive parity orbital in this shell, the $1g_{9/2}$, is at ≈2510 keV (B165) and the first negative parity state in the ^{62}Ni core is a 3^{-} state at ≈3700 keV, it is expected that positive parity levels should be first observed somewhere above 2 MeV. This state is therefore fed by what appears to be an allowed transition. Although not commonly observed in scattering reactions, ^{64}Zn(τ,α) and ^{63}Cu(d,d') (Ba65) results indicate $I^{\pi}=3/2^{-}$. In addition to the decay to the ground state this state has a weak γ transition to the 962-keV state. Thus, the γ-ray data are consistant with the $3/2^{-}$ assignment for this state.

1860.9- and 1865.7-keV States

These two states are considered together, since previously only one state has been reported in this region. That state was described as $7/2^{-}$ from the ^{64}Zn(τ,α) results. However, the log ft's of 6.8 and 7.0, respectively, indicate a slow, allowed (eliminating first-forbidden as above) β transition to each state, which would limit the spins to 5/2 at most. The 1860-keV state is observed to decay

almost equally to the ground and second excited states, while the 1865-keV state appears to decay to the ground state. This suggests an $I^{\pi}=(1/2^{-})$, $(3/2^{-})$, $5/2^{-}$ for the 1860-keV state and $1/2^{-}$, $3/2^{-}$, $5/2^{-}$ for the 1865-keV state.

2012.0-keV State

A log ft of 7.0 indicates a slow allowed β transition to this state, which is observed to decay solely to the ground state. Scattering reactions assign $I^{\pi}=1/2^{-}$ to this state. The present work is consistent with this assignment.

2062.3-keV State

This state decays to the 670-keV state with about three times the intensity of that to the ground state. The log ft for β feeding to this state is 6.0. The assignment of $I^{\pi}=1/2^{-}$ agrees with scattering results.

2081.4-keV State

The β feeding to the 2081-keV state produces a log ft of 6.5. The state in turn decays about twice as fast to the 1327-keV state as to the ground state. Since the 1327-keV state has $I^{\pi}=7/2^{-}$, the 2081-keV state is limited to $I^{\pi}=3/2^{-}$ or $5/2^{-}$. Although there is no observed decay to either $5/2^{-}$ state (a transition to the 1412-keV state would fall under the 670-keV), this state is assigned $I^{\pi}=5/2^{-}$.

2092.5-keV State

The decay of this state to the 962-keV state $(5/2^{-})$ is about three times the intensity of the decay to the ground state $(3/2^{-})$. In addition, this state receives no observable β feeding. The $^{64}Zn(\tau,\alpha)$ results indicate $I^{\pi}=7/2^{-}$. The present results agree with this assignment, although $I^{\pi}=5/2^{-}$ would also be possible.

2336.8-keV State

The 2337-keV state has a transition to the ground state ($3/2^-$), a transition with half the intensity to the 962-keV state ($5/2^-$), and an even weaker one to the 1412-keV state ($5/2^-$). The log ft for β decay to this state is 5.8, indicating most likely an allowed transition. This limits I^π to $1/2^-$, $3/2^-$, or $5/2^-$. The ^{64}Zn(t,α) results indicate a $3/2^+$ state, while the ^{62}Ni(τ,d) results indicate it to be $5/2^-$. Since there is no agreement in the scattering results, I^π of $3/2^-$ or $5/2^-$ is assigned to this state.

2497.5-keV State

β decay to this state has a log ft of 6.4 suggested an allowed or first forbidden ε decay to it. This state decays to the ground state and perhaps to the 670-keV level ($1/2^-$). The second transition has been placed by the energy difference even though the agreement was ≈2.5 keV. This state is therefore assigned $I^\pi=1/2^\pm$, $3/2^\pm$, or $5/2^\pm$. We are now in the region where positive parity states might be expected.

2512.5-keV State

This state has a single decay to the ground state and a log ft of 6.7 from ε feeding. These place few limits on the assignment of this state, only that it is $1/2^\pm$, $3/2^\pm$, or $5/2^\pm$. The results of many different scattering experiments shown in Figure 32 indicate a $9/2^+$ state at ≈2510 keV. Although this assignment would be incompatible with the feeding to and decay from this level, it is consistent with the overall ^{63}Cu results, since Mazari et al. (Ma57) report two states in this region, at 2504 and 2510 keV. The state observed in scattering could be the 2504-keV one, while the one observed in β decay experiments could be their 2510-keV level. The present assignment for the 2512-keV state is $1/2^\pm$, $3/2^\pm$, or $5/2^\pm$.

2536.2-keV State

This state has a multitude of γ transitions proceeding from it. In addition to the ground state decay ($3/2^-$), there is a γ transition of twice the intensity to the 1412-keV state ($5/2^-$), and two, each with $\simeq$1/4 the intensity, to the 1327- ($7/2^-$) and 962-keV ($5/2^-$) states. The log ft to this state is 5.4, indicating a strongly allowed transition. The assignment for this state is $I^\pi=5/2^-$.

2697.0-keV State

This state has a ε feeding with a log ft of 5.4 to it and three γ transitions proceeding from it. In addition to the ground-state decay, there is a γ transition of about 1.7 times the intensity to the 670-keV ($1/2^-$) state and one with about half the intensity to the 1547-keV ($3/2^-$) state. The ^{62}Ni(τ,d) reaction indicates $I^\pi=1/2^-$. γ-ray results are consistent with this assignment, although the $3/2^-$ and $5/2^-$ possibilities cannot be excluded.

2717.2-keV State

This state has, in addition to its ground-state decay, a decay to the 1327-keV ($7/2^-$) state of three times the intensity, one with the same intensity to the 2092-keV state, and one with one-third the intensity to the 670-keV ($1/2^-$) state. The log ft of 5.7 indicates an allowed ε transition. All of this limits the assignment to $I^\pi=3/2^-$ or $5/2^-$, with $5/2^-$ being the more probable based on γ ray intensities.

2780.6-keV State

This state decays to the 670-keV ($1/2^-$) state with about half the intensity of the ground-state decay. The log ft from the feeding is 6.1. This suggests an assignment of $I^\pi=1/2^-$, $3/2^-$, or perhaps $5/2^-$. Although a positive parity is possible, it is not probable. The results

of the ^{62}Ni(τ,d) reaction indicate an assignment of $3/2^-$.

2807.1- and 2857.8-keV States

Both states are ε fed with a log ft of 6.9 and have only a ground-state γ transition. They are therefore assigned $I^\pi=1/2^\pm$, $3/2^\pm$, or $5/2^\pm$, since both allowed and first forbidden ε decay are possible.

2889.5-keV State

The 2889-keV state has a γ transition to the 962-keV ($5/2^-$) state that is about three times the intensity of its ground-state transition. The log ft of 6.3 suggests an allowed transition but with a first forbidden decay not ruled out. The assignment for this state is most likely $I^\pi=5/2^-$ or perhaps $3/2^-$. The ^{62}Ni(τ,d) data indicate a $1/2^-$ state at $\approx$2880 keV.

3044.0-keV State

This state has an ε feeding with a log ft of 6.2 and only a ground-state γ transition. An assignment of $7/2^-$ is indicated from the results of the ^{64}Zn(t,α) reaction but could be for the level at 3032 keV reported by Mazari et al. (Ma57), since the low log ft would suggest an allowed transition. This state is therefore assigned $I^\pi=1/2^\pm$, $3/2^\pm$, or $5/2^\pm$.

3100.3-keV State

The ε feeding to this state has a log ft of 6.8, and the state has only a ground-state γ transition. It is therefore assigned $I^\pi= 1/2^\pm$, $3/2^\pm$, or $5/2^\pm$.

5.6. Systematics

Many authors have performed calculations on the ^{63}Cu nucleus. The most commonly used approach is using a quadrupole-quadrupole interaction to couple the odd proton to the ground state and the first

excited state, a 2^+ state, at 1172 keV in ^{62}Ni. Configuration admixing of the $2p_{3/2}$, $2p_{1/2}$, and $1f_{5/2}$ single particle proton states also needs to be included. Results of calculations including those using other approaches are shown in Figure 38. The percent single particle admixtures are shown when available. A percentage of zero indicates the particular single-particle state that could mix was not used in the calculations. The experimental admixtures are from the ^{62}Ni(τ,d)^{63}Cu reaction of Blair (B165).

Lawson and Uretsky (La57) applied the "center of gravity" theorem of atomic j-j coupling to the ^{63}Cu nucleus by assuming that the nucleus was a $2p_{3/2}$ proton coupled to the ^{62}Ni even-even core. The first four excited states of ^{63}Cu were then considered to be the quartet formed by coupling the proton to the 2^+ vibrational first excited state of ^{62}Ni. By applying this formalism and using the 1412-keV state in ^{63}Cu as the $3/2^-$ member of the quartet, a center of gravity for the 2^+ level was obtained at 1167 keV which compared well with the experimentally determined energy of 1172 keV. Later experiments showed the 1412-keV state to be $5/2^-$ and the necessary $3/2^-$ state has not been found below 2 MeV. No single particle admixtures were used in the calculations.

A "unified" model was used by Bouten and Van Leuvén (Bo62). The ^{62}Ni core was allowed quadrupole surface oscillations with no more than two phonons. The odd proton was in the $2p_{3/2}$, $2p_{1/2}$, or $1f_{5/2}$ states and coupled to the surface oscillations. The ground state and first two excited states were used as input parameters to obtain the single-particle level spacings. Good agreement was reached between calculated and experimental values for the electric quadrupole moment and for the $\tau(E2)$, the transition half-life, for the first two excited states. Althrough agreement

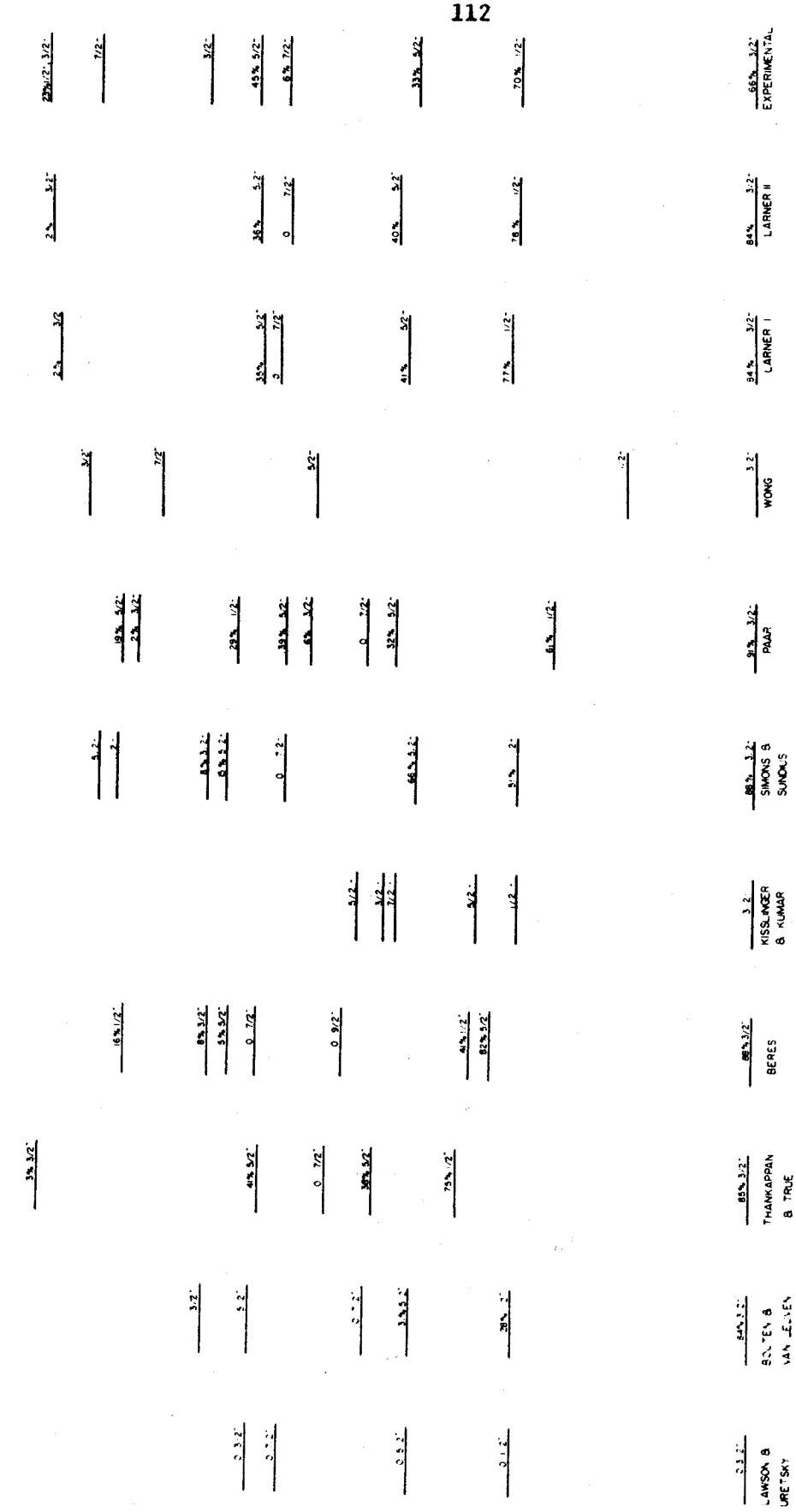

Fig. 38. Results of calculations of excited states in ^{63}Cu.

within a factor of two was also reached for the $\tau(M1)$ for these transitions, poor agreement was reached for the magnetic dipole moment.

Gove (Go63) applied the calculations of Bayman and Silverberg (Ba60) for coupling a $j=3/2$ particle to quadrupole surface oscillations to the case of ^{63}Cu. These calculations are in good agreement with the observed $B(E2)$'s. Harvey (Ha63) extended the Bayman-Silverberg model to the magnetic dipole moment and transition probabilities. He obtained good agreement for the dipole moment and for the $B(M1)$ for the transition from the 962-keV state, but his results were a factor of four faster than the $B(M1)$ experimentally obtained for the 670-keV transition.

A strong coupling model was used by Thankappan and True (Th65). The even-even ^{62}Ni core which performs quadrupole surface oscillations was coupled by a quadrupole interaction with a dipole element added to the single proton in the $2p_{3/2}$, $2p_{1/2}$, and $1f_{5/2}$ orbitals. Only the 0^+ ground state and 2^+ first excited state of ^{62}Ni were considered in this calculation. Parameters also used were the orbital spacings of Bouten and Leuvén (Bo62), however, these were adjusted for better agreement of the calculations with the experimental results. The agreement for the calculated $B(E2)$'s with experimental results is good, but the fits of the $B(M1)$'s vary from good to very bad. Also, the quadrupole moment is in good agreement as is the dipole moment.

Beres (Be66) used a very different model, namely he described the core as a quasiboson of angular momentum 2^+ and the odd proton as a quasiproton of spins $1/2^-$, $3/2^-$, and $5/2^-$. The core and the quasiproton were coupled by a quadrupole interaction. The resulting calculated $B(E2)$'s were in general agreement with experimental results. He also calculated the case of two quasineutrons interacting via a quadrupole

interaction with the quasiproton. This method gives a large number of low lying levels, and the collective quartet appears very closely spaced at about 2 MeV with the $B(E2)$ values for this quartet in agreement with those of the other method. This method, however, gives much better agreement for the higher lying positive parity states in ^{63}Cu, and good agreement is also obtained between the calculated inelastic α scattering cross sections and those observed experimentally.

The model used by Kisslinger and Kumar (Ki67) is a modified phenomenological vibrational model with its microscopic description in terms of the pairing-plus-quadrupole model. This involves the coupling of the vibrational phonon with a quasiparticle with a quasirandom phase approximation.

Simons and Sundius (Si69) used a vibrational core with up to three phonons coupled to a single particle in the $2p_{3/2}$, $2p_{1/2}$, and $1f_{5/2}$ states. They treated the phonon energy as a free parameter and obtained values somewhat greater than those of Bouten and Van Leuvén. They obtained a reasonable fit for the magnetic dipole and electric quadrupole moments, and the fits to the $B(E2)$ and $B(M1)$ for the 670-keV transition are reasonable. However, the $B(M1)$ for the 962-keV transition does not fit well at all.

A semimicroscopic model of coupling the proton to a quadrupole vibrator was used by Paar (Pa70). The vibrator was allowed up to three phonons and the proton states included the $2p_{3/2}$, $2p_{1/2}$, $1f_{5/2}$, and $1f_{7/2}$ states. The $1f_{7/2}$ was included since experimental results indicate that the $1f_{7/2}$ is not a good closed shell in this case but is partially empty producing a partially filled $2p_{3/2}$ state. Reasonably good fits were obtained for the $B(M1)$ and $B(E2)$ values and for the magnetic dipole and

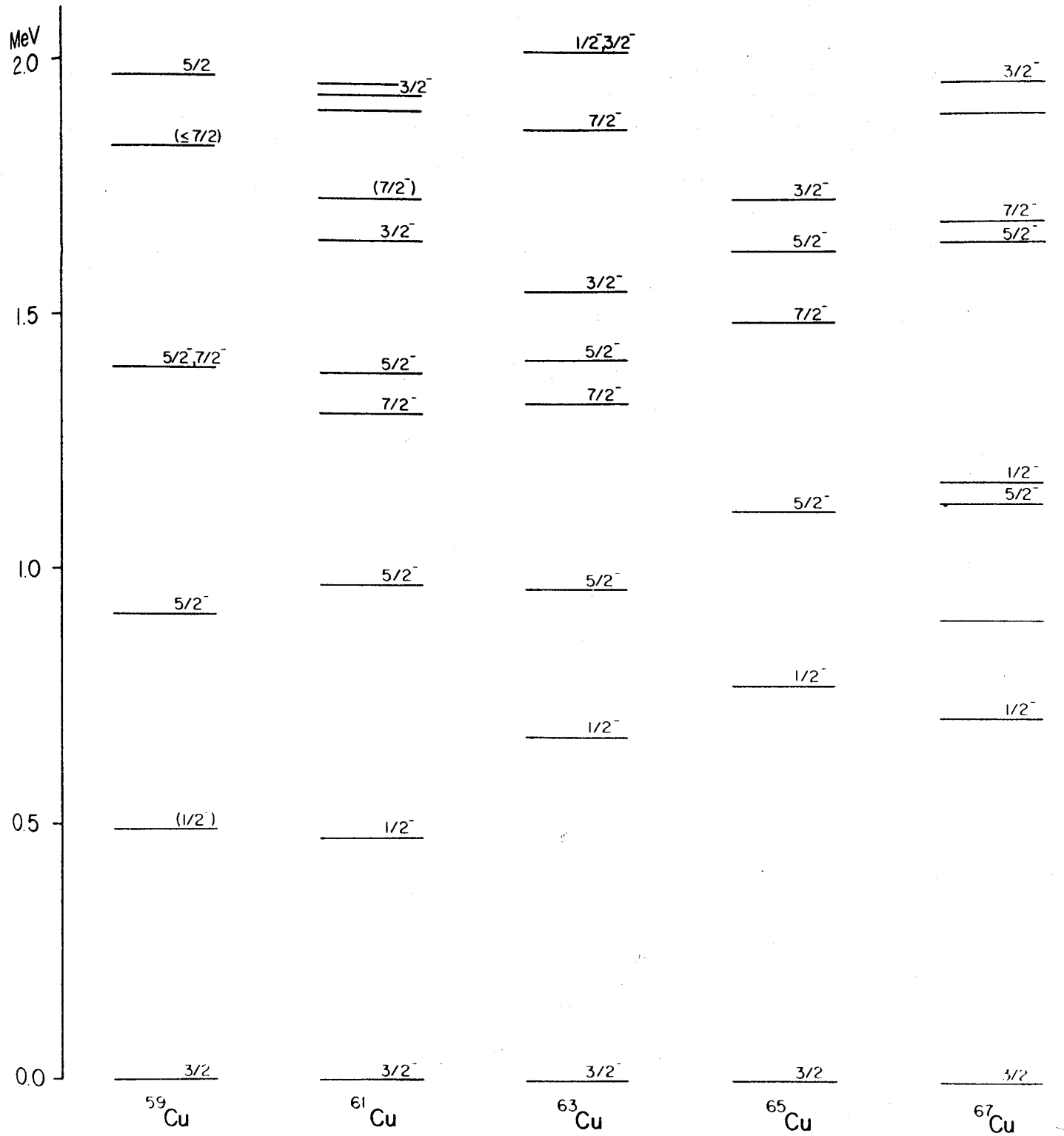

Fig. 39. Systematics of the odd mass Cu isotopes. The results shown are from ND.

electric quadrupole moments.

Wong (Wo70) performed shell model calculations for the ^{63}Cu using a weak coupling model with the $2p_{3/2}$, $2p_{1/2}$, and $1f_{5/2}$ orbitals for the proton. The energy levels produced by the shell model calculations are in poor agreement with the experimentally determined energy levels. The fits for the $B(M1)$'s and $B(E2)$'s were only fair, although better agreement was reached for the magnetic dipole and electric quadrupole moments.

The intermediate coupling model developed by Thankappan and True (Th65) was used by Larner (La70) to calculated the states in^{63}Cu. For the calculations, Larner coupled the 0^+ ground state and 2^+ first excited state of ^{62}Ni to the $2p_{3/2}$, $2p_{1/2}$, and $1f_{5/2}$ orbitals with an interaction that contained both dipole and quadrupole terms. For the first case, he used the experimental energy levels and single-particle strengths as input parameters, while the second case used the experimental energy levels and $B(E2)$ values. The results of both cases gave similar good fits to the energy levels, and the first case also gave good fits to the $B(E2)$'s.

Although most of the calculations agree on single particle admixtures, they are in disagreement with the experimental results. In particular, everyone except Paar (Pa70) assumes that the $1f_{7/2}$ shell is a good closed shell. The experimental results indicate the 1327-keV $7/2^-$ state has a 6% single particle admixture which would come from the $1f_{7/2}$ closed shell. This agrees with the results of Goode et al. (Go69) which indicate that ^{56}Ni is only 94% a doubly closed nucleus.

Figure 39 shows a comparison of the levels of the odd mass Cu isotopes. A comparison with the other Cu isotopes indicates the 1400-keV level in ^{59}Cu may be an unresolved doublet of a $5/2^-$ and a $7/2^-$ level. In general, the excited states rise in energy with neutron number.

CHAPTER VI

DECAY OF ^{62}Zn

6.1. Introduction

The odd-odd nuclide, $^{62}_{29}Cu_{33}$, contains a single proton and five neutrons outside the doubly closed $1f_{7/2}$ shell. Consequently, its states should be amenable to interpretation in fairly straightforward shell-model terms. Also, many states and trends in nearby odd-mass nuclei are known, providing reasonably trustworthy input for predicting the properties of its odd-odd states. Unfortunately, relatively few states are known in ^{62}Cu itself, and even fewer have been well characterized. Here, the decay of 9.3-h ^{62}Zn to ^{62}Cu has been reexamined using the largest Ge(Li) detectors the laboratory has been able to obtain in order to pick up weak β feedings that previously have gone undetected. The findings are then correlated with those of previous investigators and with the data from scattering reactions in an attempt to obtain a more coherent understanding of the structures of the ^{62}Cu states.

Since the discovery of ^{62}Zn by Miller et al.(Mi48), it has been studied by many other groups. Hayward (Ha50) determined the end-point energy of its β^+ spectrum to be 0.66±0.01 MeV and observed K and L conversion electrons from the 41.8±0.8-keV transition, the K/L ratio indicating it to be $E1$ or $M1$. Nussbaum et al. (Nu54) determined that the first excited state of ^{62}Cu lies at 41.3±0.3 keV and that 36±3% of the ^{62}Zn feeding passes through this state. From α_K and $K/(L+M)$ they assigned the 41.3-keV transition an $M1$ multipolarity.

The first reasonably complete decay scheme was formulated by Brun et al. (Br57) who performed extensive electron and NaI(Tl) γ-ray spectroscopy, including coincidence and γ-γ angular correlation

experiments. They deduced states in ^{62}Cu at 0, 0.042, 0.30, 0.55, 0.63, and 0.70 MeV.

In the last few years there has been a flurry of activity about the neutron-deficient members of the N=62 mass chain. Four groups (An67, Ro67, Ba68, Ho69) have reported Ge(Li) γ-ray studies on the decay of ^{62}Zn, and two other groups (Jo69, Va70) have reported on the decay of 9.9-min ^{62}Cu itself. Antman et al. (An67) performed the first high-resolution Ge(Li) γ-ray experiments (in conjunction with electron experiments), and they and Roulston et al. (Ro67) demonstrated conclusively the doublet nature of the ≈245-keV γ-ray peak and the existence of a 507.6-keV γ. These data were essential to the construction of a correct decay scheme, and the two groups arrived at almost identical decay schemes containing the first five excited states in ^{62}Cu that are populated by ^{62}Zn decay. The most precise half-life determination for ^{62}Zn, 9.2±0.1 h, is also the work of Antman et al. Bakhru (Ba68) also performed high-resolution Ge(Li) γ-ray spectroscopy, including coincidence experiments, and he measured the half-life of the 42-keV state to be 2.5±0.1 nsec. His decay scheme, however, differs in several placements from the others. The most recent paper on ^{62}Zn decay, by Hoffman and Sarantites (Ho69), again includes results from γ-γ coincidence experiments and shows a decay scheme almost identical to those of An67 and Ro67.

Nuclear reaction and in-beam studies have been reported, also. Davidson et al. (Da70) have used the ^{62}Ni(p,$n\gamma$) reaction to study the decay of the excited states in ^{62}Cu. They performed γ-ray angular correlations in addition to γ-ray singles measurements at various excitation energies in order to learn something about spins and parities as well as placements of the states. Fanger et al. (Fa70) report on similar

techniques using the $^{61}Ni(n,\gamma)$ reaction to study states in ^{62}Ni.

The points yet to be clarified are clear: 1) None of the groups studying ^{62}Zn decay was able to detect any γ rays with energies above 637 keV, although Q_ε is ≈1620 keV. Part of this problem came from the interference of γ rays from ^{62}Cu itself, which quickly grows into the sources. But now that the decay of ^{62}Cu is known (Jo69, Va70, Fa70) with some assurance, weak γ rays from ^{62}Zn can perhaps be distinguished more readily. Also, the larger Ge(Li) detectors now available, having very good peak-to-Compton ratios, should allow one to detect very weak higher-energy γ rays. 2) Very little in the way of interpretation of the structures of the ^{62}Cu states has been done. Both sides of the problem have been attacked with the following results. 1) Six new weak γ-rays that deexcite four new excited states in ^{62}Cu can be reported. 2) The structures of the ^{62}Cu states have been examined in terms of shell model states and the trends observed in this nuclear region, and this very straightforward method has been found to explain much of what is observed.

6.2. Source Preparation

The ^{62}Zn sources were prepared by irradiating natural Cu foils (69.17% ^{63}Cu, 30.83% ^{65}Cu) with 25-MeV protons accelerated by the MSU Sector-Focused Cyclotron. The reaction of interest was $^{63}Cu(p,2n)^{62}Zn$. Typically, ≈150-mg targets were bombarded with a 1-μA beam for 30-45 min. The only Zn contaminant of any consequence was 38-min ^{63}Zn, which was essentially eliminated by waiting 4 hours before counting the ^{62}Zn sources. All other possible contaminants were removed using the chemical separation described in Section 2.3.

6.3. γ-Ray Spectra

Many γ-ray spectra were taken over a long period of time, always using the largest Ge(Li) detectors at our disposal. Spectra were taken with the 2.5% and 3.6% efficient detectors, although most of the spectra were taken with the 10.4% efficient Ge(Li) detector. A typical spectrum taken with the 10.4% efficient detector is shown in Figure 40. As it was mandatory that the higher-energy portion of the spectra be optimized yet maintain a high counting rate in order to minimize stray background peaks that could mask the weak ^{62}Zn peaks, the spectra were taken through a set of absorbers and with the geometry shown in Figure 41.

Each sample was counted for several consecutive 6-h periods to insure that the peaks observed came indeed from ^{62}Zn decay. In addition to the normal procedures, however, an on-the-spot efficiency calibration with ^{110m}Ag and a background count of at least 12 h were performed for each sample. A spectrum obtained in 6 h with the 10.4% detector using the absorbers is shown in Figure 42. Note that six very weak higher-energy γ rays attributed to ^{62}Zn decay can be seen in this spectrum.

The centroids and areas of the photopeaks were determined by using the computer program SAMPO. The secondary energy calibration was performed using the stronger peaks of ^{62}Zn, its ^{62}Cu daughter, and the ^{40}K present in the natural background. The efficiency calibration for the spectra obtained both with and without the absorbers was performed using the method described in Section 2.1.3. The energies and relative intensities of the ^{62}Zn γ rays are listed in Table 8, where they are compared with the results of the other investigations that used Ge(Li) detectors. Since the point of the investigation was specifically to obtain new information about weak transitions, no coincidence experiments

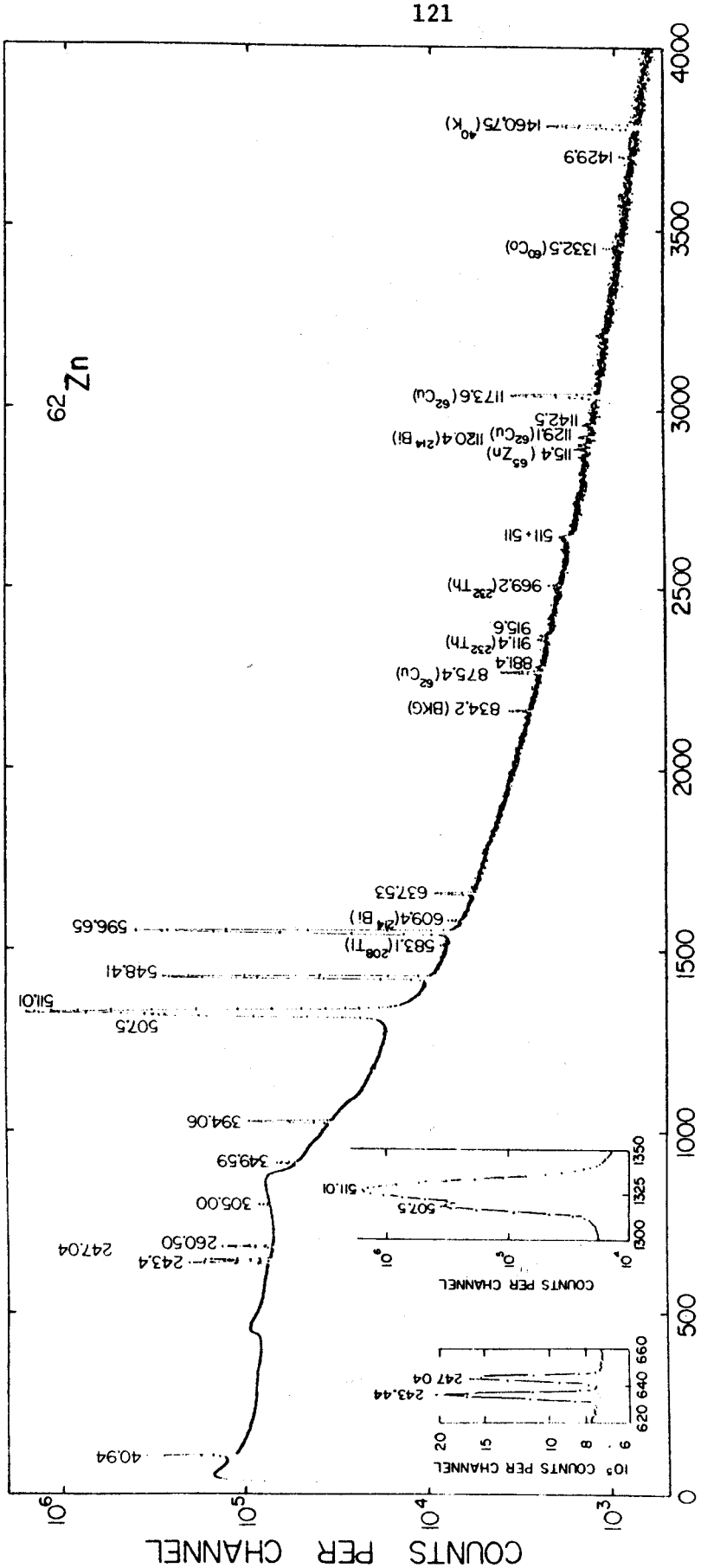

Fig. 40. A typical γ-ray spectrum of ^{62}Zn taken without absorbers. The insets show the regions at 245 keV and 511 keV in greater detail.

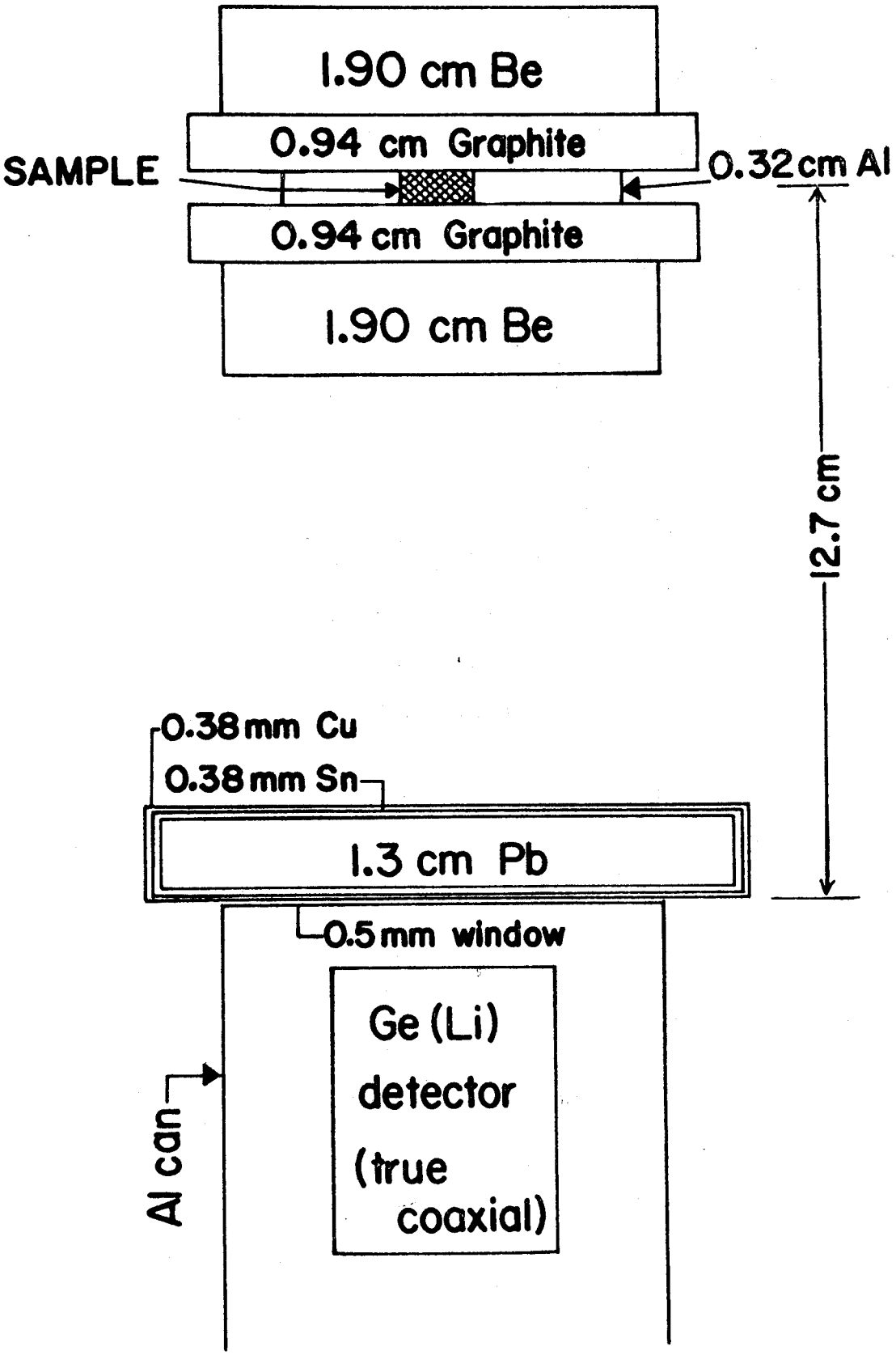

Fig. 41. A diagram of the sample and absorber placement used to study ^{62}Zn decay.

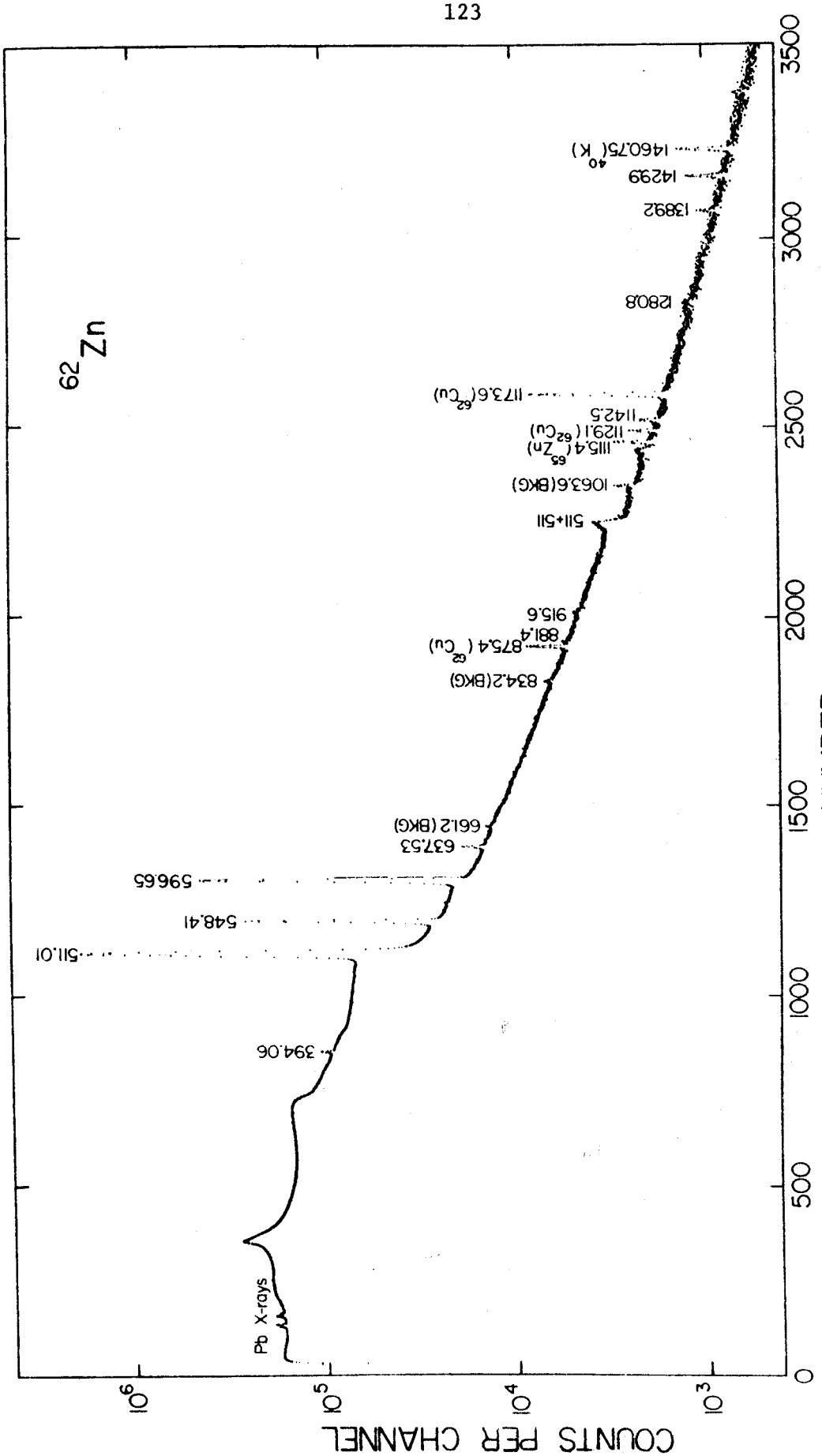

Fig. 42. A typical 6-h γ-ray spectrum of ^{62}Zn decay taken using the absorbers as shown in Figure 41.

Table 8. Energies and Intensities of γ Rays Following the Decay of ^{62}Zn

This Work		Antman, Pettersson and Suarez (An67)		Roulston, Becker, and Brown (Ro67)		Bakhru (Ba68)		Hoffman and Sarantites (Ho69)	
E_γ(keV)	I_γ	E_γ(keV)	I_γ	E_γ(keV)	I_γ[a] (±10%)	E_γ(keV)	I_γ	E_γ(keV)	I_γ
40.94±0.06	104±10	40.88±0.09	(102)[b]	41.5±0.2	(192)	42	100±5	40.84±0.13	99.4±3.5
243.44±0.03	11.1±0.5	243.40±0.05	≈7	243.7±0.5	15			243.43±0.20	10.3±0.5
247.04±0.04	8.3±0.4	247.02±0.09	≈4 11.0±0.9	247.2±0.5	12	245	10±1	247.02 0.20	8.2 0.3
260.50±0.06	5.9±0.3	260.44±0.10	2.6±0.5	260.7±0.5	8	260	4±1	260.39±0.08	5.9±0.1
305.00±0.07	1.24±0.1	---	---	305.5±1.0	0.8	---	---	304.80±0.20	1.32±0.07
349.59±0.07	1.83±0.1	349.69±0.25	≈1	349.5±1.0	1.5	---	---	349.34±0.11	1.59±0.16
394.06±0.04	9.2±0.4	394.12±0.18	6.2±1.0	394.5±0.5	10.7	395	5±1	393.80±0.06	9.16±0.12
507.5 ±0.4	58 ±10	507.57±0.13	60±15	507.5±1.0	77	505	40±3	507.41±0.15	65 ±15
548.41±0.04	60.8±1.0	548.33±0.22	59±5	548.7±0.5	65	547	60±4	548.25±0.11	62.2±0.9
596.65±0.04	≡100	596.68±0.20	100±8	597.0±0.5	100	595	100±5	596.60±0.11	≡100
637.53±0.06	0.96±0.06	636.9±0.5	≤1	638.5±1.0	1.5	---	---	637.20±0.12	3.45±0.25
---	---	---	---	---	---	682	≈4±2	---	---
881.4±0.8	0.08±0.03	---	---	---	---	---	---	---	---
915.6±0.6	0.08±0.03	---	---	---	---	---	---	---	---
1142.5±0.2	0.13±0.03	---	---	---	---	---	---	---	---
1280.8±1.5	0.03±0.01	---	---	---	---	---	---	---	---
1389.1±0.5	0.05±0.02	---	---	---	---	---	---	---	---
1429.9±0.3	0.13±0.02	---	---	---	---	---	---	---	---

[a] Normalized to $I_{597.0} \equiv 100$, retaining original number of significant figures

[b] Calculated from the adopted value for an M1 transition.

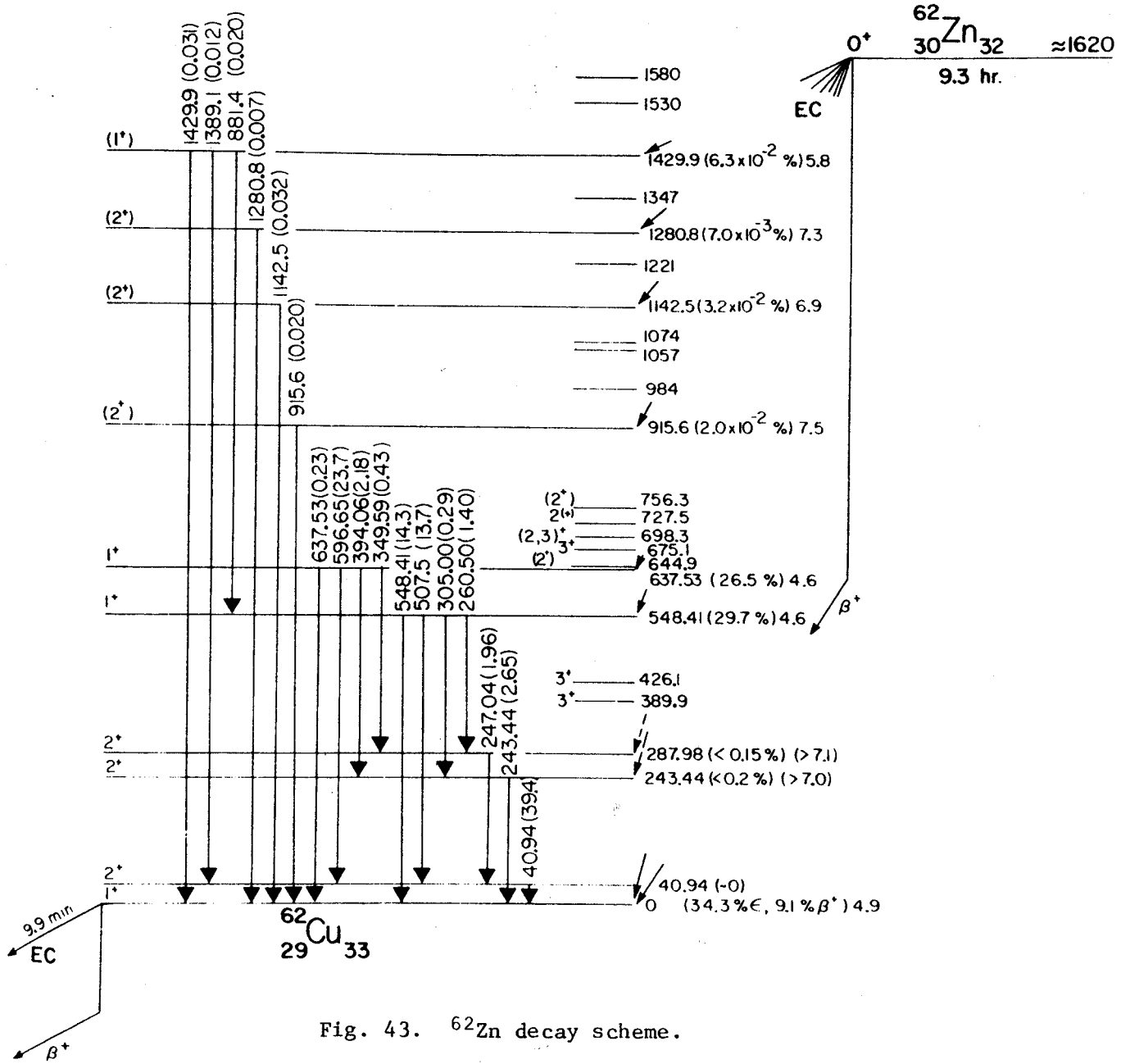

Fig. 43. ^{62}Zn decay scheme.

were performed.

A decay scheme which includes the present work is shown in Figure 43. The levels, spins and parities, and transition placements below 950 keV are from Davidson et al. (Da70), which are consistent with the other results, and the energy levels above 950 keV are from the ^{61}Ni(τ,d) reaction (Mo67). The percent feedings were determined from the percent ground state feeding determined by Hoffman et al. (Ho69) and the relative γ-ray intensities and are found on the right of the decay scheme. The log ft's based on these feedings are on the extreme right.

6.4. Discussion

$_{29}Cu^{62}_{33}$ is an odd-odd nucleus one proton and five neutrons removed from the doubly closed shell at Z=N=28. The simplest approach is to extend the the odd-group model, as normally applied to odd-even and even-odd nuclei. In this model the properties of the nuclear states are assumed to be determined primarily by the odd group of particles. In extending it to odd-odd nuclei it is assumed that the wave functions for the states and the odd-odd nuclei are simple vector-coupled product of wavefunctions of the two odd groups. If it is assumed that the residual p-n interactions are weak compared with spin orbit forces (De61) jj coupling can be used with its simplifications. With the assumption of jj coupling, a given proton and neutron configuration $|\ell_p j_p \ell_n j_n>$, can take on all integral spins, $|j_p - j_n| \leq I \leq j_p + j_n$, where the nature of the residual p-n interaction will determine the ordering of these spins. The modified Nordheim coupling rules proposed by Brennan and Bernstein (Br60) can be useful in predicting the ordering of the spins resulting from a given

configuration. Here j_p and j_n are the single-particle total angular momenta obtained from the adjacent odd-mass nuclei, while ℓ_p and ℓ_n (assumed to be pure) are the orbital angular momenta obtained from the standard shell model assignments.

Examining the systematics of the odd mass Cu isotopes, Figure 39, and the odd mass N=33 nuclei, Figure 44, the ^{62}Cu ground state is assumed to be a $(\pi p_{3/2})(\nu p_{3/2})^{-1}$ configuration for which the coupling rules would predict a ground state of 2^+ with a 1^+ first excited state. However, it is found that these two states are reversed with the 1^+ being the ground state. If the ground state configuration were $(\pi p_{3/2})(\nu p_{1/2})$, the coupling rules would predict the states in correct order. It has been found (Ph68) that there is considerable configuration mixing between these two configurations as well as others which would explain these results.

Table 9 gives the possible proton-neutron configurations in ^{62}Cu and the spins they would produce in approximate order of increasing energy. The individual proton and neutron orbitals are given in order of increasing energy as determined by the odd mass Cu and odd mass N=33 nuclei. Although the proton orbitals remain well behaved, the neutron orbitals are closely spaced and can change ordering rather easily. As a result, the relative positioning of the levels in ^{62}Cu is difficult to predict and considerable configuration mixing can occur. Therefore, a further explanation of the higher-lying states of ^{62}Cu will require more calculations on the orbitals as well as further experimental results. A comparison of the levels in ^{62}Cu with those of other odd-odd Cu isotopes is shown in Figure 45.

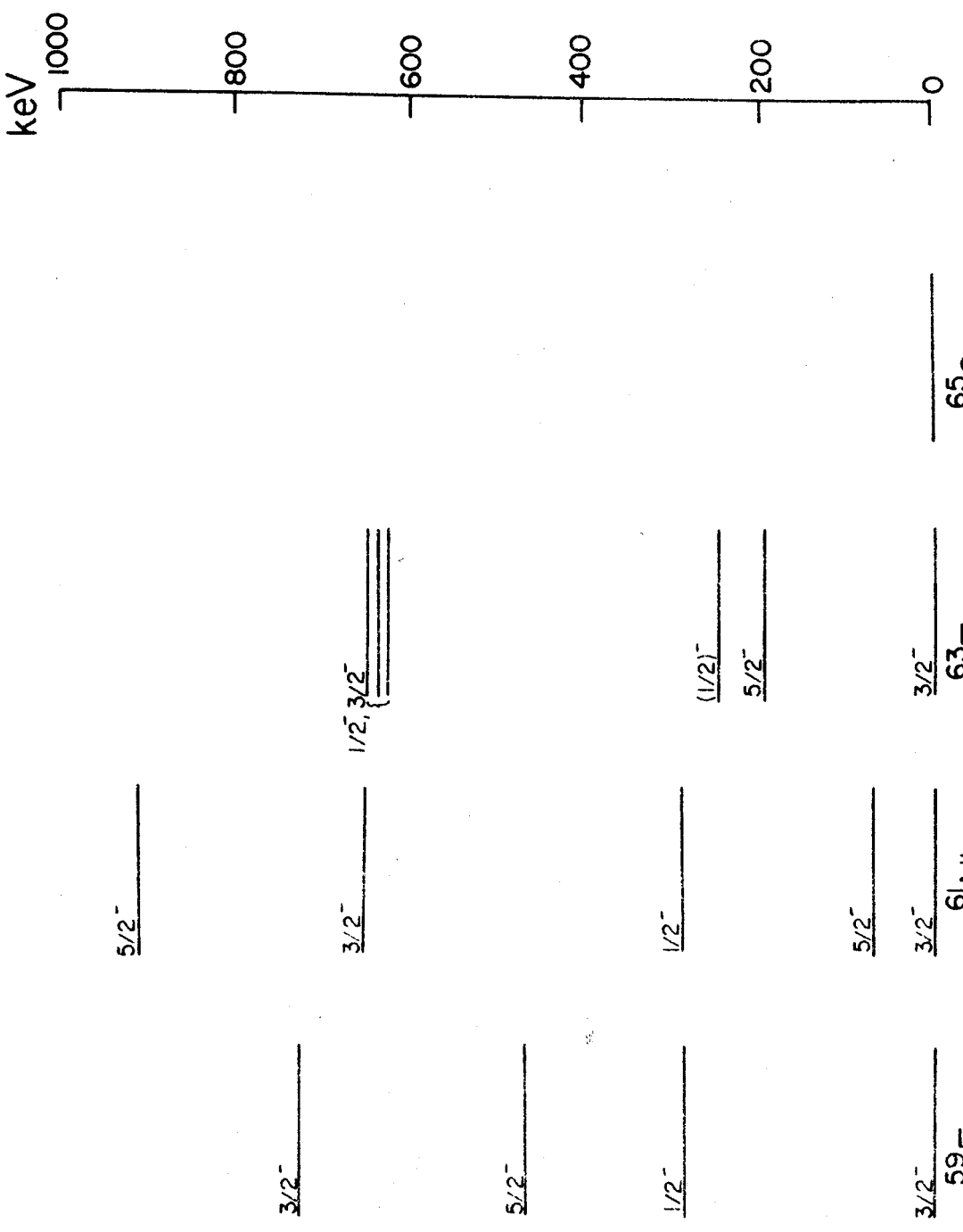

Fig. 44. Systematics of N=33 nuclei. The data is from ^{59}Fe (K167), ^{61}Ni (Co68), and ^{63}Zn (Bi66).

Table 9

States Produced by Some Low-Lying Configurations in Odd-Odd ^{62}Cu.

Proton Orbital	Neutron Orbital	States Produced
$\pi p_{3/2}$	$\nu p_{3/2}$	$2^+_+, 1^+_+, 3^+, 0^+$
	$\nu p_{1/2}$	$1^+_+, 2^+_+$
	$\nu f_{5/2}$	$1^+, 2^+, 3^+, 4^+$
$\pi p_{1/2}$	$\nu p_{3/2}$	$1^+_+, 0^+_+$
	$\nu p_{1/2}$	$1^+_+, 2^+_+$
	$\nu f_{5/2}$	$3^+, 2^+$
$\pi f_{5/2}$	$\nu p_{3/2}$	$4^+_+, 5^+_+, 3^+, 2^+, 1^+, 0^+$
	$\nu p_{1/2}$	$3^+_+, 2^+_+$
	$\nu f_{5/2}$	$1^+, 2^+, 3^+, 4^+$

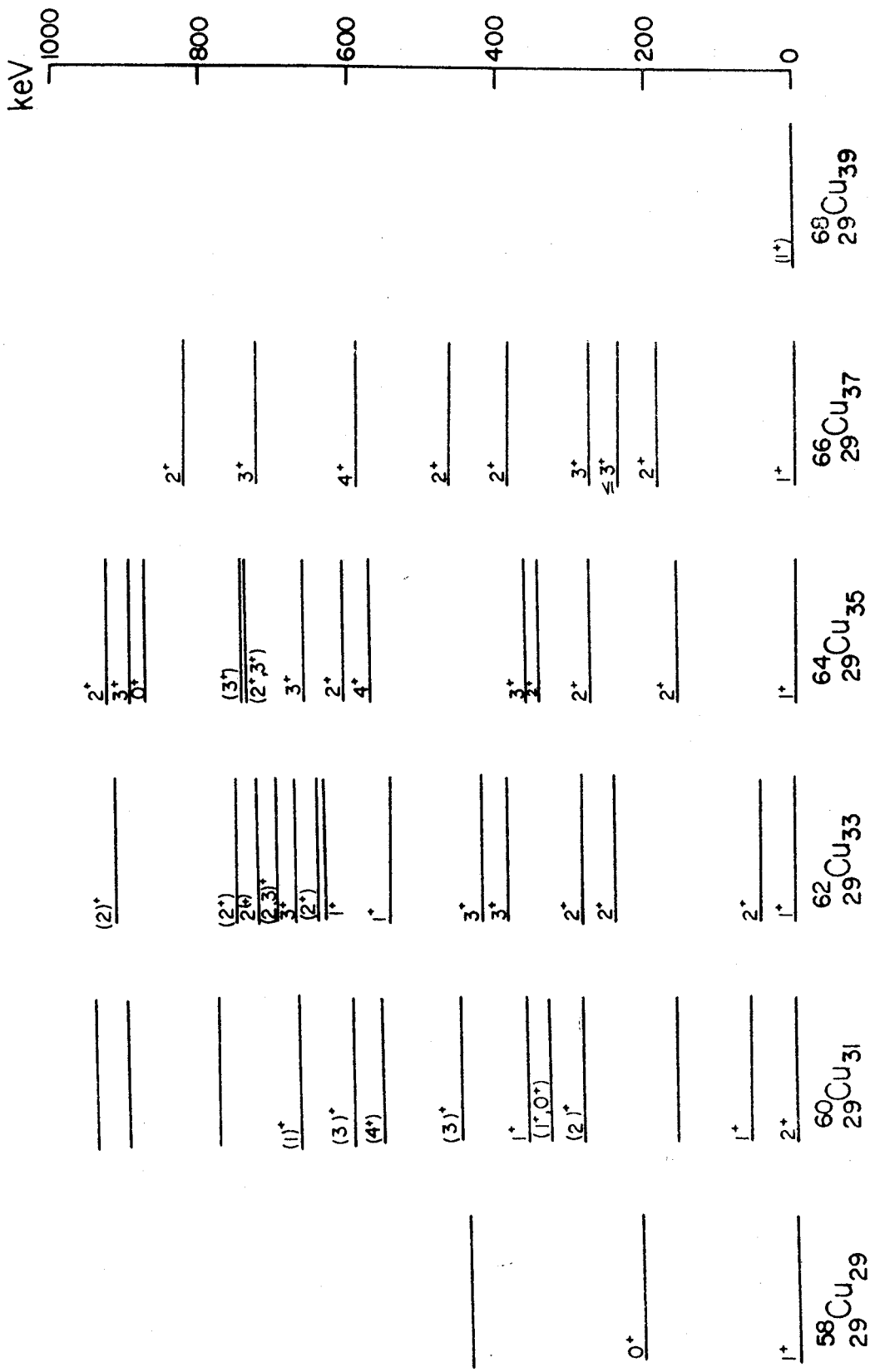

Fig. 45. Systematics of the even mass Cu isotopes. The references are ^{58}Cu (Co67), ^{60}Cu (Yo68), ^{62}Cu (Da70), ^{64}Cu (Ba70), ^{66} Cu (Da69), and ^{68}Cu (Br60).

CHAPTER VII

DECAY OF ^{63}Ga

7.1. Introduction

The first report of the production of ^{63}Ga occurred only recently, in 1965,by Nurmia and Fink (Nu65). It was discovered in their search for β-delayed α emission in the light Ga isotopes. However, the only information they reported was that it had a 33-sec half-life, and they estimated its decay energy at 5.3 MeV. Since then, a study of its decay scheme was reported by Dulfer et al. (Du70).

Other studies of the excited states of ^{63}Zn have been performed by charged particle reactions. Birstein and coworkers have reported results from ^{63}Cu(p,$n\gamma$) (Bi66) and ^{60}Ni(α,$n\gamma$) (Bi67) reactions and have reported the results of γ-ray angular distribution experiments from these reactions (Bi68). Also reported have been other ^{63}Cu(p,n) (Br55a, An62, Mc66, Ta70), ^{64}Zn(p,d) (Jo68), ^{64}Zn(d,t) (Ze60), and ^{64}Zn(τ,α) (Be67, Fo67) results. A composite comparison of these results giving both ℓ and I^{π} values with the present work is shown in Figure 46. The ^{63}Cu(p,n) results have not been reported above 1440 keV.

7.2. Experimental Procedure

The sources for the study of ^{63}Ga decay were produced by irradiating 6-mil and 10-mil thick natural Zn foils (^{64}Zn 48.89%, ^{66}Zn 27.81%, ^{67}Zn 4.11%, ^{68}Zn 18.57%, ^{70}Zn 0.62%) with 30-MeV protons from the Michigan State University Sector-Focused Cyclotron. This beam energy was chosen to maximize the production ratio of ^{63}Ga to ^{64}Ga, the principle contaminant. Figure 47 shows this ratio as a function of incident beam energy. The various energies were obtained by degrading either 40-Mev or 34-Mev

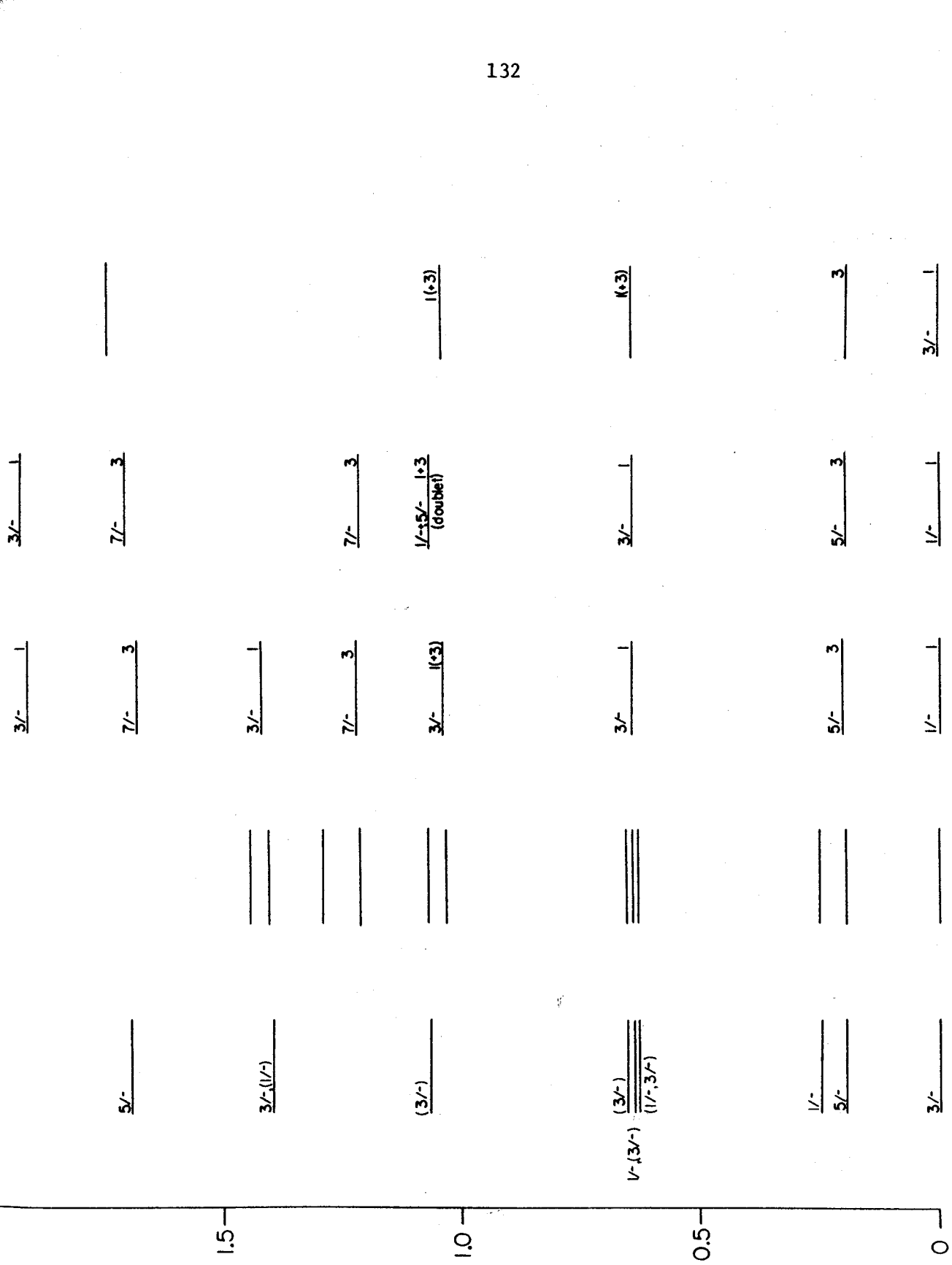

Fig. 46. A summary of the various reactions used to study the excited states in ^{63}Zn.

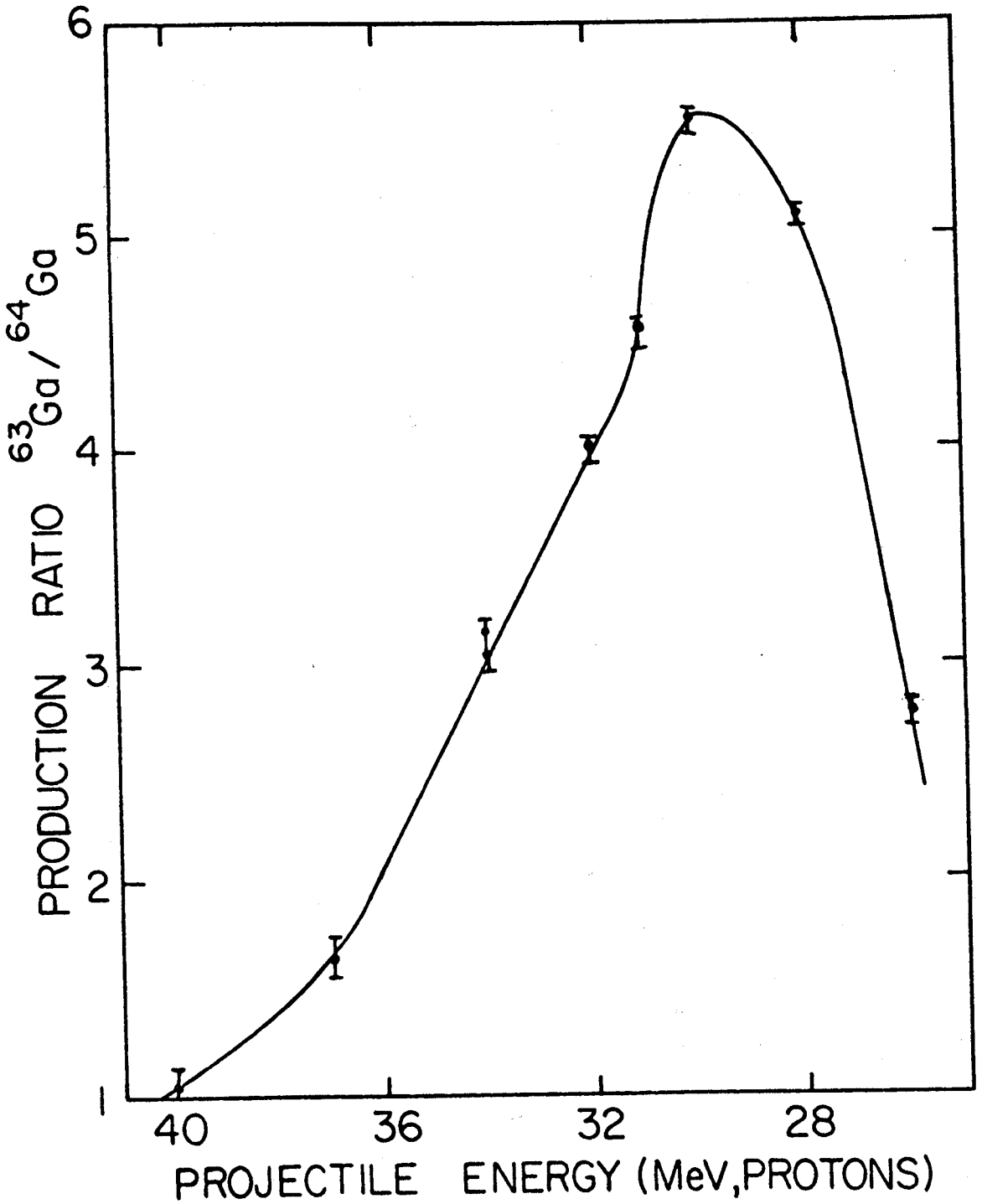

Fig. 47. Relative production of ^{63}Ga to ^{64}Ga as a function of incident beam energy.

proton beams with the appropriate thickness Al absorbers. A typical irradiation was a 1-2 second burst of an ≈0.5-μA proton beam. The targets were then moved quickly (≈7 sec) from the irradiation area to a distant counting area by a pneumatic rabbit system (Ko70). The samples were counted with either the 4.6% efficient or 10.4% efficient Ge(Li) detector and using the Ge(Li)-time coincidence system described in Section 2.1.2.C. The time length of the ramp was varied from 120 to 1560 seconds, depending on the particular experiment. In the search for low energy γ-rays, a Si(Li) x-ray detector was used in place of the Ge(Li) detector. Along with each γ-time coincidence experiment, a γ-ray singles spectrum was obtained. A typical experiment involved adding together the spectra from as many as 250 Zn foils.

An energy calibration of the stronger γ rays in the spectrum was performed by counting the Zn foils with ^{241}Am, ^{152}Eu, and ^{192}Ir as internal standards. Also used for the calibration were the γ rays from ^{63}Zn and the 1332-keV and 1791-keV γ's of ^{60}Cu which were internally present. Table 10 lists those strong γ rays from sources other than ^{63}Ga that were counted concurrently. These γ rays were then used as internal secondary standards to calibrate the weaker γ rays in the spectra. The intensity calibration was obtained from the procedure described in Section 2.1.3. The centroids and areas of the peaks were determined by the computer program SAMPO.

7.3. Experimental Results

A typical γ-ray spectrum is shown in Figure 48. Sixteen γ transitions were assigned to the ^{63}Ga decay, and their energies and intensities are listed in Table 11 along with the decay scheme results of Dulfer et al. (Du70) and the ^{63}Cu(p,$n\gamma$) results of Birstein et al. (Bi66).

Table 10

Measured γ-Ray Energies

Isotope	Energy
^{60}Cu	826.05±0.15
	909.32±0.15
	1035.12±0.20
^{64}Ga	807.85±0.10
	918.77±0.12
	991.50±0.10
	1387.35±0.10
^{65}Ga	114.97±0.10
	152.93±0.15
	751.68±0.10
	932.05±0.15
	1047.23±0.20
	1354.22±0.20

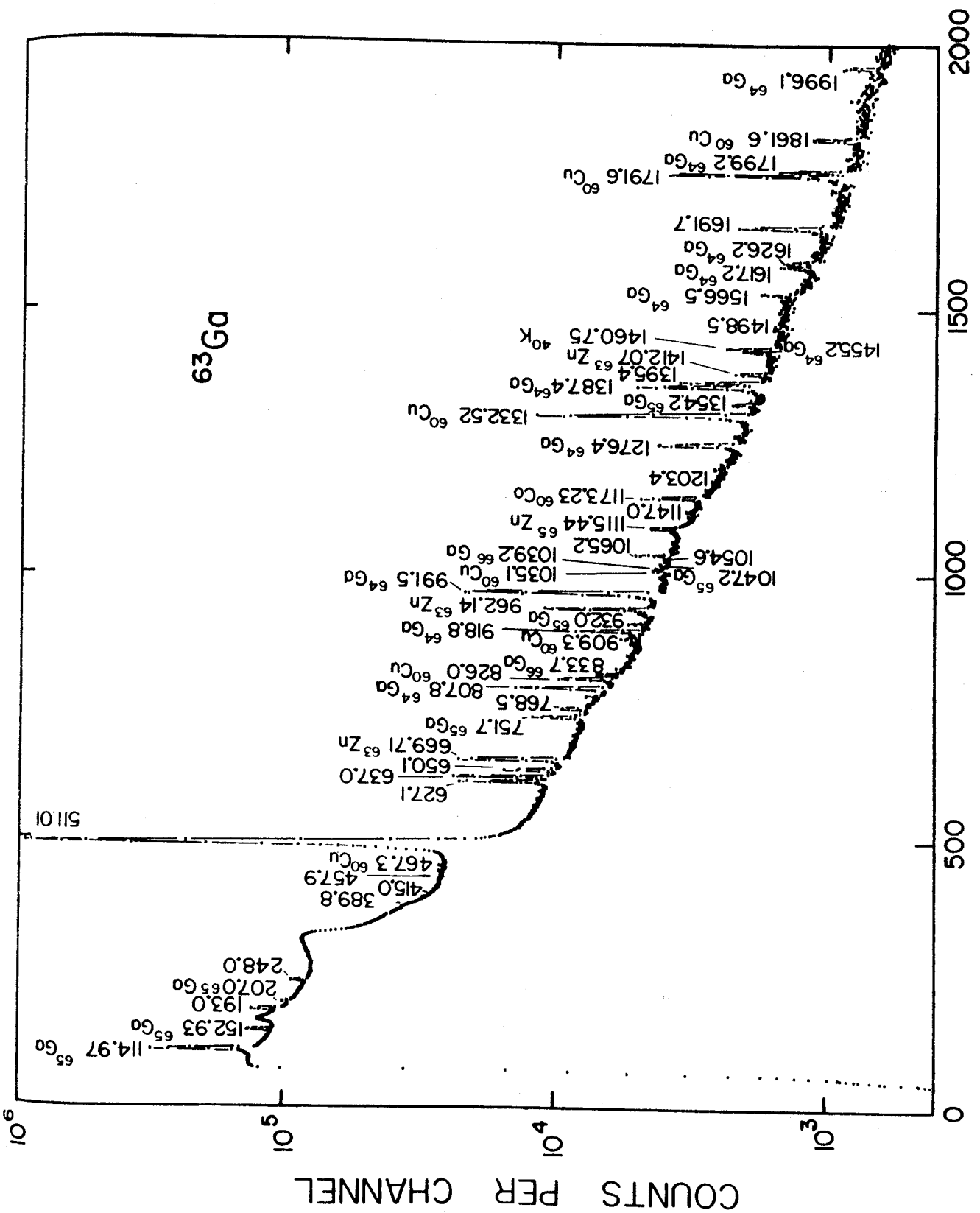

Fig. 48. A typical γ-ray spectrum from the decay of ^{63}Ga.

Table 11

γ-Ray Energies and Relative Intensities from the Decay of ^{63}Ga

Present Work		Dulfer et al.		Birstein et al.
E	*I*	*E*(Du70)	*I*	*E*(Bi66)
193.0±0.2	51.4±3.5	192.9±0.2	49	190±2
248.0±0.2	30.6±2.0	247.8±0.2	32	246±2
389.8±0.7	3.4±1.7			390
415.0±1.3	2.6±1.5			412
457.9±0.6	5.4±1.4			459
627.1±0.15	92.1±4.5	627.1±0.2	91	627±2
637.0±0.15	=100.	637.1±0.2	=100.	636±2
650.1±0.15	44.0±2.5	649.9±0.2	44	649±2
768.5±0.2	19.0±2.3	768.2±0.5	12	
1054.6±0.9	2.3±1.2			
1065.2±0.4	19.9±4.0	1065.1±0.6	18	1061±4
1147.0±0.8	3.1±0.7			
1203.4±2.0	2.4±1.2			
1395.4±0.3	37.0±7.0	1395.5±0.5	41	
1498.5±0.6	2.9±1.5			
1691.7±0.5	27.4±5.0	1691.8±1.0	28	

The uncertainties in the energies in Table 11 are based on the uncertainties in the energy standards, the height of the peaks above the background, and the reproducibility of the calculated energies from the different spectra. The relative intensities listed are the average from several spectra and their uncertainties are based on the reproducibility of the intensities and the uncertainties in our experimentally determined efficiencies for the detectors. The errors are in general 50% greater than the largest deviation of a value from the average of several runs.

There is quite good agreement between the present results and those of Dulfer et al. (Du70). Seven γ rays were observed in the present study that they did not observe. An upper limit of 2.5 in the units of Table 11 has been placed on the intensity of any unreported γ rays below 511 keV and a limit of 2.0 on those above 511 keV. A search for γ rays from ^{63}Ga in the energy range 1700 - 4000 keV was performed, but none was observed. A similar search for γ rays below 100 keV was performed using the x-ray detector, but none was observed in this region either. A half-life of 32.4 $\pm$ 0.5 sec was determined for ^{63}Ga by using 12 spectra from the γ-time coincidence system to measure the half-life of the 193-, 627-, 637-, and 650-keV γ transitions.

7.4. Decay Scheme

The decay scheme produced from the present results is shown in Figure 49. Transition and excited state energies are given in keV with the adopted energies for the states being a weighted average of several experimental runs. The Q_ε of $\approx$5.6 MeV was obtained from the mass table of Garvey et al. (Ga69). The total transition intensities, in percent of total ^{63}Ga decay, are given in the decay scheme. Since all of the internal conversion coefficients would be less than 1% of the individual γ

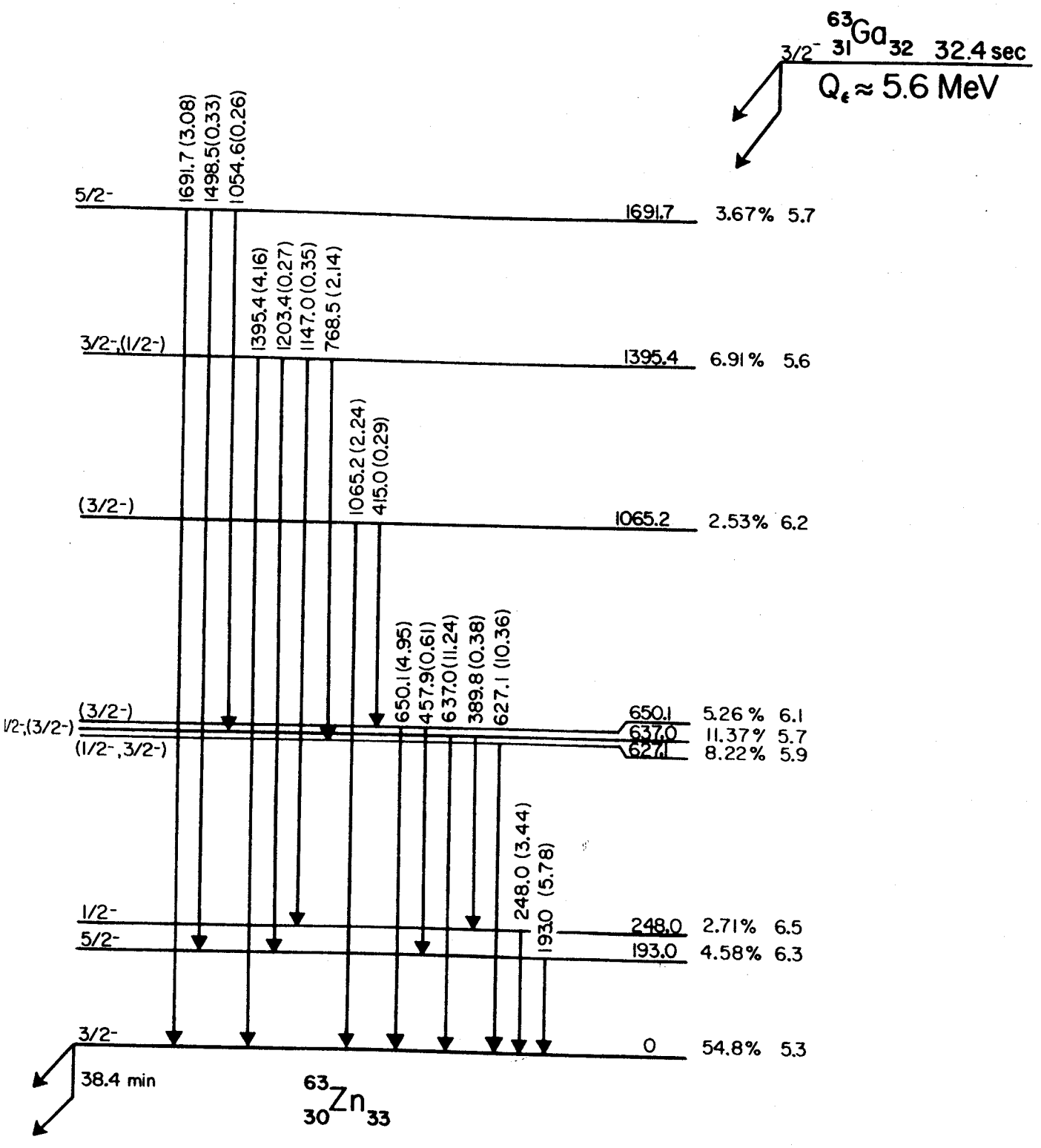

Fig. 49. Proposed decay scheme of ^{63}Ga.

intensities, they were ignored. Using the ratio of the 511-keV γ to the 627-637-650-keV γ-ray triplet measured by Dulfer et al. (Du70), with which these results are consistent, and the theoretical ε/β^+ ratios for the levels (Le66), the total relative feedings to each state were calculated. These total feedings are given in the decay scheme to the right of the energy levels. The log *ft* values based on them appear at the extreme right of the levels. The spin and parity assignments discussed in the next section are on the left of the levels. A comparison of these results with those of charged particle reactions was shown in Figure 46.

7.5. Spin and Parity Assignments

Ground State

The ground state of ^{63}Zn is assigned $I^{\pi}=3/2^-$ on the basis of charged particle scattering experiments and decay scheme systematics from its decay to states in ^{63}Cu (cf. Section 5.5.). From scattering reactions an $\ell=1$ transfer is indicated, limiting this state to $1/2^-$ or $3/2^-$. It has an allowed β decay to the $3/2^-$ ground state, $1/2^-$ first excited state, and $5/2^-$ second excited state in ^{63}Cu, thus limiting the assignment to $3/2^-$. The log *ft* of 5.3 indicated an allowed β decay from the ^{63}Ga.

193.0-keV State

Scattering results suggest an assignment of $5/2^-$. The γ-ray directional correlation experiments of Birstein et al. (Bi68) indicate the 193-keV γ to be a $5/2^-$ to $3/2^-$ transition. The log *ft* of 6.3 indicates an allowed transition from the ^{63}Ga and supports the assignment.

248.0-keV State

The log *ft* of 6.5 suggests probably allowed β decay which would limit the assignment to $1/2^-$, $3/2^-$, or $5/2^-$. This state decays solely to the ground state. Although the ^{63}Cu(p,n) results report this level, none

of the other charged particle experiments observed it. Examining the systematics of the odd-mass Zn isotopes as shown in Figure 50 and the systematics of the N=33 isotopes shown in Figure 45, a $1/2^-$ level in the region below 400 keV is strongly suggested. Since this is the only level that could fit these systematics, it is therefore assigned $I^\pi=1/2^-$.

The ground state of ^{63}Ga is assigned $I^\pi=3/2^-$ since allowed β transitions are observed to the $3/2^-$ ground state, the $5/2^-$ first excited state, and the $1/2^-$ second excited state in its ^{63}Zn daughter. This assignment is consistent with the systematics of the light odd-mass Ga isotopes and the shell model (the odd proton being in the $2p_{3/2}$ orbital).

627.1-, 637.0-, 650.1-keV States

The β feeding to these states has log ft's of 5.9, 5.7, and 6.1, respectively, all allowed transitions. Results from all the scattering experiments indicate ℓ=1 transfers, most likely $3/2^-$ states. The probability of ℓ=3 transfer was considered small. The 627-keV state decays solely to the ground state, while the 637-keV state also decays to the 248-keV state and the 650-keV state also decays to the 193-keV state. The 627-keV state is therefore assigned $I^\pi=(1/2^-, 3/2^-)$, the 637-keV state $I^\pi=1/2^-, (3/2^-)$, and the 650-keV state $I^\pi=(3/2^-)$.

1065.2-keV State

This state has a β feeding with a log ft of 6.2 and decays to the ground state and the 650-keV state. Results from ^{63}Cu(p,n) also indicate a level at 1028 keV. Scattering results indicate both ℓ=1 and ℓ=3 transfers in this region for presumably a doublet with ℓ=1, $I^\pi=3/2^-$ dominant. This state is therefore assigned $I^\pi=3/2^-$.

1395.4-keV State

This state has more γ branching than any other state in ^{63}Ga.

It decays to the ground state ($3/2^-$), the 193-keV state ($5/2^-$), the 248-keV state ($1/2^-$) and the 627-keV state (($1/2^-$, $3/2^-$). It also is populated by an allowed β transition, as indicated by a log ft of 5.6. The ^{64}Zn(p,d) results suggest a $3/2^-$ state in this region. The ^{63}Cu(p,n) results indicate two states here, with the 1395-keV state the closer to the state observed in the (p,d) results. An I^π assignment of $3/2^-$, ($1/2^-$) is suggested for this state.

1691.7-keV State

This state decays to the 193-keV state ($5/2^-$) and the 637-keV state ($1/2^-$, ($3/2^-$)) in addition to the ground state. The log ft of 5.7 for feeding to this state indicates an allowed decay. The results from charged particle scattering suggest an ℓ=3, I^π=$7/2^-$ state. Since a $7/2^-$ assignment would not permit allowed β decay, this state is assigned I^π=$5/2^-$, which is consistent with all results.

7.6. Discussion

The ^{63}Zn is in the region above the doubly closed shell occurring at ^{56}Ni. In this region the active particle states for both neutrons and protons are the $2p_{3/2}$, $2p_{1/2}$, $1f_{5/2}$, and $1g_{9/2}$. Since both $1g_{9/2}$ orbitals are well above 2 MeV (cf. Figures 39 and 50), they will be ignored. The odd nucleon in ^{63}Zn is a neutron found in the $2p_{3/2}$ orbital. In contrast to its ^{63}Cu daughter where the low-lying states are from the odd proton coupling to a core vibrational state, the first two excited states in ^{63}Zn appear to be primarily single particle states, the first being the $1f_{5/2}$ and the second the $2p_{1/2}$. These three single particle states remain rather closely spaced in the lighter Zn isotopes with the $1f_{5/2}$ being the ground state for ^{65}Zn and ^{67}Zn.

The triplet of the 627-, 637-, and 650-keV states appear to be

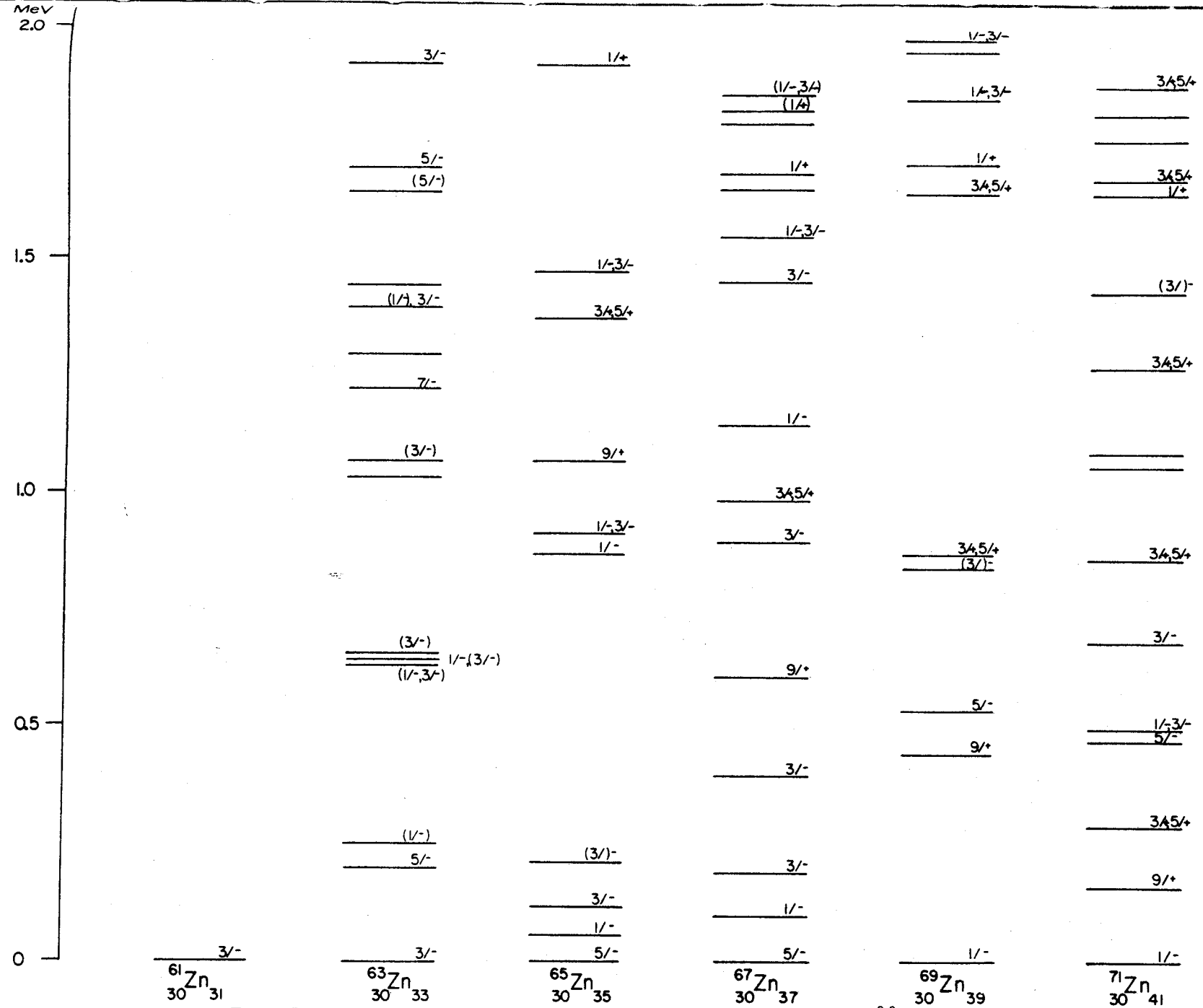

Fig. 50. Systematics of the odd-mass Zn isotopes. The ^{63}Zn results are from the present work, ^{61}Zn from ND, and the rest from Vo67.

core coupled states. Since the log ft's to these states fall between that of the ground state decay and those to the first two excited states, these states would therefore result from the coupling of the odd neutron in the $2p_{3/2}$ orbital to a ^{62}Zn core excitation. However, since little is known about the excited states in ^{62}Zn, the details of these states must be left to a later time. Not enough is known about the higher-lying states in ^{63}Zn since they occur above the pairing gap and could result from several different sources, so therefore little can be said about them here.

The β decay from ^{63}Ga to the states in ^{63}Zn presents some very interesting problems. The ground state of ^{63}Ga apparently has the odd proton in the $\pi p_{3/2}$ orbital. The ground state of ^{63}Zn appears to be $(\pi\, p_{3/2})^2(\nu f_{5/2})^2(\nu p_{3/2})^3$ or some similar neutron configuration since it has five neutrons outside a closed shell and an $I^{\pi}=3/2^-$. While a neutron configuration of $(\nu p_{1/2})^2(\nu p_{3/2})^3$ might appear to more easily explain the ground state of ^{63}Zn and the nonobservance of its 248-keV ($1/2^-$) state in all the scattering reactions, it is not a probable configuration since it would require the lower spin state of an ℓ to be below the higher spin state, and this does not occur in nuclear level systematics.

The more probable configuration suggests that the $\nu p_{3/2}$ and $\nu f_{5/2}$ states are degenerate so that both may be partially filled. The decay from the ^{63}Ga indicates a normal allowed transition to the ^{63}Zn ground state with its suggested degeneracy, while unexpectedly slow β transitions feed the supposedly pure single particle $5/2^-$ and $1/2^-$ states. A much more detailed study of this region is necessary before these states in ^{63}Zn can be fully explained.

CHAPTER VIII

^{62}Ga AND β-DELAYED α EMISSION

8.1. Introduction

The occurance of β-delayed α emission has been known for a long time. In 1935, Crane et al. (Cr35) reported the β-delayed α decay of 850-msec ^{8}Li. Alvarez (Al50) in 1950 expanded the list when he reported similar decays for 774-msec ^{8}B, 11.0-msec ^{12}N, and 405-msec ^{20}Na. Further searches for β-delayed α emission in the light elements have produced 20.4-msec ^{12}B, 7.13-sec ^{16}N, 2.09-sec ^{24}Al, and 297-msec ^{32}Cl. All of these nuclei are of the type N=Z±2, where Z is odd, β decaying to excited states in N=Z even-even nuclei. The excited states immediately decay by emitting an α particle rather than by the usual γ emission.

In their report of the discovery of 33-sec ^{63}Ga, Nurmia and Fink (Nu65) reported their purpose was to look for delayed α's from ^{62}Ga, but they did not observe any. Their search was based on calculations by Taagepera and Nurmia (Ta61) which indicated the possibility of β-delayed α emission in the nuclei just above the ^{56}Ni doubly closed shell, among other places. Fengés and Rupp (Fe68) used these calculations and the Myers and Swiatecki mass tables (My65) to predict the onset of β-delayed α and proton emission for all elements through N=84. Their results indicate that ^{64}Ga would be the heaviest possible β-delayed α emitter for Ga, with delayed proton emission expected to start with ^{62}Ga and direct proton emission expected to start with ^{60}Ga.

Figure 51 shows the mass equation-based predictions of Myers and Swiatecki (My65) for the light Ga isotopes as well as predictions based on experimental results from the ^{63}Ga decay described in Chapter 7. The figure indicates α and proton binding energies from both sources. Since

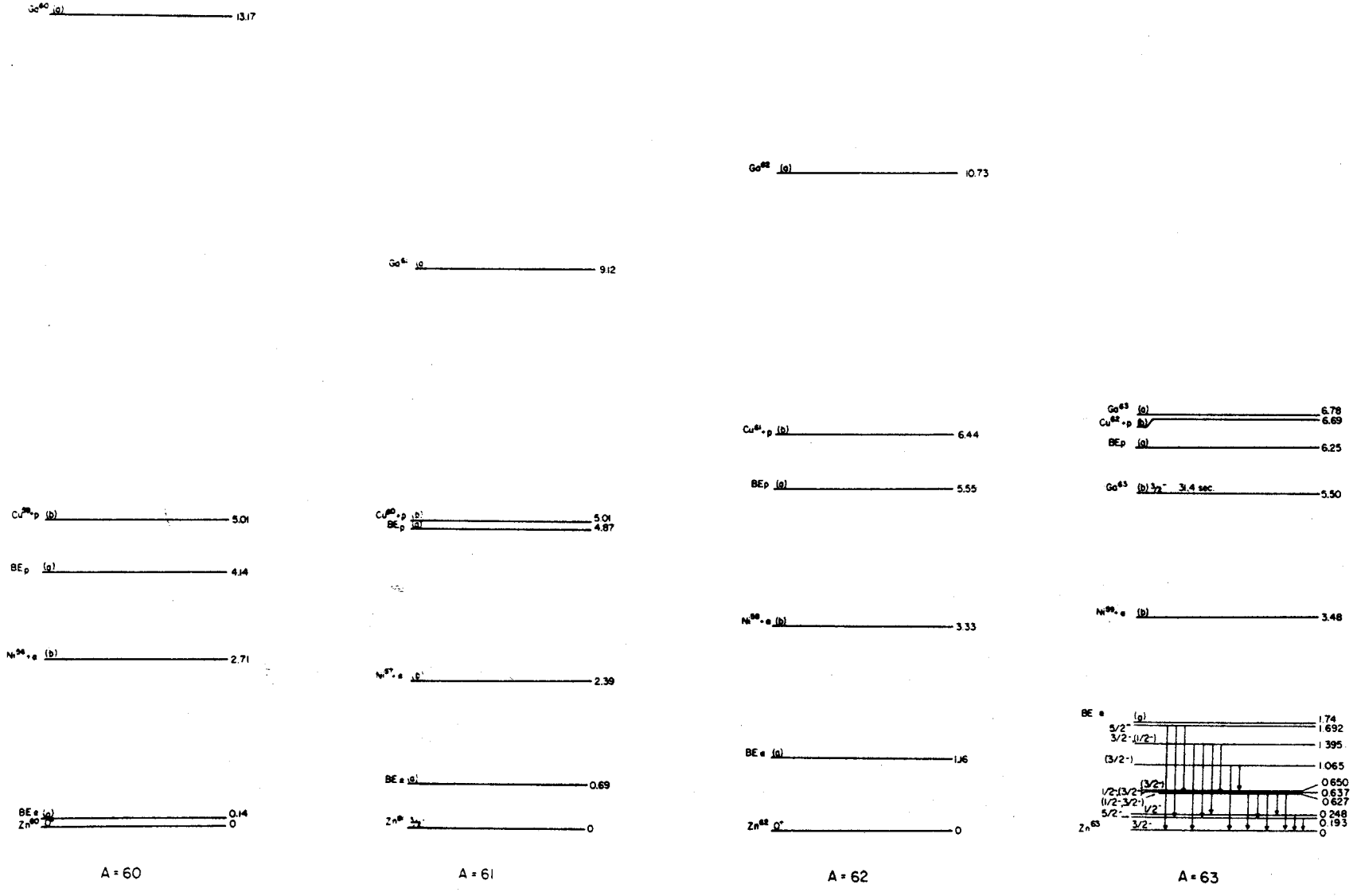

Fig. 51. Proton and α binding energies for light Zn isotopes. Those labeled (a) are from My65 and those labeled (b) are from ND. Also included are the γ-ray results from Chapter 7.

the proton binding energies are close to those for α particles, the lower Coulomb barrier could make β-delayed proton emission competitive with the β-delayed α emission. The general trend of increasing decay energy with decreasing particle binding energy is easily seen both in calculated and experimentally based binding energies. An anomaly is seen in the binding energies of ^{60}Ga. The β-delayed α emission of ^{60}Ga would lead to ^{56}Ni, a doubly closed shell nucleus. However, the experimentally based binding energy is larger than that of ^{61}Zn, and the proton binding energy is the same as that for ^{61}Zn. The corresponding calculated values from Myers and Swiatecki (My65) decrease approximately with A. With these results and calculations in mind, a search for β-delayed α emission in the light Ga isotopes was begun.

8.2. Experimental Procedure

The search for β-delayed α emission utilized the He-jet thermalizer and α detectors described in Section 2.2. In addition to the α detector, the 4.6% efficient Ge(Li) detector was also used to count the γ rays from the collected nuclei. The targets used were 0.1-mil thick natural Cu foils. Three foils were used at any one time, each separated by a 0.8 inch thick teflon block with a 1-inch ϕ hole in it. An incident beam of 70 MeV τ of about 0.4 μA current was used to produce the light Ga isotopes. Lower beam energies were obtained by degrading the beam with Al absorbers. The range of the recoils produced with this beam is 0.035 mil in Cu or 0.74 inches in the 2 atm He used. The ranges were calculated using the results reported by Harvey (Ha60). The recoils were collected on masking tape. The bombardment energies of 70, 55, and 40 MeV were chosen to represent the peak in the production cross section of ^{61}Ga, ^{62}Ga, and ^{63}Ga, respectively.

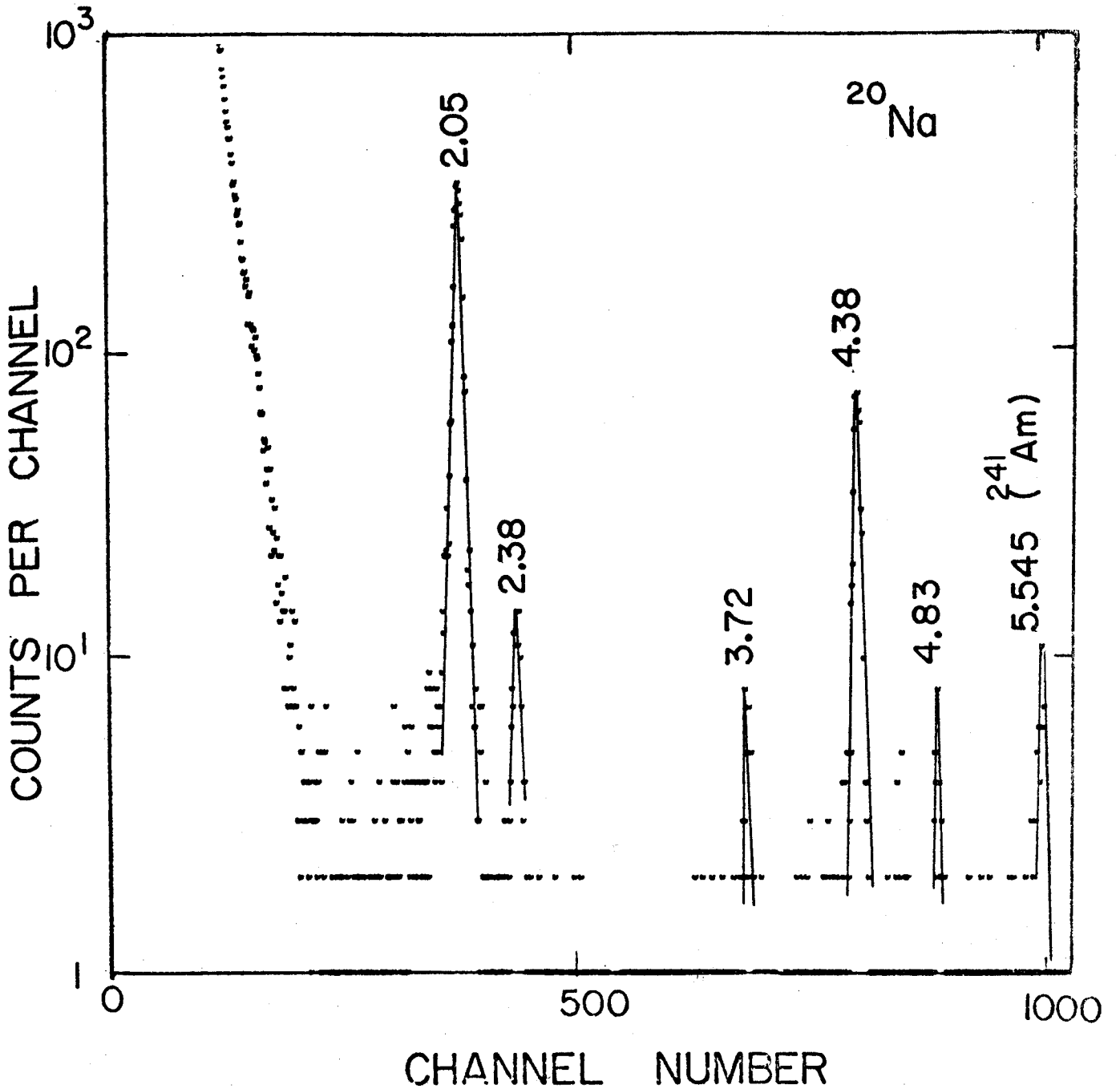

Fig. 52. An α spectrum from the β-delayed α emission of ^{20}Na (Po67).

In order to insure β-delayed α's could be observed, the β-delayed α decay of ^{20}Na (Po67) was examined. For this experiment, the Cu foils were removed and Ne gas was allowed to leak into the target chamber along with the He thermalizer gas. The results of this test are shown in Figure 52. In addition to the ^{20}Na peaks, there is a peak from ^{241}Am. This appears to be contamination on the detector face and is seen in other spectra including those with no source present. For this experiment, the recoils were collected on a cooled Al block.

8.3. Results

In Figure 53, the results of the search for β-delayed α emission in the light Ga isotopes are shown. Incident beams of 70-, 55-, and 40-MeV τ were used to bombard the Cu targets, and the results from each beam energy are shown. The only peak observed in all three spectra is the 5.545-MeV α peak from the ^{241}Am contamination on the detector. Only in the 70-MeV spectrum is there any sign of α activity. Four single channels in the region from channel 500 to channel 1000 have more than one count in them. The peak at about channel 550 has about 4 counts and the one at 905 has 3 counts, whereas the other two have only the two counts in the one channel. No counts were observed at these locations in other α spectra.

The γ-ray spectra corresponding to the α spectra shown in Figure 53 are shown in Figures 54, 55, and 56. Several isotopes appear here that were not observed in the ^{63}Ga studies. In general, the shorter lived species will not be observed since the collection tape was changed hourly and therefore allowed a buildup of the long lived species.

Examining the spectra, the ^{66}Ga is found to increase by about one third going from 40 MeV τ to 55 MeV τ and increased by about one half

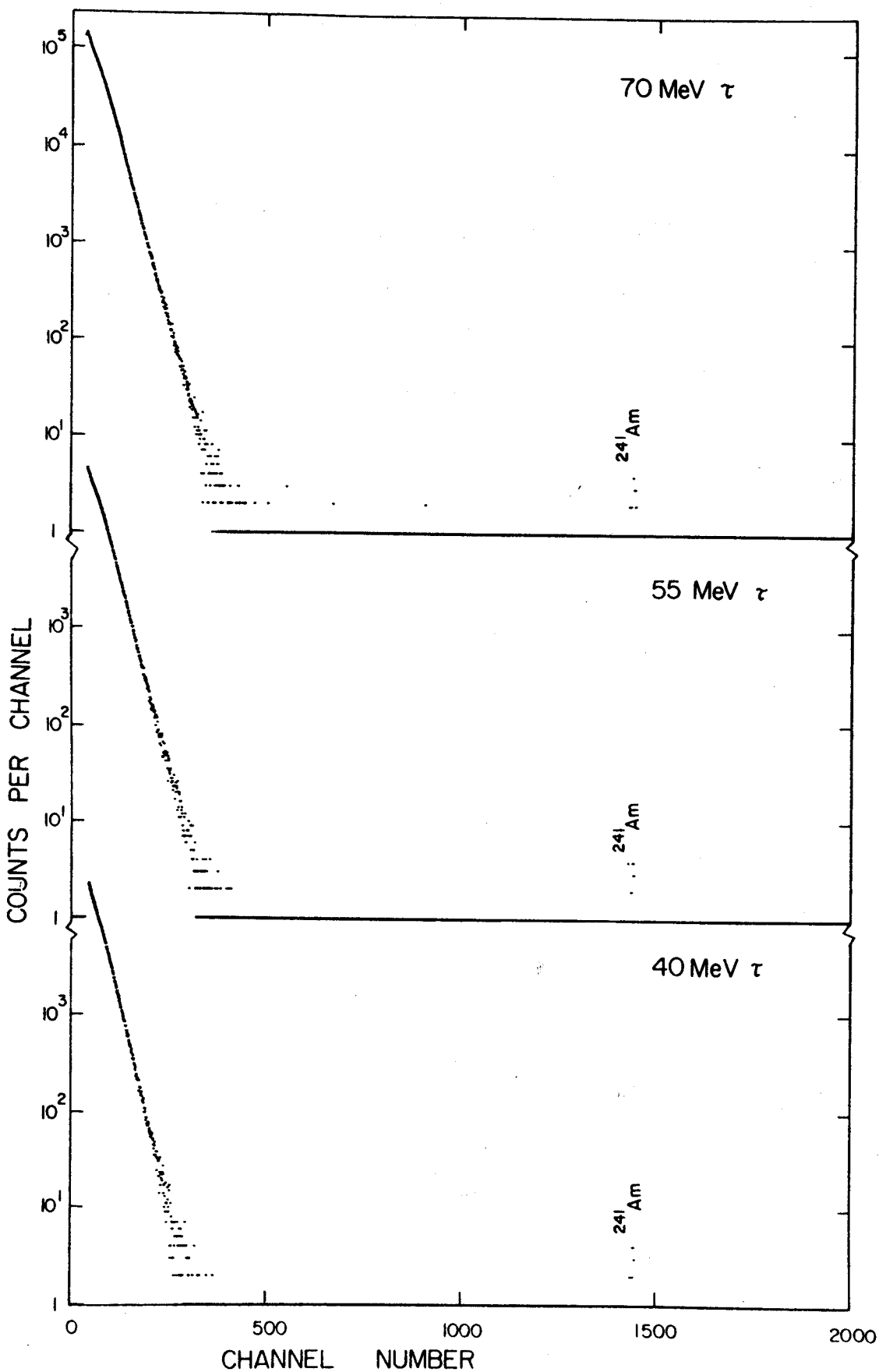

Fig. 53. A search for β-delayed α emission in light Ga isotopes.

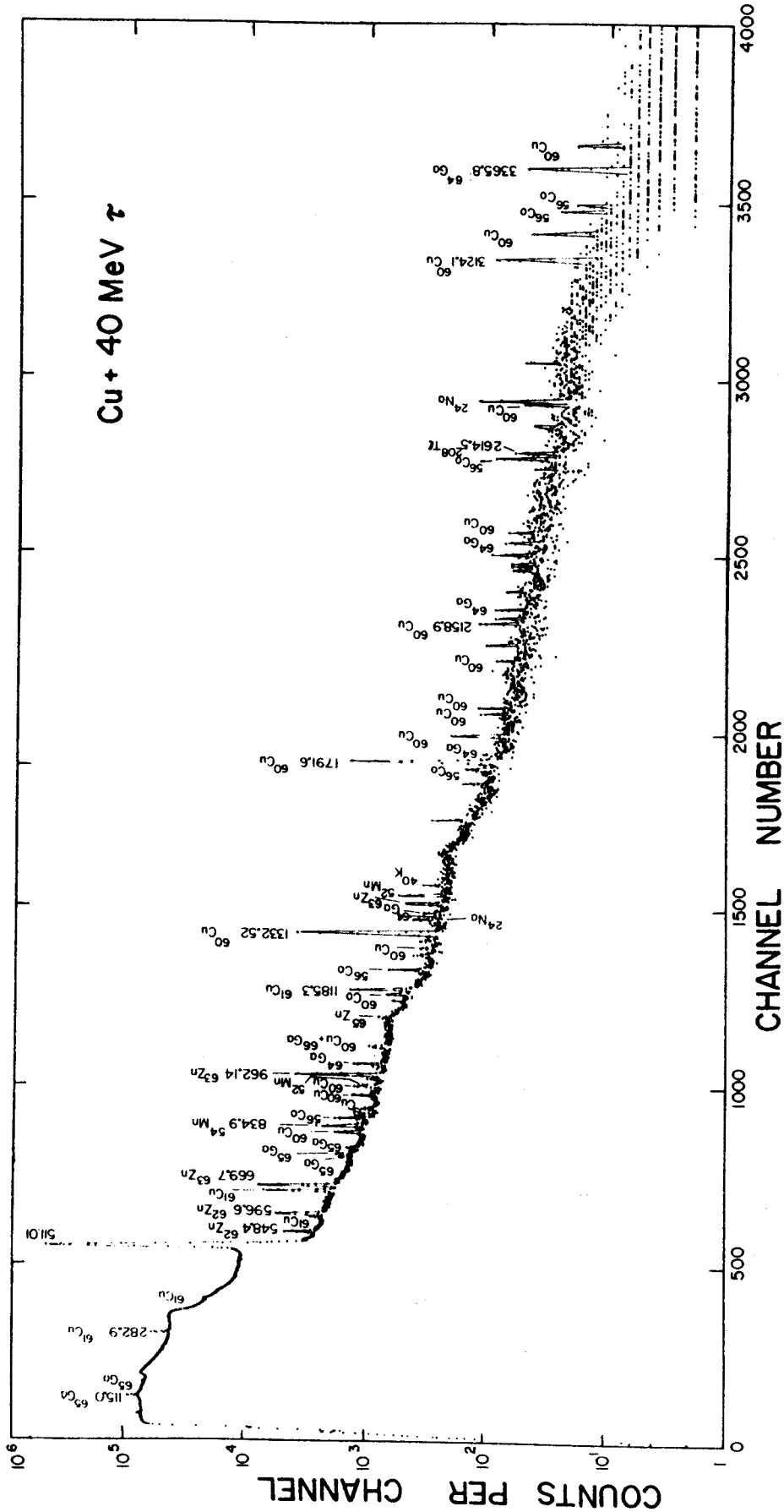

Fig. 54. γ-ray spectrum from the recoils produced from bombarding Cu with 40 MeV τ.

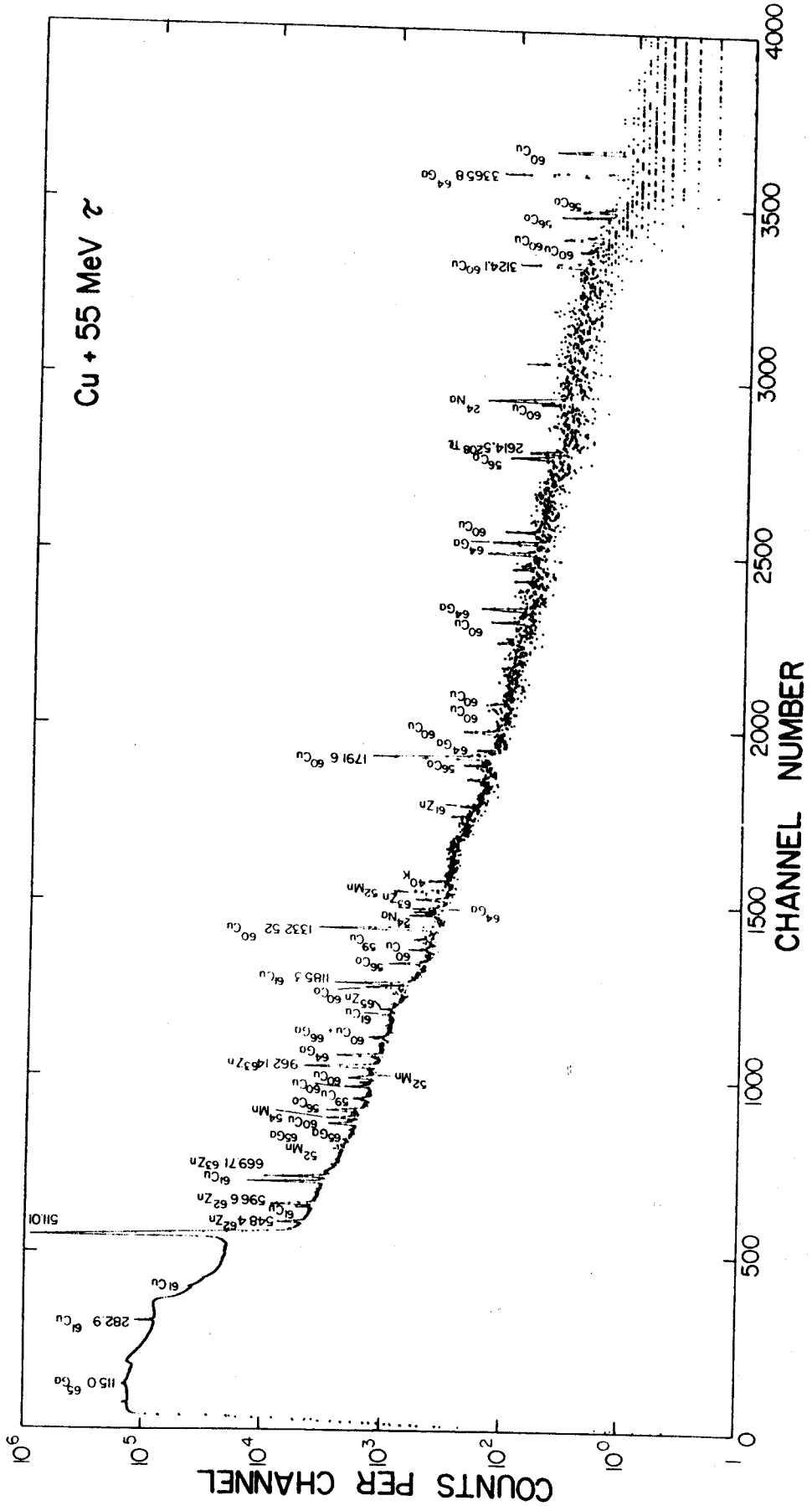

Fig. 55. γ-ray spectrum from the recoils produced by bombarding Cu with 55 MeV τ.

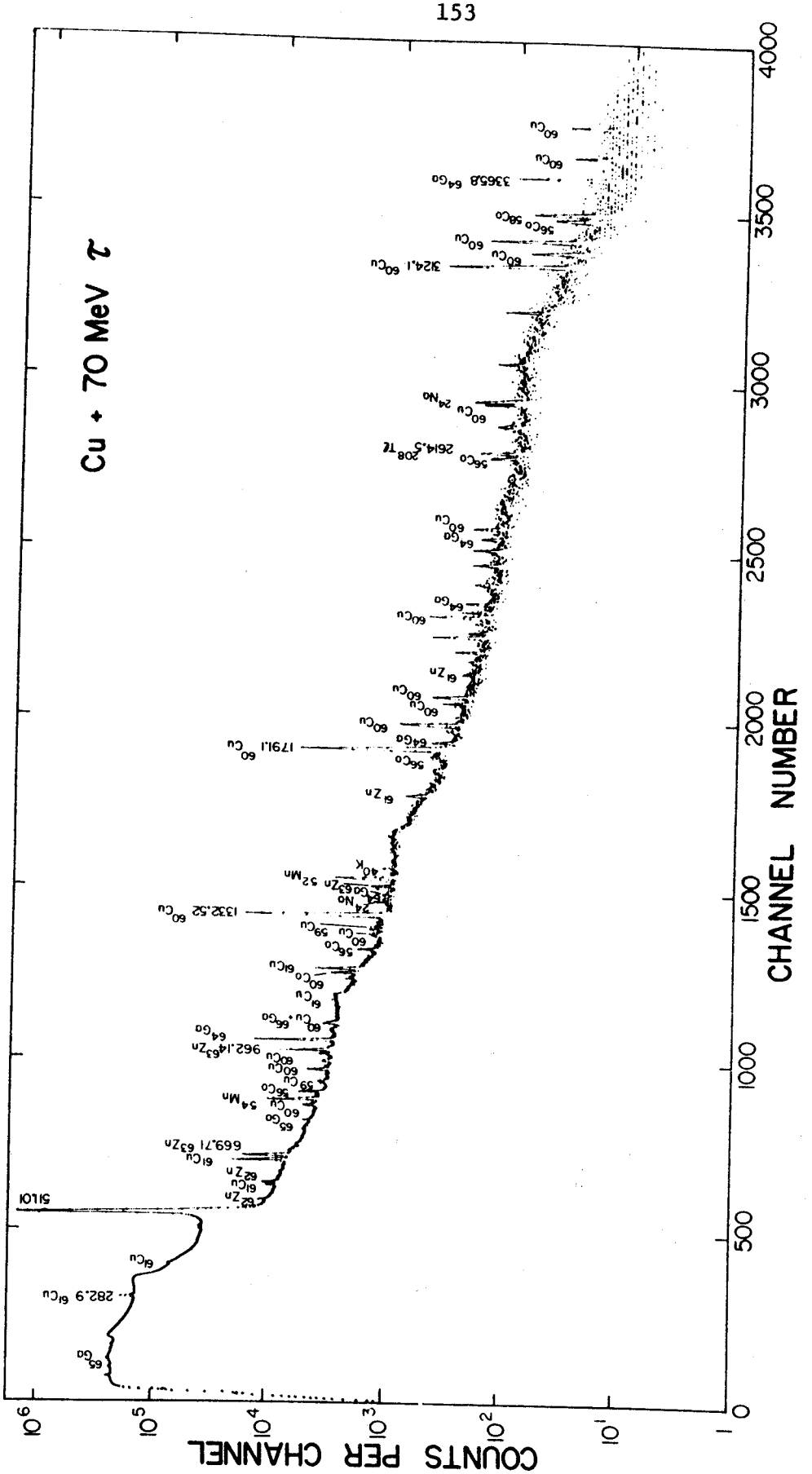

Fig. 56. γ-ray spectrum from the recoils produced by bombarding Cu with 70 MeV τ.

again going to 70 MeV τ. The ^{65}Ga in turn decreased by about 40% from 40 MeV to 55 MeV, and decreased slightly further going to 70 MeV. Both of these isotopes are only weakly seen above 40 MeV and are hard to measure accurately because the ^{66}Ga is obscured by stronger nearby γ rays from other isotopes present and the ^{65}Ga is overwhelmed by the underlying Compton background. An increase by a factor of 2.7 is noted in the ^{64}Ga intensity going from 40 to 55 MeV. The increase was reduced to only a factor of 2 for 70 MeV as compared to 40 MeV.

The ^{63}Zn daughter of ^{63}Ga increases by about one fifth from 40 to 55 MeV and increases by another half at 70 MeV, while the ^{62}Zn daughter of ^{62}Ga increases by one half at 55 MeV then drops to only about five sixths at 70 MeV. A doubling of intensity from 40 MeV to 55 MeV is noted for ^{61}Cu, with an additional increase of one half going to 70 MeV. ^{61} Zn is observed only weakly in the Compton valley from the 511-keV γ but does appear to have the same intensity relations as its more obvious ^{61}Cu daughter. The ^{60}Cu, in turn, has about the same intensity at the two lower energies, but an intensity at 70 MeV of more than 4 times that at lower energies.

Some of the peaks present result from beam interactions with the Havar foil separating the evacuated beam line and the pressurized target chamber, the Al collimator and absorbers, and the natural background. Some isotopes occuring from these sources are ^{56}Co, ^{52}Mn, ^{54}Mn, and ^{24}Na. In addition to the γ rays from these isotopes, several other γ rays, mostly weak, were observed but could not be identified, although their source is believed to be reactions with the Havar foil.

Figures 57 and 58 show the calculated cross sections for ^{63}Cu and ^{65}Cu produced by the program CS8N written by T. Sikkeland and D. Lebeck

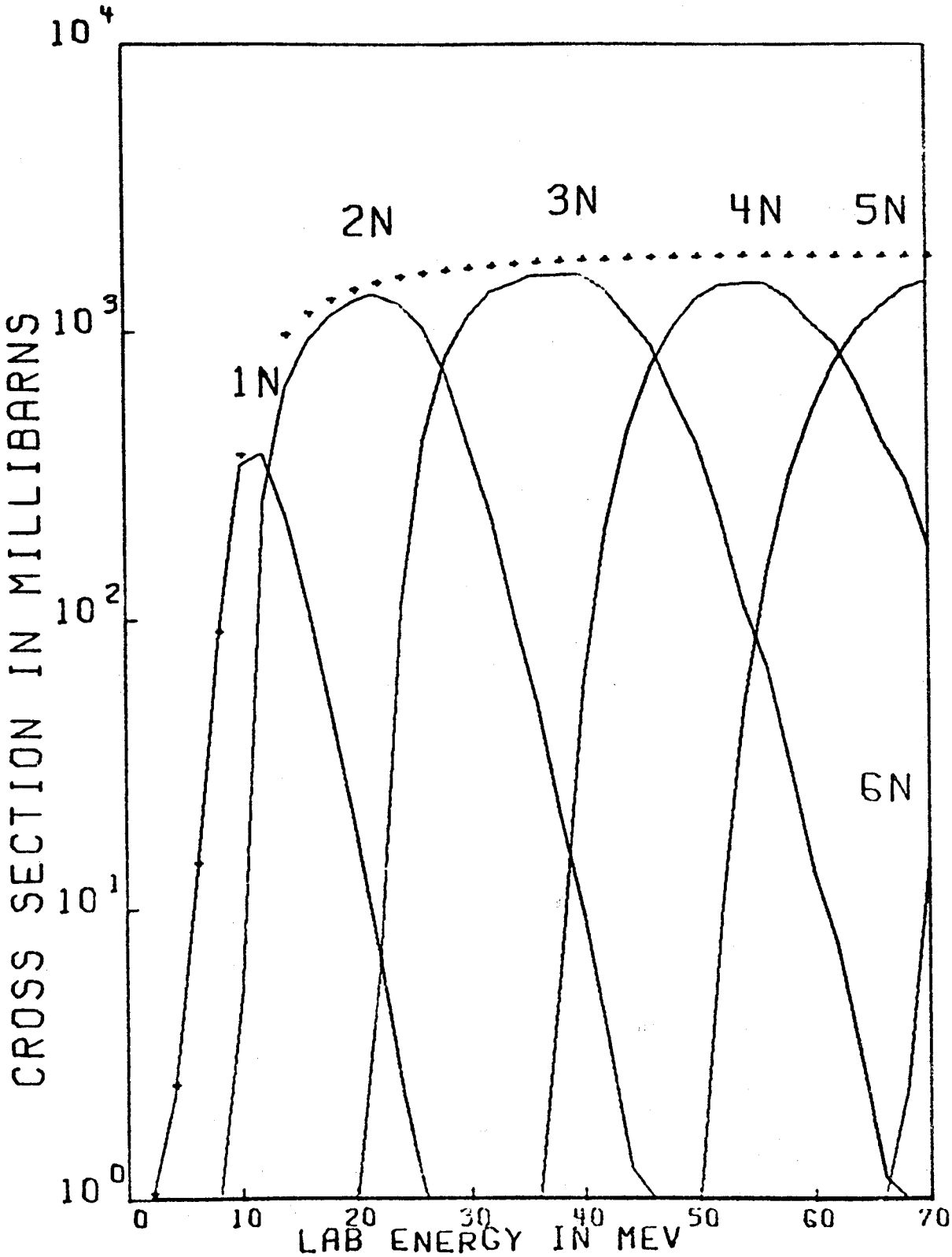

Fig. 57. The $^{63}Cu(\tau,xn)$ cross sections calculated by the program CS8N.

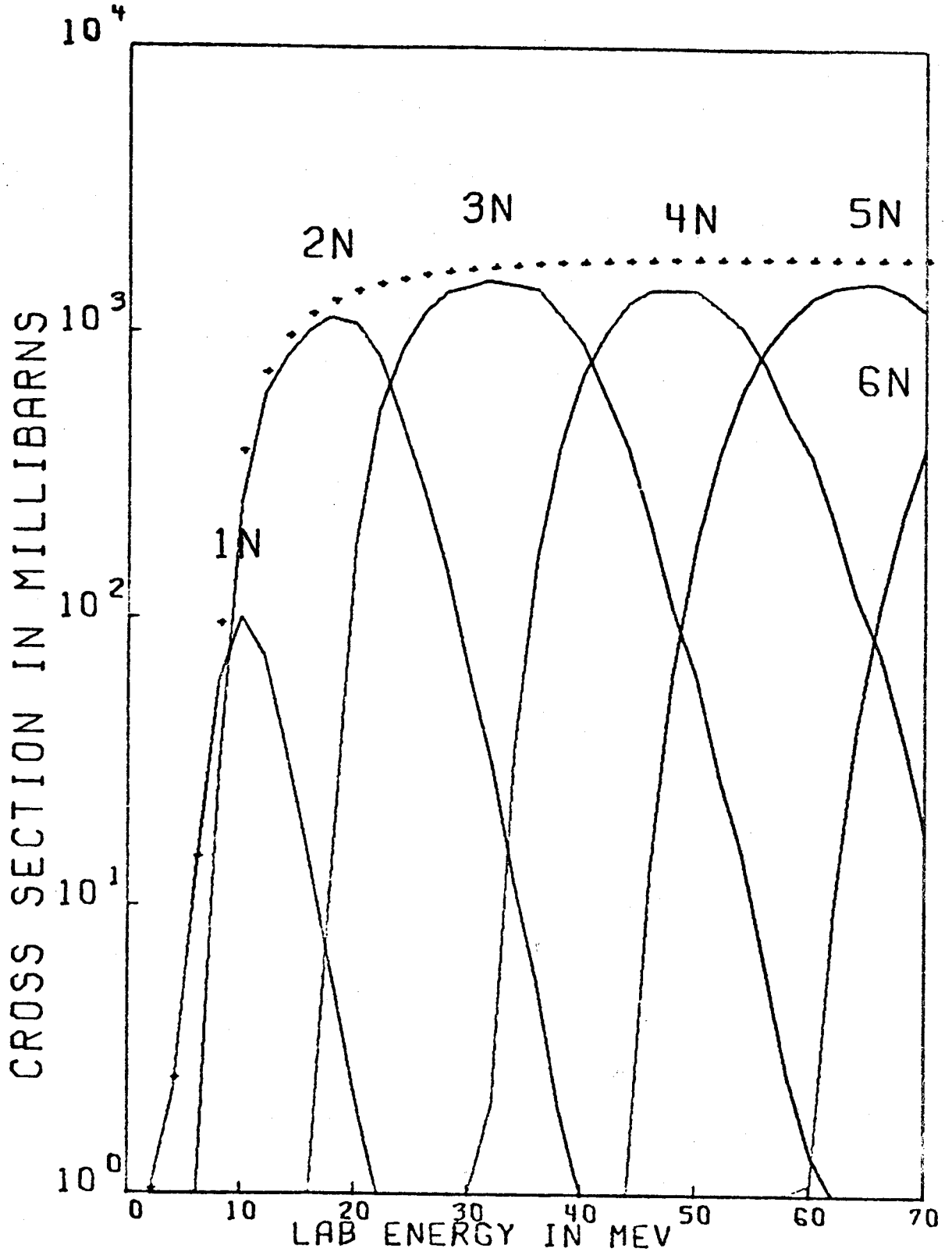

Fig. 58. The $^{65}Cu(\tau,xn)$ cross sections calculated by the program CS8N.

at the University of California, Berkeley, to calculate the results of bombarding heavy elements with heavy ions. The relative cross sections predicted by the curves are in general agreement with the experimental results, taking into account that the interacting beam degraded by the Al absorbers, is not monoenergetic like the incident beam, but has a large range of energies, the range being larger for the thicker absorbers. It should be said that the isotopes of masses 61 and heavier are considered to be daughters of the Ga isotopes produced by the Cu(τ,xn) reaction. The ^{60}Cu and lighter masses are primarily from the Cu(τ,αxn) reactions. Since ^{61}Cu and ^{61}Zn are observed as well as ^{62}Zn and ^{63}Zn, it appears that the light Ga isotopes, ^{61}Ga, ^{62}Ga, and ^{63}Ga, have been produced. Since the ^{60}Cu is present from other reactions and the presence of ^{60}Zn cannot be determined because its most intense γ rays fall at the same energy as much stronger transitions in the spectra, the production of ^{60}Ga is hard to evaluate. However, the large increase in the ^{60}Cu intensity from the 70-MeV τ beam gives a strong indication that ^{60}Ga was produced with this beam. These isotopes were not observed directly since their half-lives are expected to be seconds or less. However, based on the intensity of the daughter decays and the lack of observed α transitions, an upper limit of about ten parts per million can be placed on the β-delayed α branching of any of these isotopes. This could be due to the Coulomb barrier of the nuclei or the lack of β feeding to states above the α binding energy.

CHAPTER IX

CONCLUSIONS

Although there has been comparitively little work done on it, the region beyond the doubly closed shell at ^{56}Ni can provide significant information about the structure of the nucleus. Since ^{56}Ni is not stable and ^{58}Ni is the lightest stable nucleus in this region, the nuclei just outside the doubly closed shell are not as easily produced as those near the lighter doubly magic nuclei. To add to the difficulty in studying these nuclei, their half-lives are short, minutes or less, making decay scheme studies rather arduous.

One of the purposes of examining this region is the possibility of β-delayed α emission occuring in the light Ga isotopes. An extensive search for this α emission was conducted by producing isotopes as light as ^{60}Ga. Although some hints of delayed α emission were observed, the only definite result was the placing of an upper limit on the β-delayed α emission in this region.

Excited states in several other isotopes have also been studied in order to learn more about the systematics in this region. In the investigation of the β decay of ^{63}Zn a new level and several new γ transitions were observed. The new level is one of the doublet of the 1861- and the 1865-keV states. All previous studies of the excited states in ^{63}Cu report only a single state at ≃1863 keV. Several different coinci dence experiments were also performed to help elucidate features of the ^{63}Zn decay scheme such as the differences in ε_K/β^+ between the strongly collective states and the primarily single-particle states, all supposedly fed by allowed β transitions.

An examination of the decay scheme of ^{62}Zn revealed six new γ

transitions, one of which had been previously observed only in $^{62}Ni(p,n\gamma)$ reactions. Since ^{62}Cu is an odd-odd nucleus, the structure of its states is much more complex than other nuclei and requires considerable understanding in order to interpret it.

Seven new transitions were observed in the β decay of ^{63}Ga. No transition from this decay was observed above 1700 keV. Since the α binding energy, and therefore the lower energy limit on β-delayed α emission, lies somewhere in the range 1700 to 3300 keV depending on the mass tables used, γ transitions in this region would greatly aid in placing a firmer limit on the α binding energy and the possibility of β-delayed α emission.

Although the results reported here produce some new insights into the systematics of this region just above the doubly closed shell at ^{56}Ni, more information is needed before a good understanding of the behavior of the nuclei in this region can be obtained. More results, both experimental and theoretical, must be obtained before a consistent interpretation of the energy levels in these nuclei can be presented. The results presented here represent but a small step on the long road to this end.

BIBLIOGRAPHY

BIBLIOGRAPHY

(Al50) L. W. Alvarez, Phys. Rev. 80, 519 (1950).

(An62) J. D. Anderson, C. Wong, and J. McClure, Nucl. Phys. 36, 161 (1962).

(An67) S. Antman, H. Pettersson, and A. Suarez, Nucl. Phys. A94, 289 (1967).

(Au67) R. L. Auble, D. B. Beery, G. Berzins, L. M. Beyer, R. C. Etherton, W. H. Kelly, and Wm. C. McHarris, Nucl. Instr. Methods 51, 61 (1967).

(Ba60) B. F. Bayman and L. Silverberg, Nucl. Phys. 16, 625 (1960).

(Ba65) M. Barloutaud, J. Gastebois, J. M. Laget, and J. Quidort, Phys. Lett. 19, 306 (1965).

(Ba67) D. Bachner, R. Bock, H. H. Duhm, R. Santo, and R. Stock, Nucl. Phys. A99, 487 (1967).

(Ba68) H. Bakhru, Phys. Rev. 169, 889 (1968).

(Ba70) W. T. Bass and P. H. Stelson, Phys. Rev. C2, 2154 (1970).

(Ba71) D. L. Bayer, MSUCL-35 (1971).

(Be55) For example, the problem is considered in P. R. Bell, in *Beta- and Gamma-Ray Spectroscopy* (ed. K. Siegbahn; North-Holland Publ. Co., Amsterdam, 1955) p. 132.

(Be66) W. P. Beres, Nucl. Phys. 75, 255 (1966); and Phys. Lett. 16, 65 (1965).

(Be67) M. G. Betigeri, H. H. Duhm, R. Santo, R. Stock, and R. Bock, Nucl. Phys. A100, 416 (1967).

(Be69) D. B. Beery, Ph. D. Thesis, Michigan State University,1969.

(Be69a) F. M. Bernthal, Ph. D. Thesis, University of California, Berkeley, UCRL-18651, 1969.

(Bi66) L. Birstein, M, Harchol. A. A. Jaffe, and A. Tsukrovitz, Nucl. Phys. 84, 81 (1966).

(Bi67) L. Birstein, Ch. Drory, A. A. Jaffe, and Y. Zioni, Nucl. Phys. A97, 203 (1967).

(Bi68) L. Birstein, R. Chechik, Ch. Drory, E. Friedman, A. A. Jaffe, and A. Wolf, Nucl. Phys. A113, 193 (1968); and Phys. Lett. 26B, 220 (1968).

(Bl65) A. G. Blair, Phys. Rev. 140, B648 (1965); and Phys. Lett. 9, 37 (1964).

(Bo37) W. Bothe and W. Gentner, Z. Physik 106, 236 (1937).

(Bo62) M. Bouten and P. Van Leuven, Nucl. Phys. 32, 499 (1962).

(Bo68) E. Bożek, A. Z. Hrynkiewicz, G. Zapalski, R. Kulessa, and W. Waluś, Nucl. Instr. Methods 58, 325 (1968).

(Bo69) I. Borchert, Z. Physik 223, 473 (1969).

(Br55) H. Brysk and M. E. Rose, ORNL-1830 (1955).

(Br55a) R. M. Brugger, T. W. Bonner, and J. B. Marion, Phys. Rev. 100, 84 (1955).

(Br57) E. Brun, W. E. Meyerhof, J. J. Kraushaar, and D. J. Horen, Phys. Rev. 107, 1324 (1957).

(Br60) M. H. Brennen and A. M. Bernstein, Phys. Rev. 120, 927 (1960).

(Ca71) D. C. Camp and G. L. Meridith, Nucl. Phys. A166, 349 (1971).

(Co67) J. A. Cookson, Phys. Lett. 24B, 570 (1967).

(Co68) E. R. Cosman, D. N. Schramm, and H. A. Enge, Nucl. Phys. A109, 305 (1968).

(Cr35) H. R. Crane, L. A. Delsasso, W. A. Fowler, and C. C. Lauritsen, Phys. Rev. 47, 971 (1935).

(Da69) W. W. Daenick and Y. S. Park, Phys. Rev. 180, 1062 (1969).

(Da70) W. F. Davidson, M. R. Najam, P. J. Dallimore, J. Hellström, and D. L. Powell, Nucl. Phys. A154, 539 (1970).

(De67) D. DeFrenne, M. Dorikens, L. Dorikens-Vanpraet, and J. Demuynck, Nucl. Phys. A103, 203 (1967).

(Dr60) J. E. Draper and A. A. Fleischer, Nucl. Instr. Methods 9, 67 (1960).

(Du70) G. H. Dulfer, H. E. Beertema, and H. Verheul, Nucl. Phys. A149, 518 (1970).

(Fa70) U. Fanger, D. Heck, W. Michaelis, H. Ottmar, H. Schmidt, and R, Gaeta. Nucl. Phys. A146, 549 (1970).

(Fe68) T. Fénges and B. Rupp, ATOMKI Kozlem. 10, 116 (1968).

(Fo67) C. M. Fou, R. W. Zurmühle, and J. M. Joyce, Nucl. Phys. A97, 458 (1967).

(Ga69) G. T. Garvey, W. J. Gerace, R. L. Jaffe, I. Talmi, and I. Kelson, Rev. Mod. Phys. 41, 51 (1969).

(Gi69) G. C. Giesler, unpublished.

(Gi71) G. C. Giesler, Wm. C. McHarris, R. A. Warner, and W. H. Kelly, Nucl. Instr. Methods 91, 313 (1971).

(Gi71a) G. C. Giesler, K. L. Kosanke, R. A. Warner, Wm. C. McHarris, and W. H. Kelly, Nucl. Instr. Methods 93, 211 (1971).

(Go63) H. E. Gove, Phys. Lett. 4, 249 (1963).

(Go69) P. Goode, Bull. Am. Phys. Soc. 14, 623 HE1 (1969).

(Gu69) R. Gunnick, J. B. Niday, R. P. Anderson, and R. A. Meyer, UCID-15439 (1969).

(Ha50) R. W. Hayward, Phys. Rev. 79, 541 (1950).

(Ha60) B. G. Harvey, Ann. Rev. Nucl. Sci. 10, 235 (1960).

(Ha63) M. Harvey, Nucl. Phys. 48, 578 (1963).

(Ha68) J. Hattula, J. Kantele, and A. Sarmanto, Nucl. Instr. Methods 65, 17 (1968).

(Ha69) J. H. Hamilton and S. M. Brahmavor, *International Conference on Radioactivity in Nuclear Spectroscopy Techniques and Applications*, Abstracts, Vanderbuilt University (1969).

(Ho58) A. M. Hoogenboom, Nucl. Instr. Methods 3, 57 (1958).

(Ho66) P. Holmberg, F. Spring, and A. Lundán, Soc. Sci. Fennica, Commentationes Phys.-Math. 32, No. 12 (1966).

(Ho69) E. J. Hoffman and D. G. Sarantites, Phys. Rev. 177, 1640 (1969).

(Ja69) JANUS Timesharing Moniter See J. Kopf, Ph. D. Thesis, Michigan State University, 1969 for description of original version.

(Jo68) R. R. Johnson and G. D. Jones, Nucl. Phys. A122, 657 (1968).

(Jo69) H. W. Jongsma, B. Bengtsson, G. H. Dulfer, and H. Verheul, Physica 42, 303 (1969).

(Ka62) J. Kantele and R. W. Fink, Nucl. Instr. Methods 15, 69 (1962).

(Ka62a) J. Kantele, Nucl. Instr. Methods 17, 33 (1962).

(Ka70) J. Kantele and P. Suominen, Nucl. Instr. Methods 86, 65 (1970).

(Ki67) L. S. Kisslinger and K. Kumar, Phys. Rev. Lett. 19, 1239 (1967).

(Ki70) A. Kiuru and P. Holmberg, Z. Physik 233, 146 (1970).

(Kl67) E. D. Klema, L. L. Lee Jr., and J. P. Schiffer, Phys. Rev. 161, 1134 (1967).

(Ko70) K. L. Kosanke in Michigan State University Nuclear Chemistry Annual Report COO-1779-44 (1970).

(Ko71) K. L. Kosanke, W. C. Johnston, Wm. C. McHarris, F. M. Bernthal, R. A. Warner, and W. H. Kelly, Decay of ^{205}Bi (to be published).

(La57) R. D. Lawson and J. L. Uretsky, Phys. Rev. 108, 1300 (1957).

(La70) D. Larner, Phys. Rev. C2, 522 (1970).

(Le66) C. M. Lederer, J. M. Hollander, and I. Perlman, *Table of Isotopes*, 6th Ed., Wiley (1966).

(Ma57) M. Mazari, W. Buechner, and R. deFigueiredo, Phys. Rev. 108, 373 (1957).

(Ma71) A. L. Marusak, Ph. D. Thesis, University of Tennessee, ORNL-TM-2472, 1970.

(Mc66) L. C. McIntyre, Phys. Rev. 152, 1013 (1966).

(Mi48) D. R. Miller, R. C. Thompson, and B. B. Cunningham, Phys. Rev. 74, 347 (1948)

(Mo51) S. A. Moszkowski, Phys. Rev. 82, 35 (1951).

(Mo67) G. C. Morrison, private communication.

(My65) W. Myers and W. Swiatecki, UCRL-11980 (1965).

(ND) Nuclear Data B2, Nos. 3.5 (1967,1968).

(Nu54) R. H. Nussbaum, A. H. Wapstra, R. van Lieshout, G. J. Nijgh, and L. T. Ornstein, Physica 20, 571 (1954).

(Nu65) M. Nurmia and R. W. Fink, Phys. Lett. 14, 136 (1965).

(Pa70) V. Paar, Nucl. Phys. A147, 369 (1970).

(Ph68) E. A. Phillips and A. D. Jackson Jr., Phys. Rev. 169, 917 (1967).

(Po67) R. M. Polichar, J. E. Steigerwalt, J. W. Sunier, and J. R. Richardson, Phys. Rev. 163, 1084 (1967).

(Ro67) K. I. Roulston, E. H. Becker, and R. A. Brown, Phys. Lett. 24B, 93 (1967).

(Ro68) P. Roussel, G. Bruge, A. Bussiere, H. Faraggi, and J. E. Testoni, Nucl. Phys. A155, 306 (1970).

(Ro69) J. T. Routi and S. G. Prussin, Nucl. Instr. Methods 72, 125 (1969); and J. T. Routi UCRL-19452.

(Ru71) T. D. Rupp and S. H. Vegors Jr., Nucl. Phys. A163, 545 (1971).

(Si69) L. Simons and T. Sundius, Soc. Sci. Fennica, Commentationes Phys.-Math. 34, No. 9 (1969)

(Ta61) R. Taagepera and M. Nurmia, Ann. Acad. Sci. Fennicae, A VI, No. 78 (1961).

(Ta70) S. Tanaka, P. H. Stelson, W. T. Bass, and J. Lin, Phys. Rev. C2, 160 (1970).

(Th65) V. K. Thankappan and W. W. True, Phys. Rev. 137, B793 (1965).

(Va70) D. M. VanPatter, D. Neuffer, H. L. Scott, and C. Moazed, Nucl. Phys. A146, 427 (1970).

(Vo67) D. vonEhrenstein and J. P. Schiffer, Phys. Rev. 164, 1374 (1967).

(Wa59) A. H. Wapstra, G. J. Nijgh, and R. vanLieshout, *Nuclear Spectroscopy Tables*, North Holland Publ. Co., Amsterdam (1959).

(Wo70) S. S. M. Wong, Nucl. Phys. A159, 235 (1970).

(Yo68) H. J. Young and J. Rapaport, Phys. Lett. 26B, 143 (1968).

(Ze60) B. Zeidman, J. L. Yntema, and B. J. Raz, Phys. Rev. 120, 1723 (1960).

(Zw54) P. F. Zweifel, Phys. Rev. 96, 1572 (1954) and 107, 329 (1957).

APPENDICES

APPENDIX A

EVENT RECOVERY FORTRAN and SYMBOL Listing

```
FORTRAN
      EVENT RECOVERY
      DIMENSION SPEC(4096,10),NSPEC(4096),TITLE(10,10),T(30),MIL(10),MFL
     1(10),MI(10),MF(10),MIR(10),MFR(10),NCHAN(10),NSQ(10),NT(
     210),AL(10),A(10),AR(10),NA(10),NB(10)
      COMMON SPEC
      EQUIVALENCE(SPEC,NSPEC)
C     SPEC(I,J)=COUNTS IN CHANNEL I OF THE JTH DISPLAY SPECTRUM
C
C
C        KX=MOST  SIGNIFICANT HALF WORD
C        KY=LEAST SIGNIFICANT HALF WORD
      NR=0
   26 JI=0
   20 DO 4 J=1,10
      READ(105,2,END=8)MIL(J),MFL(J),MI(J),MF(J),MIR(J),MFR(J),NCHAN(J),
     1NA(J),NB(J),NT(J),NSQ(J),NSQEZ(J),(TITLE(I,J),I=1,10)
    2 FORMAT(715,5I1,10A4)
      IF(NCHAN(J).EQ.0)NCHAN(J)=1024
    5 DO 6 I=1,4096
    6 SPEC(I,J)=0.
      AL(J)=0.
      AR(J)=0.
      IF(MFL(J).EQ.0)GO TO 4
      AL(J)=MFL(J)-MIL(J)+1
      AR(J)=MFR(J)-MIR(J)+1
    4 CONTINUE
      J=11
    8 J=J-1
      JK=JI*10+J
      IF(JK.LE.0)GO TO 31
      IF(J.EQ.0)GO TO 26
      PRINT 25,((MIL(L),MFL(L),MI(L),MF(L),MIR(L),MFR(L),NCHAN(L),NT(L),
     1NA(L),NB(L),NSQ(L),NSQEZ(L),(TITLE(I,L),I=1,10)),L=1,J)
   25 FORMAT(1H0,'MIL  MFL  MI   MF   MIR  MFR  NCHAN NTAPE XADC  NB
     1  NSQ  NSQEZ      TITLE'/(3X,2I5,2(I4,I3),I6,5I5,4X,10A4))
      IF(NR.EQ.1)CALL CHAIN(18S)
   18 NEVENT=0
      NTAPE=NT(1)
      CALL SETUP(NA,NB,NSQ,SPEC,AL,AR,MIL,MFL,MI,MF,MIR,MFR,J)
```

C — AL,AR=A(J)/(AL(J)*2) FACTORS FOR LEFT AND RIGHT GATE SPECTRA USED BELOW

C — A(J)=MF(J)-MI(J)+1 LEFT,RIGHT, AND CENTER GATES

C — NCHAN(J)=1024 CHANNELS IN SPECTRUM

```
      DO 19 L=1,NTAPE
      READ(109,1) T
    1 FORMAT(30A4)
      PRINT 3,T
    3 FORMAT(2X,30A4)
      NLAST=NTAPE-L
      CALL DATA(NLAST,NEVENT,NBAD,19S)
   19 CONTINUE
      DO 30 K=1,J
      NC=NCHAN(K)
      IF(NC.EQ.1)GO TO 30
      IF(NSQEZ(K).LT.2)GO TO 23
      NC=NCHAN(K)/NSQEZ(K)
      DO 22 I=1,NC
      SPEC(I,K)=0.
      NH=I*NSQEZ(K)
      NL=NH-NSQEZ(K)+1
      DO 21 L=NL,NH
   21 SPEC(I,K)=SPEC(I,K)+SPEC(L,K)
   22 CONTINUE
   23 DO 24 L=1,NC
      NSPEC(L)=SPEC(L,K)
      IF(NSPEC(L).LT.0)NSPEC(L)=0
   24 CONTINUE
      JK=JI*10+K
      PUNCH 29,NC,(TITLE(L,K),L=1,10),JK
   29 FORMAT('*C     1',I4,4X,10A4,I24)
      CALL CPUNCH(NSPEC,NC,JK)
   30 CONTINUE
      PRINT 28,NEVENT,NBAD
   28 FORMAT(/ ' THE NUMBER OF EVENTS =',I7,10X,'THE NUMBER OF BAD COUNT
     1S = ',I7///)
      NR=1
      IF(J.LT.10)GO TO 26
      JI=JI+1
      GO TO 20
   31 END
```

```
 1                          *        SUBROUTINE SETUP(NA,NB,NSQ,SPEC,AL,AR,MIL,MFL,MI,MF,MIR,MFR,J)
 2                          *
 3                          *        LOADS POINTERS INTO LOCATIONS FOR USE IN SUBROUTINE DATA
 4                          *
 5                                   DEF      SETUP
 6                                   DEF      DATA,CHAIN
 7                                   REF      F:109
 8  00000  00000000  A      NA       DATA     0                    ADC SET USED
 9  00001  00000000  A      NB       DATA     0                    POINTER FOR NB
10  00002  00000000  A      NSQ      DATA     0                    POINTER FOR NSQ
11  00003  00000000  A      SPEC     DATA     0                    POINTER FOR SPEC
12  00004  00000000  A      AL       DATA     0                    POINTER FOR AL
13  00005  00000000  A      AR       DATA     0                    POINTER FOR AR
14  00006  00000000  A      J        DATA     0                    NUMBER OF CONTROL CARDS
15  00007  00000000  A      NEVENT   DATA     0
16  00008  00000000  A      NBAD     DATA     0
17  0000A                             BOUND    8                    SET UP AS DOUBLE WORDS
18  0000A                  LIMITS     RES      60                   STACK FOR LIMITS
```

```
19                                          PAGE
20          00046                   SETUP   EQU     $               ENTRY POINT
21  00046       3270000D    A               LW,7    13              GET LOCATION OF ARGUMENTS
22  00047       326E0001    A               LW,6    1,7             GET POINTER FOR NA
23  00048       B2600006    A               LW,6    *6              GET NA
24  00049       35600000                    STW,6   NA              AND STORE IT
25  0004A       326E0002    A               LW,6    2,7             GET POINTER FOR NB
26  0004B       35600001                    STW,6   NB              AND STORE IT
27  0004C       326E0003    A               LW,6    3,7             GET POINTER FOR NSQ
28  0004D       35600002                    STW,6   NSQ             AND STORE IT
29  0004E       326E0004    A               LW,6    4,7             GET POINTER FOR SPEC
30  0004F       35600003                    STW,6   SPEC            AND STORE IT
31  00050       326E0005    A               LW,6    5,7             GET POINTER FOR AL
32  00051       35600004                    STW,6   AL              AND STORE IT
33  00052       326E0006    A               LW,6    6,7             GET POINTER FOR AR
34  00053       35600005                    STW,6   AR              AND STORE IT
35  00054       320E0007    A               LW,0    7,7             GET POINTER FOR MIL
36  00055       321E0008    A               LW,1    8,7             GET POINTER FOR MFL
37  00056       322E0009    A               LW,2    9,7             GET POINTER FOR MI
38  00057       323E000A    A               LW,3    10,7            GET POINTER FOR MF
39  00058       324E000B    A               LW,4    11,7            GET POINTER FOR MIR
40  00059       325E000C    A               LW,5    12,7            GET POINTER FOR MFR
41  0005A       326E000D    A               LW,6    13,7            GET POINTER FOR J
42  0005B       32600006    A               LW,6    *6              AND GET J
43  0005C       35600006                    STW,6   J               AND STORE IT
44  0005D       22700000    A               LI,7    0               INITIALIZE POINTER
45  0005E       35700007                    STW,7   NEVENT          RESET EVENT COUNTER
46  0005F       35700008                    STW,7   NBAD            RESET BAD EVENT COUNTER
47  00060       B28E0000    A       SET1    LW,8    *0,7            LOAD MIL
48  00061       B29E0001    A               LW,9    *1,7            LOAD MFL
49  00062       158E000A                    STD,8   LIMITS,7        STORE LEFT LIMITS
50  00063       B28E0002    A               LW,8    *2,7            LOAD MI
51  00064       B29E0003    A               LW,9    *3,7            LOAD MF
52  00065       158E001E                    STD,8   LIMITS+20,7     STORE PEAK LIMITS
53  00066       B28E0004    A               LW,8    *4,7            LOAD MIR
54  00067       B29E0005    A               LW,9    *5,7            LOAD MFR
55  00068       158E0032                    STD,8   LIMITS+40,7     STORE RIGHT LIMITS
56  00069       20700001    A               AI,7    1               INCREMENT POINTER
57  0006A       31700006    A               CW,7    6               IS IT LAST CARD
58  0006B       69100060                    BL      SET1            LOOP IF NOT
59  0006C       B0D0000D    A               AW,13   *13             GET ADDRESS OF LAST ARGUMENT
60  0006D       20D00001    A               AI,13   1               SKIP TO NEXT LOCATION
61  0006E       E8D0000D    A               B       *13             AND GO THERE
```

```
                                        PAGE
                                *
                                *       SUBROUTINE DATA(NLAST,NEVENT,NBAD,&19)
                                *
                                *       PERFORMS OPERATIONS WITH EVENT RECORDER TAPES
                                *       TAPES READ FROM F:109  UP TO 60 WORD RECORDS
                                *
                                *       NORMAL ENTRY WITH NLAST INDICATING IF LAST TAPE
                                *       NORMAL RETURN WITH NEVENT GIVING NUMBER OF COINCIDENCE EVENTS,
                                *       NBAD GIVING THE NUMBER OF SINGLE COUNTS TO END ADDRESS &19
                                *       IF READ ERROR, FORGET IT AND GET ANOTHER RECORD
                                *
00000003                ARG     EQU     3               FORTRAN ARGUMENT REGISTER
00000006                R6      EQU     6
00000007                R7      EQU     7
00000008                SR1     EQU     8
0000000A                SR3     EQU     10
0000000D                RET     EQU     13              FORTRAN LINK REGISTER
0000000D                R13     EQU     13              SAVE FLOAT MODE
                                *
00070                           BOUND   8
00070   01000000    A   EOFCODES DATA    X'01000000',X'06FFFFFF'
00071   06FFFFFF    A
00072                   BUF     RES     60                                              170
000AE   00000078    A   VAL     DATA    120
000AF   00000078    A   SIZE    DATA    120
000B0   41100000    A   A       DATA    FS'1.0'
000B1   10000000    N   READ    GEN,8,24 X'10',F:109    FPT FOR READ OPERATION
000B2   F0000010    A           DATA    X'F0000010'
000B3   00000000    N           DATA    ERR
000B4   00000000    N           DATA    ABN
000B5   00000072            BUF DATA    BUF
000B6   000000F0    A           DATA    240
000B7   01000000    N   REWIND  GEN,8,24 1,F:109        REWIND TAPE
000B8   03000000    N   CVOL    GEN,8,24 X'03',F:109    CHANGE VOLUME CALL
000B9   80000000    A           GEN,1,31 X'1',X'0'
000BA   00000000    F           PZE     ABN
```

```
                                    PAGE
                          *
          000BB           DATA      EQU       $              SUBROUTINE ENTRY POINT
                          *
          000BB           NEXT      EQU       $              ENTRY FOR COINCIDENCE PAIR
   000BB    7400000D  A             STCF      R13            SAVE FLOAT MODE
   000BC    02300000  A             LCFI      0,0            AND SET LIGHTS TO OFF
   000BD    68000000  F             B         NEXT1          GET FIRST VALUE
   000BE    33100008      NEXT2     MTW,1     NBAD           INCREMENT BAD READ COUNTER
   000BF    331000AE      NEXT1     MTW,1     VAL            SET POINTER TO NEXT VALUE
   000C0    323000AE                LW,ARG    VAL            GET POINTER
   000C1    313000AF                CW,ARG    SIZE           IS IT TOO BIG
   000C2    69100000  F             BL        GETIT          IF NOT, USE IT
   000C3    C41000B1      ERR       CAL1,1    READ           ELSE READ ANOTHER RECORD
   000C4    22300004  A             LI,ARG    4              GET OFFSET FOR ACTUAL RECORD SIZE
   000C5    32360000  X             LW,ARG    F:109,ARG      AND PICK IT UP
   000C6    2530006E  A             SLS,ARG   -18            ALIGN AS HALFWORD COUNT
   000C7    353000AF                STW,ARG   SIZE           AND STORE
   000C8    22300000  A             LI,ARG    0              THEN
   000C9    353000AE                STW,ARG   VAL            RESET POINTER
   000CA    32700000      GETIT     LW,R7     NA             GET ADCS USED
   000CB    21700004  A             CI,R7     4              IS IT OLD EVENT RECORDER
   000CC    69300000  F             BNE       GETNEW         IF NOT, JUMP
   000CD    20300001  A             AI,ARG    1              SET POINTER
   000CE    68000000  F             B         GETOLD         JUMP TO GET DATA
   000CF    52660072      GETNEW    LH,R6     BUF,ARG        LOAD FIRST HALF WORD
   000D0    25600072  A             SLS,R6    -14            GET ITS ADC
   000D1    4B600000  F             AND,R6    =X'3'          MASK OFF GARBAGE
   000D2    32700000                LW,R7     NA             LOAD XADC
   000D3    31700006  A             CW,R7     R6             COMPARE TO CHECK IF CORRECT
   000D4    693000BE                BNE       NEXT2          IF NOT,GET NEW COUNT,INCREMENT BAD COU
   000D5    20300001  A             AI,ARG    1              LOOK AT YADC
   000D6    52660072                LH,R6     BUF,ARG        LOAD SECOND HALF WORD
   000D7    25600072  A             SLS,R6    -14            GET ITS ADC
   000D8    4B600000  F             AND,R6    =X'3'          MASK OFF GARBAGE
   000D9    20700001  A             AI,R7     1              GET SECOND ADC
   000DA    31700006  A             CW,R7     R6             COMPARE THESE TWO
   000DB    693000BE                BNE       NEXT2          IF NOT,GET NEW COUNT,INCREMENT BAD COU
   000DC    52760072      GETOLD    LH,R7     BUF,ARG        LOAD Y SIDE
   000DD    4B700000  F             AND,R7    =X'1FFF'       MASK OFF GARBAGE
   000DE    68200000  F             BLEZ      ZERO           JUMP IF X=0
   000DF    203FFFFF  A             AI,ARG    -1             GET LOCATION OF X EVENT
   000E0    52660072                LH,R6     BUF,ARG        GET X EVENT
```

```
000E1       48600000  F             AND,R6    =X'1FFF'      MASK OFF GARBAGE
000E2       68200000  F             BLEZ      ZERO          JUMP IF Y=0
000E3       331000AE                MTW,1     VAL           SET POINTER TO NEXT EVENT
000E4       33100007                MTW,1     NEVENT        INCREMENT EVENT COUNTER
      000E5                 EXIT    EQU       $             NORMAL EXIT WITH DATA
000E5       7030000D  A             LCF       R13           RESTORE FLOAT MODE
000E6       68000000  F             B         STORE         JUMP TO STORAGE ROUTINE
                            *
000E7       331000AE        ZERO    MTW,1     VAL           SET POINTER TO NEXT EVENT
000E8       33100007                MTW,1     NEVENT        INCREMENT EVENT COUNTER
000E9       680000BF                B         NEXT1         AND GET NEXT EVENT
                            *
                            *       HERE IF ABNORMAL CONDITION
      000EA                 ABN     EQU       $
000EA       19A00070                CLM,SR3   EOFCODES      DOES IT LOOK LIKE EOF
000EB       E9900008  A             BCS,9     *SR1          IGNORE IF NOT
000EC       041000B7                CAL1,1    REWIND        REWIND TAPE
000ED       3270000D  A             LW,R7     RET           GET LOCATION OF ARGUMENTS
000EE       327E0001  A             LW,R7     1,R7          GET POINTER FOR NLAST
000EF       52700007  A             LW,R7     *R7           GET NLAST
000F0       68200000  F             BLEZ      RETURN        JUMP IF LAST TAPE
000F1       041000B8        CHAIN   CAL1,1    CVOL          CHANGE VOLUME CALL
      000F2                 RETURN  EQU       $             RETURN FROM CHANGE VOLUME
000F2       7030000D  A             LCF       R13           RESTORE FLOAT MODE
000F3       3270000D  A             LW,R7     RET           GET LOCATION OF ARGUMENTS
000F4       327E0002  A             LW,R7     2,R7          GET POINTER FOR NEVENT
000F5       32600007                LW,R6     NEVENT        GET NUMBER OF EVENTS
000F6       B5600007  A             STW,R6    *R7           AND STORE IT
000F7       3270000D  A             LW,R7     RET           GET LOCATION OF ARGUMENTS
000F8       327E0003  A             LW,R7     3,R7          GET POINTER FOR NBAD
000F9       32600008                LW,R6     NBAD          GET NUMBER OF BAD COUNTS
000FA       B5600007  A             STW,R6    *R7           AND STORE IT
000FB       B0D0000D  A     RETURN1 AW,RET    *RET          GET LAST ARGUMENT(ERROR ADDRESS)
000FC       B2D0000D  A             LW,RET    *RET
000FD       E800000D  A             B         *RET          AND GO THERE
```

```
                                     PAGE
                            *
                            *        R4 CØNTAINS INDEX I
                            *        R5 CØNTAINS X+Y
                            *        R6 CØNTAINS X
                            *        R7 CØNTAINS Y
                            *
          000FE             STØRE    EQU       $                ENTRY TØ DATA STØRAGE RØUTINE
000FE        21601FFF  A             CI,6      8191             IS X BUFFER FILLER
000FF        69100102                BL        $+3              SKIP IF NØT
00100        21701FFF  A             CI,7      8191             IS Y BUFFER FILLER
00101        681000BB                BGE       NEXT             IF BØTH ARE, GET NEXT EVENT
00102        22400000  A             LI,4      0                INITIALIZE CØNTRØL CARD INDEX
00103        32500006  A             LW,5      6                LØAD X
00104        30500007  A             AW,5      7                ADD Y
          00105             7S       EQU       $
00105        B2380002                LW,3      *NSQ,4           GET TYPE ØF GATING
00106        68060000  F             B         9S,3             GØ TØ ITS STØRE RØUTINE     NSQ
00107        68000000  F    9S       B         27S              DISPLAY X  GATE Y            0
00108        68000000  F             B         12S              DISPLAY Y  GATE X            1
00109        68000000  F             B         15S              ANY X                        2
0010A        68000000  F             B         16S              ANY Y                        3
0010B        68000000  F             B         18S              ANY SUM                      4
0010C        68000000  F             B         19S              DISPLAY X  GATE SUM          5
0010D        68000000  F             B         22S              DISPLAY Y  GATE SUM          6
0010E        68000000  F             B         17S              UNUSED CØNTRØL PARAMETER     7
0010F        68000000  F             B         17S              UNUSED CØNTRØL PARAMETER     8
00110        68000000  F             B         17S              UNUSED CØNTRØL PARAMETER     9
                            *
                            *        DISPLAY X  GATE Y
                            *
00111        1978000A       27S      CLM,7     LIMITS,4         IS Y IN LØWER BACKGRØUND
00112        69100000  F             BCS,1     17S              IF BELØW  GØ TØ NEXT CARD
00113        69800000  F             BCS,8     10S              IF ABØVE  GØ TØ PEAK
00114        22301000  A             LI,3      4096             LØAD ARRAY SIZE
00115        37300004  A             MW,3      4                ØBTAIN ARRAY LØCATIØN
00116        30300006  A             AW,3      6                ADD CHANNEL ADDRESS
00117        B2A60003                LW,10     *SPEC,3          LØAD CHANNEL
00118        BCA80004                FSS,10    *AL,4            SUBTRACT WEIGHTED BACKGRØUND
00119        B5A60003                STW,10    *SPEC,3          AND STØRE
0011A        68000000  F             B         17S              GØ TØ NEXT CARD
0011B        1978001E       10S      CLM,7     LIMITS+20,4      IS Y IN PEAK
0011C        69100000  F             BCS,1     17S              IF BELØW  GØ TØ NEXT CARD
```

```
219  0011D  69800000  F          BCS,8    11S          IF ABOVE  GO TO UPPER BACKGROUND
220  0011E  22301000  A          LI,3     4096         LOAD ARRAY SIZE
221  0011F  37300004  A          MW,3     4            OBTAIN ARRAY LOCATION
222  00120  30300006  A          AW,3     6            ADD CHANNEL ADDRESS
223  00121  B2A60003              LW,10    *SPEC,3      LOAD CHANNEL
224  00122  3DA0000B0             FAS,10   A            ADD ONE COUNT
225  00123  B5A60003              STW,10   *SPEC,3      AND STORE
226  00124  68000000  F          B        17S          GO TO NEXT CARD
227  00125  19780032       11S   CLM,7    LIMITS+40,4  IS Y IN UPPER BACKGROUND
228  00126  69900000  F          BCS,9    17S          IF NOT  GO TO NEXT CARD
229  00127  22301000  A          LI,3     4096         LOAD ARRAY SIZE
230  00128  37300004  A          MW,3     4            OBTAIN ARRAY LOCATION
231  00129  30300006  A          AW,3     6            ADD CHANNEL ADDRESS
232  0012A  B2A60003              LW,10    *SPEC,3      LOAD CHANNEL
233  0012B  BCA80005              FSS,10   *AR,4        SUBTRACT WEIGHTED BACKGROUND
234  0012C  B5A60003              STW,10   *SPEC,3      AND STORE
235  0012D  68000000  F          B        17S          GO TO NEXT CARD
236                        *
237                        *      DISPLAY Y  GATE X
238                        *
239  0012E  1968000A       12S   CLM,6    LIMITS,4     IS X IN LOWER BACKGROUND
240  0012F  69100000  F          BCS,1    17S          IF BELOW  GO TO NEXT CARD
241  00130  69800000  F          BCS,8    13S          IF ABOVE  GO TO PEAK
242  00131  22301000  A          LI,3     4096         LOAD ARRAY SIZE
243  00132  37300004  A          MW,3     4            OBTAIN ARRAY LOCATION
244  00133  30300007  A          AW,3     7            ADD CHANNEL ADDRESS
245  00134  B2A60003              LW,10    *SPEC,3      LOAD CHANNEL
246  00135  BCA80004              FSS,10   *AL,4        SUBTRACT WEIGHTED BACKGROUND
247  00136  B5A60003              STW,10   *SPEC,3      AND STORE
248  00137  68000000  F          B        17S          GO TO NEXT CARD
249  00138  1968001E       13S   CLM,6    LIMITS+20,4  IS X IN PEAK
250  00139  69100000  F          BCS,1    17S          IF BELOW  GO TO NEXT CARD
251  0013A  69800000  F          BCS,8    14S          IF ABOVE  GO TO UPPER BACKGROUND
252  0013B  22301000  A          LI,3     4096         LOAD ARRAY SIZE
253  0013C  37300004  A          MW,3     4            OBTAIN ARRAY LOCATION
254  0013D  30300007  A          AW,3     7            ADD CHANNEL ADDRESS
255  0013E  B2A60003              LW,10    *SPEC,3      LOAD CHANNEL
256  0013F  3DA0000B0             FAS,10   A            ADD ONE COUNT
257  00140  B5A60003              STW,10   *SPEC,3      AND STORE
258  00141  68000000  F          B        17S          GO TO NEXT CARD
259  00142  19680032       14S   CLM,6    LIMITS+40,4  IS X IN UPPER BACKGROUND
260  00143  69900000  F          BCS,9    17S          IF NOT  GO TO NEXT CARD
261  00144  22301000  A          LI,3     4096         LOAD ARRAY SIZE
```

```
00145     37300004  A            MW,3      4          ØBTAIN ARRAY LØCATIØN
00146     30300007  A            AW,3      7          ADD CHANNEL ADDRESS
00147     B2A60003               LW,10     *SPEC,3    LØAD CHANNEL
00148     BCA80005               FSS,10    *AR,4      SUBTRACT WEIGHTED BACKGRØUND
00149     B5A60003               STW,10    *SPEC,3    AND STØRE
0014A     68000000  F            B         17S        GØ TØ NEXT CARD
                          *
                          *      ANY X
                          *
0014B     22301000  A     15S    LI,3      4096       LØAD ARRAY SIZE
0014C     37300004  A            MW,3      4          ØBTAIN ARRAY LØCATIØN
0014D     30300006  A            AW,3      6          ADD CHANNEL ADDRESS
0014E     B2A60003               LW,10     *SPEC,3    LØAD CHANNEL
0014F     3DA000B0               FAS,10    A          ADD ØNE CØUNT
00150     B5A60003               STW,10    *SPEC,3    AND STØRE
00151     68000000  F            B         17S        GØ TØ NEXT CARD
                          *
                          *      ANY Y
                          *
00152     22301000  A     16S    LI,3      4096       LØAD ARRAY SIZE
00153     37300004  A            MW,3      4          ØBTAIN ARRAY LØCATIØN
00154     30300007  A            AW,3      7          ADD CHANNEL ADDRESS
00155     B2A60003               LW,10     *SPEC,3    LØAD CHANNEL
00156     3DA000B0               FAS,10    A          ADD ØNE CØUNT
00157     B5A60003               STW,10    *SPEC,3    AND STØRE
00158     68000000  F            B         17S        GØ TØ NEXT CARD
                          *
                          *      ANY SUM
                          *
       00159              18S    EQU       $
00159     32800005  A            LW,8      5          GET SUM
0015A     B2280001               LW,2      *NB,4      GET TYPE ØF SUM
0015B     21200001  A     18C    CI,2      1          WHAT TYPE ØF SUM
0015C     69100000  F            BL        18A        IF LESS, GØ TØ STØRAGE
0015D     69200000  F            BG        18B        IF GREATER, GØ TØ X<Y
0015E     31600007  A            CW,6      7          IS X>Y
0015F     68200000  F            BLE       17S        IF NØT  GØ TØ NEXT CARD
00160     68000000  F            B         18A        ØTHERWISE STØRE IT
00161     31600007  A     18B    CW,6      7          IS X<Y
00162     68100000  F            BGE       17S        IF NØT  GØ TØ NEXT CARD
00163     22301000  A     18A    LI,3      4096       LØAD ARRAY SIZE
00164     37300004  A            MW,3      4          ØBTAIN ARRAY LØCATIØN
00165     30300008  A            AW,3      8          ADD CHANNEL ADDRESS
```

```
00166   B2A60003            LW,10    *SPEC,3      LOAD CHANNEL
00167   3DA000B0            FAS,10   A            ADD ONE COUNT
00168   B5A60003            STW,10   *SPEC,3      AND STORE
00169   68000000  F         B        17S          GO TO NEXT CARD
                      *
                      *     DISPLAY X  GATE SUM
                      *
        0016A         19S   EQU      $
0016A   B2280001            LW,2     *NB,4        GET TYPE OF SUM
0016B   68300000  F         BEZ      19A          IF NONE  GO TO STORAGE ROUTINE
0016C   21200001  A         CI,2     1            IS IT X>Y
0016D   69300000  F         BNE      19B          IF NOT  GO TO X<Y
0016E   31600007  A         CW,6     7            IS X>Y
0016F   68200000  F         BLE      17S          IF NOT  GO TO NEXT CARD
00170   68000000  F         B        19A          OTHERWISE STORE IT
00171   31600007  A   19B   CW,6     7            IS X<Y
00172   68100000  F         BGE      17S          IF NOT  GO TO NEXT CARD
00173   1958000A      19A   CLM,5    LIMITS,4     IS SUM IN LOWER BACKGROUND
00174   69100000  F         BCS,1    17S          IF BELOW  GO TO NEXT CARD
00175   69800000  F         BCS,8    20S          IF ABOVE  GO TO PEAK
00176   22301000  A         LI,3     4096         LOAD ARRAY SIZE
00177   37300004  A         MW,3     4            OBTAIN ARRAY LOCATION
00178   30300006  A         AW,3     6            ADD X ADDRESS
00179   B2A60003            LW,10    *SPEC,3      LOAD CHANNEL
0017A   BCA80004            FSS,10   *AL,4        SUBTRACT WEIGHTED BACKGROUND
0017B   B5A60003            STW,10   *SPEC,3      AND STORE
0017C   68000000  F         B        17S          GO TO NEXT CARD
0017D   1958001E      20S   CLM,5    LIMITS+20,4  IS SUM IN PEAK
0017E   69100000  F         BCS,1    17S          IF BELOW  GO TO NEXT CARD
0017F   69800000  F         BCS,8    21S          IF ABOVE  GO TO UPPER BACKGROUND
00180   22301000  A         LI,3     4096         LOAD ARRAY SIZE
00181   37300004  A         MW,3     4            OBTAIN ARRAY LOCATION
00182   30300006  A         AW,3     6            ADD X ADDRESS
00183   B2A60003            LW,10    *SPEC,3      LOAD CHANNEL
00184   3DA000B0            FAS,10   A            ADD ONE COUNT
00185   B5A60003            STW,10   *SPEC,3      AND STORE
00186   68000000  F         B        17S          GO TO NEXT CARD
00187   19580032      21S   CLM,5    LIMITS+40,4  IS SUM IN UPPER BACKGROUND
00188   69900000  F         BCS,9    17S          IF NOT  GO TO NEXT CARD
00189   22301000  A         LI,3     4096         LOAD ARRAY SIZE
0018A   37300004  A         MW,3     4            OBTAIN ARRAY LOCATION
0018B   30300006  A         AW,3     6            ADD X ADDRESS
0018C   B2A60003            LW,10    *SPEC,3      LOAD CHANNEL
```

```
0018D      BCA80005         FSS,10   *AR,4         SUBTRACT WEIGHTED BACKGROUND
0018E      B5A60003         STW,10   *SPEC,3       AND STORE
0018F      68000000  F      B        17S           GO TO NEXT CARD
                       *
                       *    DISPLAY Y  GATE SUM
                       *
      00190            22S  EQU      $
00190      B2280001         LW,2     *NB,4         GET TYPE OF SUM
00191      68300000  F      BEZ      22A           IF NONE  GO TO STORAGE ROUTINE
00192      21200001  A      CI,2     1             IS IT X>Y
00193      69300000  F      BNE      22B           IF NOT  GO TO X<Y
00194      31600007  A      CW,6     7             IS X>Y
00195      68200000  F      BLE      17S           IF NOT  GO TO NEXT CARD
00196      68000000  F      B        22A           OTHERWISE STORE IT
00197      31600007  A 22B  CW,6     7             IS X<Y
00198      68100000  F      BGE      17S           IF NOT  GO TO NEXT CARD
00199      1958000A    22A  CLM,5    LIMITS,4      IS SUM IN LOWER BACKGROUND
0019A      69100000  F      BCS,1    17S           IF BELOW  GO TO NEXT CARD
0019B      69800000  F      BCS,8    23S           IF ABOVE  GO TO PEAK
0019C      22301000  A      LI,3     4096          LOAD ARRAY SIZE
0019D      37300004  A      MW,3     4             OBTAIN ARRAY LOCATION
0019E      30300007  A      AW,3     7             ADD Y ADDRESS
0019F      B2A60003         LW,10    *SPEC,3       LOAD CHANNEL
001A0      BCA80004         FSS,10   *AL,4         SUBTRACT WEIGHTED BACKGROUND
001A1      B5A60003         STW,10   *SPEC,3       AND STORE
001A2      68000000  F      B        17S           GO TO NEXT CARD
001A3      1958001E    23S  CLM,5    LIMITS+20,4   IS SUM IN PEAK
001A4      69100000  F      BCS,1    17S           IF BELOW  GO TO NEXT CARD
001A5      69800000  F      BCS,8    24S           IF ABOVE  GO TO UPPER BACKGROUND
001A6      22301000  A      LI,3     4096          LOAD ARRAY SIZE
001A7      37300004  A      MW,3     4             OBTAIN ARRAY LOCATION
001A8      30300007  A      AW,3     7             ADD Y ADDRESS
001A9      B2A60003         LW,10    *SPEC,3       LOAD CHANNEL
001AA      3DA000B0         FAS,10   A             ADD ONE COUNT
001AB      B5A60003         STW,10   *SPEC,3       AND STORE
001AC      68000000  F      B        17S           GO TO NEXT CARD
001AD      19580032    24S  CLM,5    LIMITS+40,4   IS SUM IN UPPER BACKGROUND
001AE      69900000  F      BCS,9    17S           IF NOT  GO TO NEXT CARD
001AF      22301000  A      LI,3     4096          LOAD ARRAY SIZE
001B0      37300004  A      MW,3     4             OBTAIN ARRAY LOCATION
001B1      30300007  A      AW,3     7             ADD Y ADDRESS
001B2      B2A60003         LW,10    *SPEC,3       LOAD CHANNEL
001B3      BCA80005         FSS,10   *AR,4         SUBTRACT WEIGHTED BACKGROUND
```

```
391  001B4    B5A60003           STW,10   *SPEC,3        AND STORE
392  001B5    68000000  F        B        17S            GO TO NEXT CARD
393                        *
394                        *     HERE TO NEXT CARD
395                        *
396           001B6        17S   EQU      *
397  001B6    20400001  A        AI,4     1              INCREMENT INDEX BY ONE
398  001B7    31400006           CW,4     J              WAS IT LAST CARD
399  001B8    69100105           BL       7S             IF NOT  L000000P
400  001B9    680000BB           B        NEXT           IF SO  GO TO NEXT EVENT
401                                END
     001BA    00000003  A
     001BB    00001FFF  A
```

```
FORTRAN
      1          C     MOIRAE ENERGY AND INTENSITY CALIBRATION
      2                DIMENSION A(300),SDA(300),Y(300),NPKLO(300),NPKHI(300),Q(300),X(30
      3               10),E(40),F(40),NEC(40),COFT(4),TITLE(16),U(7)
      4                REAL LOG
      5             22 READ(105,10,END=12)NPTS,NGECC,NENCO,XM,XN,TITLE
      6             10 FORMAT(3I2,2F5.2,16A4)
      7             81 READ 11,(F(I),I=1,NPTS)
      8             11 FORMAT(8F10.0)
      9                IF(XM.NE.0.)READ 11,U
     10                IF(NENCO.NE.0)GO TO 95
     11                NU=1
     12                NENCO=NPTS
     13                DO 3 I=1,NPTS
     14              3 E(I)=F(I)
     15                GO TO 19
     16             95 READ 99,(NEC(L),L=1,NENCO)
     17             99 FORMAT(40I2)
     18                LI=1
     19                DO 4 L=1,NPTS
     20                DO 5 LL=1,NENCO
     21                IF(NEC(LL).NE.L)GO TO 5
     22                I=LL
     23                GO TO 9
     24              5 CONTINUE
     25                I=NENCO+LI
     26                LI=LI+1
     27              9 READ 1,NURUN,A(I),SDA(I),X(I),NPKLO(I),NPKHI(I)
     28                E(I)=F(L)
     29              4 CONTINUE
     30                NU=NPTS+1
     31             19 DO 2 I=NU,300
     32             20 READ(105,1,END=21)NURUN,A(I),SDA(I),X(I),NPKLO(I),NPKHI(I)
     33              1 FORMAT (I5,   F14.0,F10.2,F7.2,2I4)
     34              2 CONTINUE
     35             21 NEWX=I-1
     36             23 PRINT 93,NURUN,(TITLE(L),L=1,16)
     37             93 FORMAT ('1' 9X 'RUN NUMBER' I5, 10X,16A4/)
     38                NTERM=3
     39                IF(NENCO.LE.3)NTERM=2
     40                CALL BESTFIT(E,X,NENCO,NTERM,COFT)
     41                PRINT 96
     42             96 FORMAT('0',5X,'COEFFICIENTS OF CALCULATED LEAST SQUARES FIT ARE:')
```

```
      DO 50 M=1,NTERM
      N=M-1
      PRINT 97,N,COEFT(M)
   97 FORMAT (9X,'A',I2,'  =',F20.10)
   50 CONTINUE
      PRINT 91
   91 FORMAT('0',9X,'C',7X,'E',13X,'E FITTED     DEVIATION IN KEV')
      SD=0.
      DO 52 N=1,NENCO
      Y(N)=0.
      DO 53 M=1,NTERM
      MA=M-1
      Y(N)=Y(N)+COEFT(M)*(X(N)**MA)
   53 CONTINUE
      DEV=E(N)-Y(N)
      SD=SD+DEV*DEV
      PRINT 92,X(N),E(N),Y(N),DEV
   92 FORMAT(F13.2,F9.2,F18.2,F12.3)
   52 CONTINUE
      SD=SQRT(SD/(NENCO-1))
      PRINT 6,SD
    6 FORMAT('0    STANDARD DEVIATION IN CALIBRATION ENERGIES',F12.4)
      NE=NENCO+1
      IF(NE.GT.NEWX)GO TO 71
      DO 70 N=NE,NEWX
      Y(N)=0.0
      DO 61 M=1,NTERM
      MA=M-1
   61 Y(N)=Y(N)+COEFT(M)*(X(N)**MA)
   70 CONTINUE
   71 X1=0.0
      X2=0.0
      X3=0.0
      X4=0.0
      X5=0.0
      X6=0.0
      X7=1.0
      IF(NGECO.EQ.0)GO TO 16
      IF(NGECO.NE. 1)GO TO 30
C         3.6% DETECTOR AT  0 INCHES GOOD > 400 KEV
      X1=-2.8481884003
      X2= 0.6668965220
      X3=-0.0361465663
```

```
      X4=-2.8481884003
      X5= 0.6668965220
      X6=-0.0361465663
      X7= 1.0
      GO TO 18
   30 IF(NGECC.NE. 2)GO TO 31
C        3.6% DETECTOR AT  2 INCHES
      X1=16.3561859131
      X2=-2.0367994308
      X3= 0.0909128785
      X4=-45.8184967041
      X5=  8.4092130661
      X6= -0.4991983175
      X7=EXP(81.4209289551+45.2146911621*0.78001-1.40676)
      GO TO 18
   31 IF(NGECC.NE. 3)GO TO 32
C        3.6% DETECTOR AT 10 INCHES
      X1=17.6195983887
      X2=-2.2184772491
      X3= 0.0994535089
      X4=-45.1457977295
      X5=  7.2898702621
      X6= -0.3815773129
      X7=EXP(90.6882563448+48.1047210693*0.78525+0.18718)
      GO TO 18
   32 IF(NGECC.NE.11)GO TO 33
C        2.5% DETECTOR AT  0 INCHES
      X1= 10.4776115417
      X2= -1.2133836746
      X3=  0.0528133996
      X4=-30.7291870117
      X5=  2.8710823059
      X6=0.0
      X7=EXP(81.5283508301+31.3188476563*0.74116-0.48050)
      GO TO 18
   33 IF(NGECC.NE.12)GO TO 34
C        2.5% DETECTOR AT  2 INCHES
      X1= 14.0573759079
      X2= -1.7552604675
      X3=  0.0800320506
      X4=-53.1406250000
      X5=  9.4473867416
      X6= -0.5440220237
```

```
129               X7=EXP(96.499542236+39.167388916-0.73961-0.24043)
130               GO TO 18
131            34 IF(NGECC.NE.13)GO TO 35
132          C       2.5% DETECTOR AT 10 INCHES
133               X1= 17.8550262451
134               X2= -2.2473268509
135               X3=  0.1011717319
136               X4=-41.9310455322
137               X5=  7.3369789124
138               X6= -0.4129428864
139               X7=EXP(77.860824585+48.8855133057-0.82155-1.19690)
140               GO TO 18
141            35 IF(NGECC.NE.21)GO TO 36
142          C       XRAY DETECTOR AT  0 INCHES
143               GO TO 17
144            36 IF(NGECC.NE.22)GO TO 37
145          C       XRAY DETECTOR AT  2 INCHES
146               GO TO 17
147            37 IF(NGECC.NE.23)GO TO 38
148          C       XRAY DETECTOR AT 10 INCHES
149               GO TO 17
150            38 IF(NGECC.NE.31)GO TO 39
151          C       7CC  DETECTOR AT  0 INCHES IS NOT AVAILABLE
152               GO TO 17
153            39 IF(NGECC.NE.32)GO TO 40
154          C       7CC  DETECTOR AT  2 INCHES IS NOT AVAILABLE
155               GO TO 17
156            40 IF(NGECC.NE.33)GO TO 41
157          C       7CC  DETECTOR AT  8 INCHES GOOD < 1700 KEV
158               X1=-10.2557344437
159               X2=  1.9886932373
160               X3= -0.1093124151
161               X4=-10.2557344437
162               X5=  1.9886932373
163               X6= -0.1093124151
164               X7=1.0
165               GO TO 18
166            41 IF(NGECC.NE.44)GO TO 42
167          C       4.6% DETECTOR AT  5 INCHES
168               GO TO 17
169            42 IF(NGECC.NE.42)GO TO 43
170          C       4.6% DETECTOR AT  2 INCHES
171               GO TO 17
```

```
   43 IF(NGECC.NE.43)GO TO 44
C          4.6% DETECTOR AT 10 INCHES
      X1=  3.7981853
      X2=  -.3336803
      X3=   .0137885
      X4=-42.398132
      X5=  7.2985811
      X6=  -.4063828
      X7=EXP(93.173646)
      GO TO 18
   44 IF(NGECC.NE.54)GO TO 45
C          10.4% DETECTOR AT  5 INCHES
      X1=  4.27583
      X2=  -.47926
      X3=   .022849
      X4=-62.71104
      X5= 11.03814
      X6=  -.638647
      X7=EXP(117.20301+14.04565-.35542-.71738)
      GO TO 18
      GO TO 18
   45 IF(NGECC.NE.52)GO TO 46
C          10.4% DETECTOR AT  2 INCHES
      X1=2.0880670547
      X2=-.1455207467
      X3= .0061463341
      X4=-64.8149871826
      X5= 11.4318428040
      X6=  -.6618534923
      X7=EXP(117.89775 8545+13.79627418 2+2.41350-5.18760)
      GO TO 18
   46 IF(NGECC.NE.53)GO TO 47
C          10.4% DETECTOR AT 10 INCHES
      X1=  2.136800766
      X2=  -.1194006205
       X3=   .0033111656
       X4=-48.95594787 6
      X5=  8.2206764221
      X6=  -.4499259591
      X7=EXP(95.148223877+9.730970382 -.16362-.50244)
      GO TO 18
   47 IF(NGECC.NE.61)GO TO 48
C          FOR FUTURE EXPANSION
```

```
      GO TO 17
   48 IF(NGECC.NE.62)GO TO 49
C        FOR FUTURE EXPANSION
      GO TO 17
   49 IF(NGECC.NE.63)GO TO 82
C        FOR FUTURE EXPANSION
      GO TO 17
   82 CONTINUE
   16 IF(XM.EQ.0)GO TO 17
      X1=U(1)
      X2=U(2)
      X3=U(3)
      X4=U(4)
      X5=U(5)
      X6=U(6)
      X7=EXP(U(7))
      GO TO 18
   17 PRINT 8
    8 FORMAT('0    EFFICIENCY CURVE NOT AVAILABLE    UNCORRECTED RATIOS
     1OF AREAS ARE GIVEN')
   18 Q(1)=100.
      ALOGY1=LOG(Y(1))
      G1=Y(1)**(X1+X2*ALOGY1+X3*ALOGY1*ALOGY1)
      IF(Y(1).LT.400.)G1=X7*Y(1)**(X4+X5*ALOGY1+X6*ALOGY1*ALOGY1)
      DO 7 I=2,NEWX
      ALOGYI=LOG(Y(I))
      IF(Y(I).LT.400.)GO TO 15
      QI=Y(I)**(X1+X2*ALOGYI+X3*ALOGYI*ALOGYI)
      GO TO 14
   15 QI=Y(I)**(X4+X5*ALOGYI+X6*ALOGYI*ALOGYI)*X7
   14 Q(I)=(100*A(I)/A(1))*QI/G1
      IF(Q(I).LE.1.E-6)Q(I)=0.0
      IF(Q(I).GE.1.E 6)Q(I)=0.0
    7 CONTINUE
      NE=NPTS+1
      PRINT 94,((N,X(N),Y(N),E(N),Q(N),A(N),SDA(N),NPKLO(N),NPKHI(N)),N=
     11,NPTS)
   94 FORMAT('0  N  CENTROID CALC E CALIB E REL INTENSITY PEAK AREA  ARE
     1A SD PKLO PKHI'/(I4,1X,3F8.2,F12.4,F11.0,F10.2,2I5))
      IF(NE.GT.NEWX)GO TO 22
      PRINT 98,((N,X(N),Y(N),Q(N),A(N),SDA(N),NPKLO(N),NPKHI(N)),N=NE,NE
     1WX)
   98 FORMAT(I4,1X,2F8.2,8X,F12.4,F11.0,F10.2,2I5)
```

```
258               GO TO 22
259            12 END


1                 SUBROUTINE BESTFIT (Y,X,NPT ,NTERM,COFT)                    8SEPT69
2           C     THIS ROUTINE DOES A LEAST SQUARES FIT TO THE FOLLOWING FUNCTION--
3           C      Y=COFT(1)+COFT(2)*X+COFT(3)*X**2+...+COFT(NTERM)*X**(NTERM-1)
4                 DIMENSION Y(NPT),X(NPT),COFT(NTERM)
5                 DOUBLE PRECISION A(23,23),YD(200),XD(200),XTERM(41)
6                 IF(NTERM.GT.21)GO TO 3
7                 IF(NPT.GE.NTERM)GO TO 9
8                 PRINT 16
9              16 FORMAT(10X,'NOT ENOUGH DATA POINTS FOR NUMBER OF TERMS')
10                GO TO 14
11             9  ND=2*NTERM-1
12                DO 1 I=1,41
13             1  XTERM(I)=0.0D0
14                DO 2 I=1,23
15                DO 2 J=1,23
16             2  A(I,J)=0.0D0
17                DO 4 I=1,NPT
18                XD(I)=X(I)
19             4  YD(I)=Y(I)
20          C     FILLS X PART OF MATRIX
21                XTERM(1)=NPT
22                DO 5 I=2,ND
23                DO 5 J=1,NPT
24             5  XTERM(I)=XTERM(I)+XD(J)**(I-1)
25                DO 8 I=1,NTERM
26                DO 8 J=1,NTERM
27                IND=I+J-1
28             8  A(I,J)=XTERM(IND)
29          C     FILLS Y PART OF MATRIX
30                DO 6 J=1,NPT
31             6  A(1,NTERM+1)=A(1,NTERM+1)+YD(J)
32                DO 7 I=2,NTERM
33                DO 7 J=1,NPT
34             7  A(I,NTERM+1)=A(I,NTERM+1)+YD(J)*(XD(J)**(I-1))
```

```
C       SETS THE PIVIOT
        A(1,NTERM+2)=1.0
C       INVERTS THE MATRIX
        N1=NTERM+1
        N2=NTERM+2
        DO 11 I=1,NTERM
        DO 10 J=2,N2
     10 A(N1,J)=A(1,J)/A(1,1)
        DO 11 J=1,NTERM
        DO 11 K=1,N1
     11 A(J,K)=A(J+1,K+1)-A(J+1,1)*A(N1,K+1)
        DO 12 I=1,NTERM
     12 COFT(I)=A(I,1)
        GO TO 14
      3 PRINT 15
     15 FORMAT(' DIMENSIONS OF BESTFIT WERE EXCEEDED, ZEROS RETURNED')
        DO 13 I=1,NTERM
     13 COFT(I)=0.0
     14 CONTINUE
        RETURN
        END
```